DOT/FAA/TC-12/51

Federal Aviation Administration
William J. Hughes Technical Center
Aviation Research Division
Atlantic City International Airport
New Jersey 08405

Evaluation of Friction Stir Weld Process and Properties for Aircraft Applications

October 2018

Final Report

U.S. Department of Transportation
Federal Aviation Administration

NOTICE

Technical Report Documentation Page

1. Report No.	2. Government Accession No.	3. Recipient's Catalog No.
DOT/FAA/TC-12/51		

4. Title and Subtitle	5. Report Date
EVALUATION OF FRICTION STIR WELD PROCESS AND PROPERTIES FOR AIRCRAFT APPLICATIONS	October 2018
	6. Performing Organization Code

7. Author(s)	8. Performing Organization Report No.
D. Burford, S. Jurak, P. Gimenez Britos, and E. Boldsaikhan	

9. Performing Organization Name and Address	10. Work Unit No. (TRAIS)
Advanced Joining and Processing Lab National Institute for Aviation Research Wichita State University 1845 North Fairmount Wichita, KS 67260-0093	11. Contract or Grant No.

12. Sponsoring Agency Name and Address	13. Type of Report and Period Covered
Mark Freisthler U.S. Department of Transportation Federal Aviation Administration Northwest Mountain Region−Transport Airplane Directorate 1601 Lind Avenue, SW Renton, WA 98057	Final Report
	14. Sponsoring Agency Code AIR-100

15. Supplementary Notes

The FAA William J. Hughes Technical Center Aviation Research Division Technical Monitors were Curtis Davies and Lynn Pham.

16. Abstract

Friction stir joining processes and joint properties were evaluated for aircraft applications by staff and students of the National Institute for Aviation Research Advanced Joining & Processing Lab of Wichita State University. The work was performed between 2004 and 2010. Both friction stir welding (FSW) and friction stir spot welding (FSSW) are joining technologies that are being developed for a variety of applications throughout the aerospace industry. These applications are typically developed on a case-by-case basis to take advantage of manufacturing and implementation cost savings associated with these relatively new processes, such as part count reduction, improved material buy-to-fly ratios, cycle time reduction, reduced lead-time requirements, and lowered environmental impacts. Because these are relatively new innovations, industry standards and design (allowables) data for FSW and FSSW are still not firmly established. Consequently, developing and implementing applications incorporating these technologies require significantly more effort (testing and verification) than conventional joining technologies (i.e., installed fasteners). To facilitate the establishment of standards and specifications for friction stir technologies, a proposal to evaluate FSW and FSSW for potential inclusion in Metallic Materials Properties Development and Standardization (MMPDS) was presented to the MMPDS coordinating committee in April 2006. A round-robin test program was subsequently conducted by MMPDS members. This study found evidence that different processing paths can achieve similar material properties. The work was then introduced to the Aerospace Metals and Engineering Committee of SAE International to coordinate the drafting of Aerospace Material Specifications for friction-stirred materials. This study also showed that new electronic nondestructive evaluation techniques are becoming available that may provide a greater probability of detection than conventional nondestructive evaluation techniques. This study indicates that with fiction stir welding is becoming an acceptable joining method suitable for aircraft application.

17. Key Words	18. Distribution Statement
Friction stir welding, Friction stir spot welding, Metallic materials properties development and standardization, Mechanical tests, Standards, Specifications.	This document is available to the U.S. public through the National Technical Information Service (NTIS), Springfield, Virginia 22161. This document is also available from the Federal Aviation Administration William J. Hughes Technical Center at actlibrary.tc.faa.gov.

19. Security Classif. (of this report)	20. Security Classif. (of this page)	21. No. of Pages	22. Price
Unclassified	Unclassified	153	

ACKNOWLEDGEMENTS

Funding for this multiyear program was provided through a grant from the FAA and a cost-matching grant from the State of Kansas through the National Institute for Aviation Research (NIAR)-Industry-State (NIS) Program. The executive administrator for these programs is Dr. John Tomblin, Executive Director, National Institute for Aviation Research (NIAR).

The Principal Investigator for this program was Dr. Dwight A. Burford. The FAA William J. Hughes Technical Center Technical Monitors were Curtis Davies and Lynn Pham. The NIS FY2010 Industry Executive Committee included Greg Smith, The Boeing Company IDS; Ivan Vlatko and Jim Ambridge, Bombardier Learjet; Jim Krone and Amit Tamhane, Cessna; Dennis Schmidt and Ed Petkus, Hawker Beechcraft; and Jim Westerman and Farhad Tadayon, Spirit AeroSystems. Prior-year members are referenced in the respective NIS annual reports.

Over the course of the program, each of the following individuals served at least 1 year as an industry point of contact for the company under which his or her name is listed:

Boeing

- John Baumann
- Marc Matsen
- David Ogan
- Raj Talwar

Learjet/Bombardier Aerospace

- Alexandre Bourgeois
- Jennifer Graham-Rateliff*
- Leo Kok
- Richard Meeske
- Gary Moore
- Krish Patni
- Russ Penner
- Ken Poston
- Bruce Thomas

Cessna Aircraft Company

- Ali Eftekhari
- Michael Hannigan*
- Chris Hurst
- Uma Ramasubramanian*
- Jason Scheuring*
- Ron Weddle*

Lockheed Martin Aeronautics Company

- John Barnes
- Ashley Norris
- Jennifer Takeshita

Hawker Beechcraft (formerly Raytheon)

- Robert Cerney
- Byron Colcher
- Phil Douglas*
- Bill Jones
- Ken Minks
- Ron Preston

Spirit AeroSystems

- Casey Allen*
- Mike Cumming
- Robert Kay
- Mark Ofsthun
- Gil Sylva

(*Formerly with the company represented.)

In addition to the grant funding, industry partners provided materials and services for several project phases and tasks of this program. Also, The Welding Institute provided three tool designs for the Metallic Material Properties Development and Standardization (MMPDS) round-robin studies. The Fracture and Fatigue Laboratory of NIAR completed many of the mechanical tests. The NIAR Research Machine Shop fabricated most all friction-stir welding tools tested in this program. Aluminum Company of Canada, Aluminum Company of America, and Kaiser provided material for the MMPDS round-robin test program.

The results represented in this report were generated and assembled through the efforts of many individuals over the course of the program. Much of the welding, mechanical tests, and metallography were completed by graduate and undergraduate student assistants. One Doctoral dissertation and multiple Master's theses were completed under this program. Research prepared for two Master's theses in particular are featured in this report in sections 4 and 5. The following people are recognized for their individual contributions to this work (based on their current relationship with the NIAR Advanced Joining and Processing (AJ&P) Lab).

AJ&P Staff

- Enkhsaikhan Boldsaikhan, Ph.D.
- Jeremy Brown
- Pedro Gimenez Britos
- James Gross
- Bruce Handyside
- T.J. Lam
- Ece Toros

Graduate Research Assistants

- Farzad Baratzadeh
- Jeff Buller
- Vishwanath Iyer
- Vien Nguyen
- Sarah Jurak

Student Assistants

- Raeann M. Edson
- Adam J. Knolla
- Brady Sexson
- Santiago Vera Torres
- Siddharth M. Vyawahare
- Christian Walden
- Galen Werth

Other NIAR Staff

- Brijesh Kumar, Ph.D.
- Mark Murrell
- Lamia Salah
- Indika U. Thevarapperuma

WSU Faculty

- George Talia, Ph.D.

Formerly Associated with NIAR

- Farhan Aktar
- Dale Cope, Ph.D.
- Kishore Dupally
- Jason Grube
- Jessi Irving
- Adam Jahns
- Josh Merry
- Heath Misak
- Paul Nething
- Kyle Nilsen
- Huy Pham
- Nicholas Thurlby
- Bryan Tweedy
- Christian Widener, Ph.D.
- Karin Witthar

The following Wichita State University faculty members have served as graduate academic advisors to various students conducting research under this program:

- Ramazan Asmatulu, Ph.D.
- George Talia, Ph.D. (deceased)
- Kurt Soschinske, Ph.D. (deceased)
- Brian Driessen, Ph.D.
- Mike McCoy, Ph.D.
- Walter Horn, Ph.D.
- Gamal Weheba, Ph.D.
- Hamid Lankarani, Ph.D.

TABLE OF CONTENTS

APPENDICES

LIST OF FIGURES

LIST OF TABLES

LIST OF ACRONYMS

AJ&P	Advanced Joining & Processing
Al	Aluminum
ALCAN	Aluminum Company of Canada
ALCOA	Aluminum Company of America
AMEC	Aerospace Metals and Engineering Committee (of SAE)
AMS	Aerospace Material Specifications
ANOVA	Analysis of variance
AWS	American Welding Society
CAA	Chromic acid anodized
CNT	Carbon nanotubes
DFT	Discrete Fourier transformation
DOE	Design of experiments
e-NDE	Electronic nondestructive evaluation
ETWG	Emerging Technologies Working Group
FAA	Federal Aviation Administration
FPT	Fixed probe tool
FSP	Friction stir processing
FSW	Friction stir welding
FSSW	Friction stir spot welding
HAZ	Heat-affected zone
HRS	High rotational speed
HV	Vickers hardness
ipm	Inches per minute
LM	Lockheed Martin
LOP	Lack of penetration
MMDPS	Metallic Material Properties Development and Standardization
NASM	National Aerospace Standard, Metric
NDE	Nondestructive evaluation
NIAR	National Institute for Aviation Research
NIS	NIAR-Industry-State
NN	Neural network
PDS	Process Development System
POD	Probability of detection
rpm	Revolutions per minute
RPT	Retractable probe tool
SAE	SAE International
TEM	Transmission electron microscopy
TMAZ	Thermomechanically affected zone
TWI	The Welding Institute
UPA	Ultrasonic phased array
UTS	Ultimate tensile strength
WSU	Witchita State University

EXECUTIVE SUMMARY

This report presents annual summaries and selected focus areas of a comprehensive research program conducted from October 2004 through December 2010 by the staff and students of the Advanced Joining & Processing Lab of the Wichita State University National Institute for Aviation Research in Wichita, Kansas. This study was initiated to determine opportunities for standardization of the friction stir-welding (FSW) process to provide efficiencies in certification. This project assessed the process dependency of the processes currently available and assessed the material and process controls needed to allow the publication of design related properties in industry handbooks like the Metallic Materials Properties Development and Standardization (MMPDS). The project initiated in October 2004 to evaluate friction stir-joining processes and joint properties for potential aircraft applications. Initial evaluations of the process were completed and, in 2006, the program emphasis was placed on supporting the development of design data based on advancements in the technology and the emerging industry process specifications.

This report presents an outline of possible approaches for developing design data and supporting property standards for friction stir technologies. A proposal was made to the MMPDS coordination committee to conduct this study. In April 2006, an industry-based round-robin evaluation program began in the MMPDS Emerging Technologies Working Group (ETWG) (formerly the Process Intensive Materials Working Group). After successfully completing the ETWG round-robin evaluation program, preliminary work to formulate a road map to coordinate draft Aerospace Material Specifications for friction-stirred materials and joints was presented to the Aerospace Metals and Engineering Committee (AMEC) of SAE International (October 2008). Once the proposal was approved by AMEC members, draft specifications based on the MMPDS round-robin program were presented to the committee.

In this research, advances in FSW and friction stir spot welding (FSSW) tooling and process innovations were evaluated and found to potentially provide improved robustness over previously used FSW and FSSW practices. Additionally, based on results from an industry-based round-robin program, signal analysis of process forces provided greater probability of detection of internal flaws than conventional nondestructive evaluation techniques. The results of this study indicate that with proper material and process controls, it may be possible to develop relevant design data using MMPDS procedures.

1. INTRODUCTION

Since The Welding Institute (TWI) filed the friction stir welding (FSW) patent in December of 1991 [1–2], many researchers have investigated this unique subsolidus welding technology for joining aluminum (Al) structural alloys and product forms [3–4]. Advanced components, such as a space shuttle's external tank [5–6] and the fuel tanks for the Boeing Delta family of rockets [7–8], are among the earliest applications developed for aerospace. The hundreds of friction stir-related patents held by aerospace companies and their suppliers demonstrate the continuing interest in deploying friction stir-related technologies on airframe structures [9].

1.1 APPLICATION OF FSW IN AEROSPACE

The FSW and friction stir spot welding (FSSW), a variant of FSW, are emergent joining technologies that are under development for a variety of applications throughout the aerospace industry [10]. To date, however, they are found only in a limited number of commercial, space, and military aviation structures and assemblies [11]. These applications typically have been developed on a case-by-case basis to take advantage of manufacturing and implementation cost savings associated with these relatively new processes, such as part count reduction, improved material buy-to-fly ratios, cycle time reduction, reduced lead-time requirements, lowered environmental impacts, and less manufacturing time and complexity.

The first commercial aviation implementation was the fabrication of the fuselage and tail assemblies of the Eclipse 500 (a very light jet) [12–13]. Friction stir-welded cargo nose barrier beams for the B-747-400F were developed in early 2000 [14–15] and have been in service since 2005. FSSW is currently being developed to replace resistance spot welding in the Hawker Beechcraft Baron and Bonanza cabin doors [16]. European Aeronautics Defense and Space Company also developed a FSW process to be incorporated in their aircraft design [17] and introduced a weld tool with a stationary shoulder for licensing, referred to as the Delta N tool [18–19]. Prototype structures produced with FSW reportedly have been developed for military aircraft [20]. The first production of a military application was the cargo ramp toenails for the C-17 [15]. This application of FSW reportedly provided significant cost and weight savings.

Embraer reported on a development program for FSW mid-size aircraft [21–22]. They noted that there is a growing demand for lower-cost aircraft that maintain or exceed the performance and efficiencies of those based on current manufacturing approaches [23]. Investing in environmentally friendly manufacturing technologies that can also provide safe structures, such as FSW, is key to meeting such requirements. FSW is an attractive alternative to current fabrication technologies. Therefore, Embraer tested a cylindrical barrel section to evaluate the skin and stringer lap joint as well as a skin butt joint. The stringers were an L or slightly Z shape and made of 0.05-inch-thick AA7050-T76511. The skin was 0.063-inch, bare AA2024-T3. The primary interest was to evaluate the fatigue and damage tolerance behavior of the test article. It lasted five design life cycles without cracking, demonstrating excellent fatigue behavior. The FSW barrel section also demonstrated satisfactory crack propagation response.

Bombardier recently reported on an ongoing technology-readiness program initiated more than 5 years ago to advance FSW to near-production levels for butt and lap joints in dissimilar aerospace aluminum alloys [24]. The program involved multiple Bombardier divisions and industry collaborators. Both coupon-level and full-scale panel tests were conducted. Full-scale component fuselage panels were fabricated and tested to evaluate both static and dynamic mechanical properties. Stiffened panels tested for residual strength failed in a manner similar to machined monolithic structures. For the fatigue and damage-tolerance properties assessment of friction stir-welded lap joints, the panels were subjected to a spectrum loading protocol simulating a regional aircraft life cycle. At the time of this publication, a second-lifetime test was in progress for damage tolerance assessment at a facility capable of applying torque and bending as well as pressurization of the stiffened panels. Thus far, the assessment shows that FSW can be used in the construction of regional aircraft with little technical risk.

1.2 FSW OVERVIEW

FSW involves forcing a spinning, nonconsumable tool into and along the joint between two or more components to be permanently joined. Figure 1 shows the basic process and tool elements typically used to fabricate a butt joint between two plates using FSW.

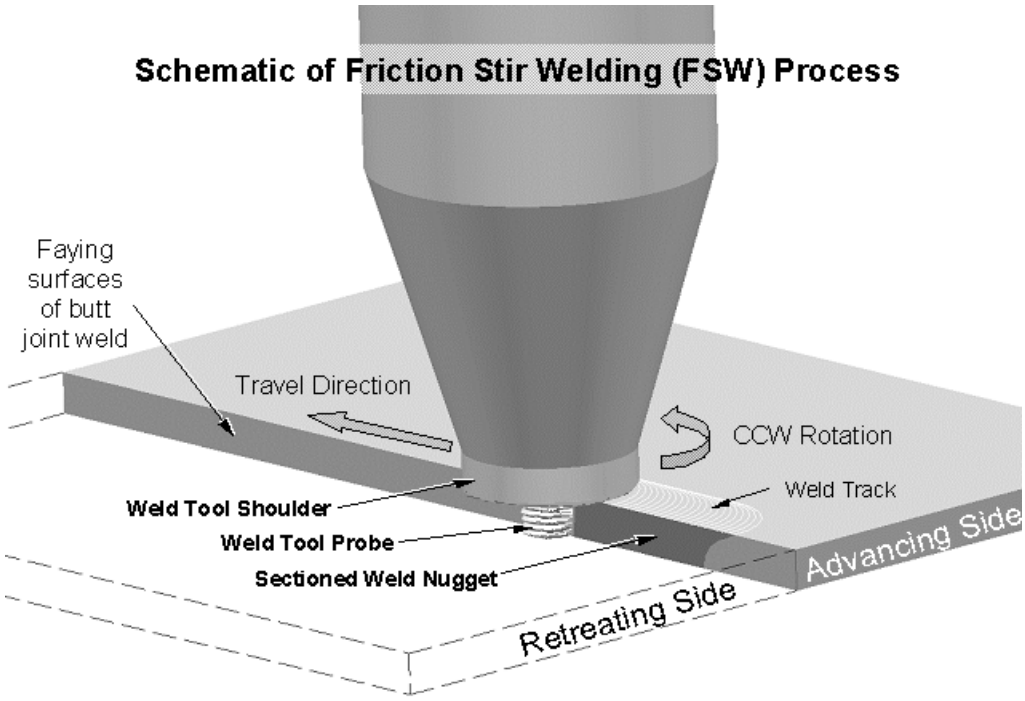

Figure 1. Basic FSW butt joint [14]

A conventional FSW tool, as shown in figure 1, consists of a tool body with a probe and a shoulder. The probe extends from the end of the weld tool and is the portion of the tool that is forced into and along the joint interface between the workpieces being joined. The probe provides through-the-thickness stirring of the joint interface. The shoulder is the surface on the end of the weld tool (less the probe). It progresses along the surface and the joint line between the workpieces during the FSW process. It provides both thermal heating and containment of the joint material to keep it from escaping the work zone around the probe.

In high rotational speed (HRS) FSW, discussed in section 2.3, a stationary or fixed (nonrotating) shoulder may be used instead of the rotating-style shoulder shown in figure 1. In the fixed-shoulder tool configuration, only the probe spins. This eliminates the heat generating on the workpiece surfaces from the rotating shoulder and, therefore, leads to a more uniform thermal condition produced through the thickness of the workpiece. A practical concern with fixed-shoulder FSW is the seepage of joint material into the dynamic interface between the rotating probe and the nonrotating (fixed) shoulder. During HRS, FSW joint material was observed leaking into the interface, which caused erosion around the circumference of the tool probe inside the shoulder. The high wear rates observed on the side of the probe were attributed to some of the thin, hot aluminum extruding into the interface and turning into alumina (an excellent abrasive), which then abraded the rotating probe.

The probe and shoulder of the weld tool provide the necessary work surfaces for stirring and containing the joint material during FSW. A typical weld cycle begins with plunging the weld tool probe slowly into the starting location of the joint until the weld tool shoulder contacts the weldment surface. After a dwell time of a few seconds (or possibly zero), the weld tool is advanced along the joint line under either a constant axial load or a fixed axial position control, both of which are controlled through the actuation of the machine tool spindle. At the end of the weld, the weld tool is typically extracted from the workpiece while it continues to rotate.

The rotating and compacting motion of the weld tool surfaces on the workpiece introduces three necessary elements to produce a sound friction weld:

- Heat
- Pressure
- Relative translation of the adjoining materials

The heat necessary for plastically straining the joint material around the weld tool is generated in the workpiece material immediately surrounding the tool probe and under the shoulder through mechanical stirring and frictional heating. The pressure to form a fully consolidated joint is provided by the weld tool shoulder compressing the joint material against a supporting backing surface (backing bar), as shown in figure 2. Relative translation between the materials to be joined is provided through the locally complex forging and extruding action induced in the joint material by the spinning, which advances the weld tool probe and shoulder. Through the simultaneous application of these processes, a metallic bond is established between the metal components without melting the base materials (workpieces).

Process parameters for FSW are dependent on the metal alloys and thicknesses being joined as well as the joint configuration and weld tool geometry selected for joining the workpieces. The following are the primary process parameters:

- Spindle rotational speed
- Weld tool travel speed
- Axial weld tool force (shoulder pressure) or location (displacement control)

Joint fit and part rigidity must also be sufficient to ensure that the parts do not shift under the high applied loads involved in the process during FSW.

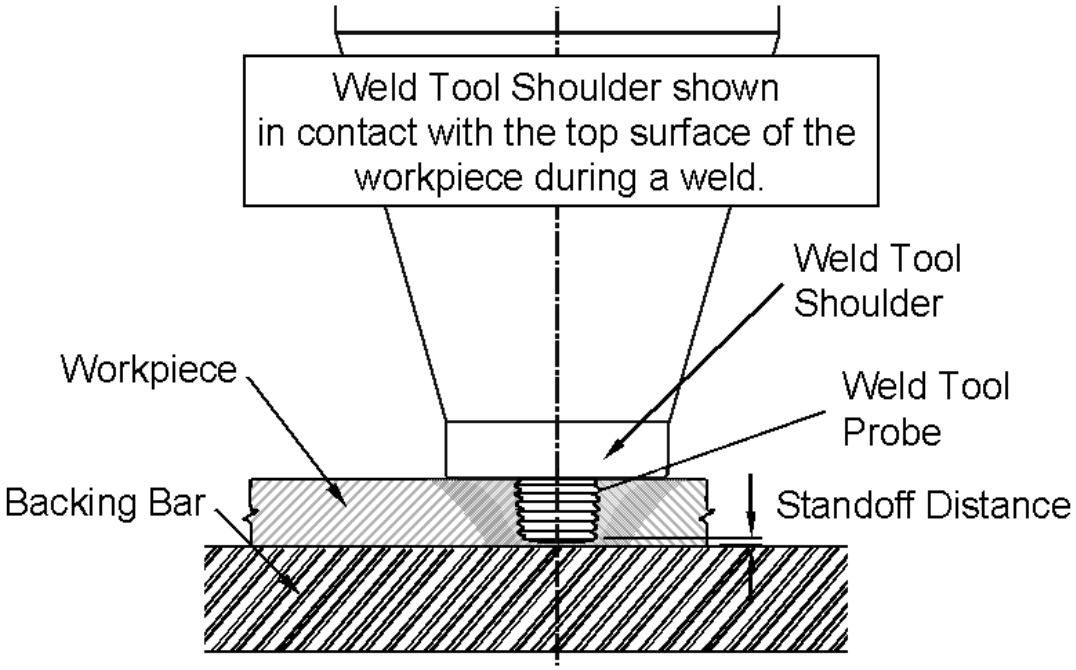

Figure 2. Cross section of a simple friction stir-welded butt joint with the weld tool at full depth [14]

Because of the forces required by the process, FSW machines must be able to apply and sustain the substantial loads necessary to produce sound, fully compacted joints (determined by design and experimentation). To ensure consistent and reproducible process results at the high loads involved in FSW, typically machines are also numerically controlled. Furthermore, because the process relies on locally generated heating, variations in the heat capacity and thermal conductivity of the workpiece and fixture along the joint line (e.g., as a result of changing section sizes) can lead to variations in metallurgical properties and, thus, variations in mechanical properties along the joint. This effect and how it is addressed is described more fully in section 3.2.1.

1.3 FEATURED FOCUS AREAS

This report is divided into the following sections to highlight key results and findings of this research program as well as to provide recommendations for implementing FSW and FSSW in constructing aircraft structures and assemblies.

- Section 2: Annual Research Summaries
- Section 3: Development of Design Data for FSW and FSSW
- Section 4: Multipath Manufacturing and the Metallic Material Properties Development and Standardization (MMPDS) Round-Robin test program
- Section 5: Electronic Nondestructive Evaluation (e-NDE) and Probability of Detection (POD)
- Section 6: Recommendations
- Section 7: Summary

2. ANNUAL RESEARCH SUMMARIES

Investigators from the Advanced Joining & Processing (AJ&P) Lab of the Wichita State University (WSU) National Institute for Aviation Research (NIAR) in Wichita, Kansas conducted research for the Federal Aviation Administration (FAA) program, "Evaluation of Friction Stir Weld Process and Properties for Aircraft Applications," and a companion NAIR-Industry-State (NIS) project, "Friction Stir Welding and Related Topics." During this time period, research was performed in the following areas:

- The FSW of typical aerospace aluminum alloys in both butt and lap joint configurations
- The FSSW with faying sealants, aluminum cladding, and various forms anodize and Alodine® finishes
- Tool evaluations for optimizing FSW and FSSW for aerospace applications
- Evaluation of material and structures performance, including materials evaluations (e.g., corrosion resistance), structural tests, and analysis of process innovations
- Standards and specification development
- Robotic FSW and FSSW
- HRS FSW and FSSW
- Design data for FSW and FSSW joints, which is considered foundational to a broader and more widespread application of friction stir technologies in aerospace structures

A brief summary of the research and development work conducted under this joint FAA-NIS program is provided in sections 2.1 through 2.7.

2.1 THE 2004 RESEARCH SUMMARY

The preliminary research results generated from this program during 2004 were published in an annual progress report [25]. The most important results from that report are summarized in sections 2.1.1–2.1.3 of this report.

2.1.1 Initial Investigation

The objective of the initial study was to gain insight into the value of various types of mechanical and corrosion tests, which are required to obtain a comprehensive assessment of the quality and performance of FSW butt joints. It was also to establish baseline properties of FSW joints at the current level of technology and understanding. Initially, the potential for using FSW to join two of the most common and widely used aluminum alloys for aeronautical applications, AA2024 and AA7075, was explored. The tests that were performed were tensile, exfoliation corrosion, fatigue, fatigue crack propagation, fracture toughness, and stress corrosion cracking. Performing a comprehensive evaluation of these welds using these tests was important because a literature survey showed that only a few of these tests were typically represented for a given sample set, giving an incomplete picture of weld performance. In many instances, only tensile tests were performed, with no fatigue-, corrosion-, or damage tolerance-type tests being done. Because these are the primary tests of interest for aeronautical applications, a more comprehensive approach was taken.

2.1.2 Findings for Preliminary Static Testing

The preliminary data demonstrated the potential of FSW as a viable manufacturing technique for use in aerospace applications. Therefore, it was concluded that FSW merits further investigative research. Specifically, tension tests were selected to provide comparisons with the limited published material properties. For the AA2024 and AA7075 aluminum alloy FSW joints, better percentages of parent metal strength (i.e., joint efficiencies) were obtained in 0.125-inch-thick specimens when compared to 0.040-inch-thick specimen results. As expected, the tool for the 0.040-inch-thick sheet stock differed in configuration from the tool for the 0.125-inch gage material. The tool for the 0.040-inch sheet also required more optimization. In both cases, values obtained were between 80% and 93% of the parent metal strength. For each gage, a single tool was used for all welds. There should be no bias toward one result or the other; objectivity precludes preference.

2.1.3 Findings From Preliminary Dynamic and Corrosion Tests

Fatigue, fatigue crack propagation, and fracture toughness results were much more difficult to compare to published parent material data because of the limited number of prior reports that provide this type of information. From the comparisons that could be made, test results indicated that FSW joints reasonably maintain the fatigue, fatigue crack propagation, and fracture toughness properties of the parent metal. However, because of the insufficient amount of available data, further study is needed to determine this trend. The resistance to corrosion and stress corrosion cracking of FSW joints produced in this preliminary study were not satisfactory. In the as-welded state, AA2024 and AA7075 friction stir-welded material had a greater susceptibility to corrosion

and stress corrosion cracking than the parent material. Nevertheless, sufficient published research in this area suggested that this can be adequately addressed through various types of post-weld treatments. Consequently, post-weld treatment of FSW joints became one of the primary focuses of the research program in 2005.

2.2 THE 2005 RESEARCH SUMMARY

The 2005 research results generated from this program were published in an annual progress report under the title, "Friction Stir Welding and Related Topics" [26]. The most important results from that report are summarized in sections 2.2.1–2.2.3.

2.2.1 Post-weld Treatments Investigated [27–28]

An MTS® ISTIR™ Process Development System (PDS) FSW machine was installed in the WSU NIAR AJ&P Lab in January 2005. The addition of the 5-axis ISTIR PDS machine provided the needed capability to perform FSW research and prototyping. A post-weld heat treatment investigation was then started to determine if thermal treatments could restore the exfoliation and stress corrosion resistance of 0.125-inch-thick friction stir butt welds in AA7075-T73 and AA2024-T3 aluminum alloys. If so, an investigation to determine the effect of selected treatments on mechanical properties would take place. A significant second-stage finding of the material test program conducted during this year was that exfoliation resistance could be restored for friction stir-welded AA2024-T3 and AA7075-T73 with proper post-artificial aging, although there was some loss in tensile and yield strengths. However, there was little effect on the fatigue crack propagation when compared to the parent material properties. Therefore, it was concluded that a suitable post-weld artificial age is achievable for certain alloy and temper combinations.

2.2.2 Fixed Shoulder Investigation [29]

The fixed-shoulder tool had an observable impact on the microstructure and resulting microhardness. As expected, it also had a significant quenching effect over a rotating shoulder. This effect was expected to be enhanced by the addition of cooling lines to the fixed-shoulder tool to maintain a large temperature differential. Since it is well known that AA2024 and AA7075 alloys are very quench-rate sensitive (with higher strengths produced for higher quench rates), this innovation may provide a new way to enhance the mechanical properties of friction stir welds in AA2XXX and AA7XXX alloys. It was also anticipated that this tool development could significantly improve the fatigue life of the welded material because a potential stress raiser at the material shoulder interface, which is generally associated with flash production, has been eliminated. It was also expected that a layer of compressive stresses was built into the top surface of the weld area from the fixed-shoulder tool.

2.2.3 The FSW Structures Modeling and Analyses [30]

Flat, 2′ x 2′ stiffened panels were fabricated with friction stir lap welds and conventional riveting technology for compression, tension, and shear tests. The objective was to establish the capability to predict the static and residual strength of stiffened panels fabricated with FSW. The approach was to use finite element analyses to assess the structural integrity of the test panels. A finite

element model was created in Patran™ and solved as a nonlinear static solution in ABAQUS™. Element data from the FSW zone of the coupon was extracted from the model results and used to generate the stress-strain curve to compare with the test data. A similar modeling philosophy was used to evaluate the lap-joint stiffened panel configuration. Finite element models were then produced for the 2′ x 2′ stiffened panels (typical airframe structure) to predict the static tensile and compressive strength of the panels. Based on this initial work, a plan was developed to continue the structural test plan in fiscal year 2006. In particular, the tension, compression, and shear tests of 2′ x 2′ stiffened panels fabricated in fiscal year 2005 would be performed, and the results would be compared to finite element models to evaluate their ability to predict the load-carrying capability of unitized FSW structures. The results would be compared directly to identical riveted panels for evaluating the static strength performance of the FSW panels.

2.3 THE 2006 RESEARCH SUMMARY

The research results generated from this program during 2006 were published in an annual progress report [31]. The most important results from that report are summarized in sections 2.3.1 through 2.3.4.

2.3.1 Fit-up Tolerances [32]

Part fit-up variations are critical to the joint quality produced by joining operations like FSW. Typical fit-up issues may include gaps, misalignment between the weld path and joint line, setup-related variations, voids or holes in the weld path, and mismatches between materials being joined. These and other factors potentially result in variations in mechanical properties between the start and finish of the weld and lead to the possible formation of defects along the joint line. The purpose of this study was to determine the robustness of the FSW process to imperfections in joint fit-up between plates in butt welding. Specifically, it includes a study of the effect of part fit-up variations on the transverse joint tensile strength of 0.125-inch-thick friction stir butt-welded AA7075-T73 aluminum plate. Welds were performed on an MTS ISTIR PDS FSW machine at NIAR. It was determined that the FSW process was capable of creating a sound defect-free joint for a range of typical fit-up discontinuities. The tolerance zone for weld path misalignment to the joint line was related to the formation of fine nugget grain structure at the bottom of the weld, with two-thirds of the tolerance zone located on the advancing side of the pin. It was also determined that a certain amount of plate gap or voids in the weld path can be tolerated without a decrease in tensile strength; beyond that point, volumetric defects form in the nugget. Otherwise, there is little variation in tensile properties along the weld joint when care is taken to ensure gap and alignment tolerances are not exceeded.

2.3.2 Material Testing [33]

The material test portion of the project consisted primarily of a post-weld heat treatment investigation to determine if thermal treatments could restore the exfoliation and stress corrosion resistance of 0.125-inch friction stir butt welds in AA7075-T73 and AA2024-T3 aluminum alloys. The primary purpose of this work was to evaluate and document selected fundamental properties of FSW joints to optimize material properties for the design of structures using this advanced joining technology. Additionally, in this portion of the research program, possible areas of concern

were identified and recommendations were made regarding methods for addressing these concerns. Dissimilar alloy joints were produced with AA2024-T81 on the advancing side of the joint and then given post-weld artificial aging to enhance their resistance to corrosion. The results were compared to 0.250-inch-thick, naturally aged dissimilar joints of AA2024-T3 and AA7075-T73 [34]. The microhardness tests on dissimilar joints of AA2024 and AA7075 clearly revealed the division between the higher-strength AA7075 material and the lower-strength AA2024 material. The effect of FSW with and without post-weld artificial aging on the electrical conductivity of friction stir-welded AA2024-T81 to AA7075-T73 was reviewed. In both cases, the electrical conductivity in the weld nugget was found to be increased by post-weld heat treatments.

2.3.3 Fixed-Shoulder FSW [29]

In 2004, a fixed-shoulder tool was developed at WSU for use in HRS FSW. In 2006, it was demonstrated to be applicable to conventional FSW using the MTS I-STIR PDS machine in NIAR's AJ&P Lab. This new development combined a fixed shoulder that surrounded the traditional rotating pin and shoulder of the fixed-pin FSW machine, compressing the material in the vicinity of the joint, which resulted in the elimination of weld flash, giving a smooth surface finish on both the top and bottom sides of the weld. The goal of this portion of the research was to integrate the fixed-shoulder tool design into the material test program as a mechanical surface treatment, then determine the effect of the FSW joint on mechanical properties and corrosion resistance due to the expected lower-heat input from a fixed-shoulder design.

2.3.4 Structural Tests [10]

When this work was planned, only a limited number of investigations covering the behavior of monolithic structures manufactured using FSW had been published in the open literature. Therefore, it became the goal of this portion of the research to determine basic properties of common aerospace structures constructed using FSW as the primary joining technique. An investigation of the integrity of stiffened panels fabricated by FSW for aircraft applications was performed by comparing the mechanical properties of FSW panels to the mechanical properties of panels made with conventional riveting. The skin of the panels was made from 0.040-inch-thick AA2024-T3, and the stiffeners were made of AA7075-T73. Prior to the fabrication of stiffened panels, friction stir-welded lap joint coupons were produced and tested with dissimilar aluminum alloys (AA2024-T3 and AA7075-T6) to simulate a joint between a stiffener (AA7075-T6) and a skin (AA2024-T3). A satisfactory set of processing parameters based on low-magnification optical microscopy was developed for the dissimilar alloy lap joints. Two centrally located BAC1498-96 hat section stiffeners were joined to each panel on 8-inch centers with friction stir lap welds. Panels were then tested in compression (in the direction of the length of the stringers), in tension (transverse to the length of the stringers), and in shear (at 45 degrees to the length of the stringers). Panels were fabricated with both continuous FSW and FSSW. An extra set of shear panels was produced with FSSW, with the discrete FSSW joints spaced equal to the rivet spacing on the riveted panels. In tension, the FSW panels showed a 10% increase in ultimate tensile strength (UTS) and a 41% increase in total elongation over the riveted panels. The failure mode for both the friction stir-welded and the riveted panels was stiffener separation at the joint line. In compression, the ultimate load for both the friction stir-welded and the riveted panels appeared to be approximately equivalent. This was the expected result because the stiffener is the primary load-

carrying component of the panel. The peak stress for the FSW and riveted panels was measured at 21.7 and 21.4 ksi, respectively (within experimental scatter). However, the friction stir-welded panel had a greater crosshead deflection than the riveted panel. For both panels, stiffener buckling appeared to be the failure mode. The friction stir-welded panels appeared to continue to buckle after failure while the riveted panel failed catastrophically as evidenced by the increasing strain. In the shear tests, the riveted panel exhibited failure at an ultimate load of approximately 32,300 lb. The friction stir-welded panels failed on average at 35,100 lb, a nominally 8% higher panel load-carrying capability than the riveted panel. The FSSW shear test panel produced an ultimate strength comparable to that of the continuous friction stir-welded panel. However, unlike the continuous friction stir-welded and riveted panels, the stiffeners on the FSSW panel remained substantially intact with failure occurring only at a small percentage of joint locations by sheet pullout.

2.4 THE 2007 RESEARCH SUMMARY

The 2007 research results were published in an annual progress report [35]. The most important results from that report are summarized in sections 2.4.1 through 2.4.5.

2.4.1 Process Varibility and Integral Fastener Initiatives [36–38]

To publish generally accepted FSW design allowables in a handbook such as MMPDS, industry material and process specifications are needed. In the case of FSW, there are many parameters involved (e.g., friction head design, rotational speed, and advancement speed through the materials). The model being developed is based on performance specifications. Customer performance requirements are defined and established through performance specifications. Supplier process specifications are based on their capabilities and expertise and are designed to meet stated customer performance requirements. At the same time, each individual manufacturer needs to define and control the processing parameters for their unique equipment and manufacturing methods. Incorporation of mechanical properties data for joints produced by friction stir-related technologies into the MMPDS handbook requires industry wide specifications, which are available to all companies. For a company to use MMPDS values in products being certified, they need to demonstrate that these values are relevant to their particular manufacturing processes. In the case of FSW, the ability to publish a relevant design data in MMPDS is dependent on the ability to show that sources of variation in the FSW process are clearly understood sufficiently to allow different FSW equipment to produce the same end results. This program was conducted to validate that different variations of equipment may be controlled to yield the same result.

2.4.2 The Effect of Surface Treatments on the Faying Surface of— an in situ Integral Fastener System [39]

FSSW has shown great potential for reducing manufacturing steps, simplifying structural design, and lowering overall costs in automotive and aerospace applications. A variant of the FSW process, FSSW, involves plunging and retracting a weld tool into the materials to be joined at a single location or at a series of locations along a joint line. Because of rapid processing times and increased reliability, the process is an attractive alternative to existing joining techniques, such as riveting and resistance spot welding. The purpose of this portion of the project was to investigate the effect of engineered materials, such as chemical conversion coatings, aluminum cladding, and anodizing placed on the faying surface to prevent or reduce corrosion of FSSW and the adjoining structure. Results are presented on the use of interfacial and faying surface treatments and the effectiveness of processing parameters developed for a new pin tool design and weld pattern. Effectiveness of the process was measured by the degree in which the interfacial and faying surface treatment was dispersed without producing detrimental effects on the mechanical integrity of the weld.

2.4.3 Fundamental Properties of Friction Stir-Welded Al 7136, Including Effects of Post-weld Artificial Aging [40]

Recently, a new AA7XXX series aluminum alloy, designated AA7136, was developed for aerospace applications by Universal Alloy Corporation. Base material properties of AA7136 are compared to friction stir-welded joint properties. Additionally, an investigation into post-weld artificial aging and corrosion was conducted. The FSW joint properties and aging behavior of AA7136 were also compared to AA7075-T73 and some of the replacement alloys for AA7075-T6 that were identified by the U.S. Navy, specifically AA7055-T74 and AA7249-T76. Trends in the overall aging behavior of AA7XXX series alloys friction stir welded in the T7x condition are discussed. Preliminary results show that the corrosion resistance of AA7XXX series alloys welded in the T7x condition can be significantly enhanced by the application of post-weld aging following FSW. Post-weld aging is also required to stabilize the microstructure in AA7XXX series alloys, which would otherwise continue to naturally age indefinitely, as indicated in the literature. Microhardness, electrical conductivity, tensile and exfoliation corrosion test results, as well as an assessment of the metallurgical characteristics, are presented.

2.4.4 Influence of Shoulder Configuration and Geometric Features on FSW Track Properties [41]

Several shoulder configurations have been incorporated into FSW and processing weld tool designs, including featureless concave shoulders and flat and convex scrolled shoulders. Examination of welds produced in aluminum alloys by tools with various shoulders confirms that surface roughness and metal deformation in the uppermost layers of welds are greatly influenced by the shoulder design. Therefore, in an effort to reduce surface damage in butt joints, lap joints, and friction stir-processed material, tools with different scroll patterns were tested to improve weld tool track material properties. Measurable smoothing of the surface finish was achieved by incorporating a unique feature, termed the Wiper™ [42], on the shoulder face. In addition to reducing surface roughness, the Wiper appears to result in a reduction of shearing deformation

damage in the microstructure just beneath the contact surface and, thus, provides better fatigue-resistant properties in the as-welded tool track.

2.4.5 High-Rotational Speed FSW With a Fixed Shoulder [29]

FSW is an innovative solid-state joining technique that produces high-quality joints in the range of 200 to 2000 revolutions per minute (rpm). Work at WSU, however, has demonstrated that FSW and processing with much higher spindle speeds is possible. The principal advantage of operating at higher rotation speeds is the ability to reduce the spindle torque and forging loads. The primary disadvantage is that reduced forging loads create more opportunities for the formation of weld defects like voids, wormholes, and increased porosity. One way to overcome that challenge is through the introduction of a nonrotating shoulder surrounding the rotating pin to maintain the necessary forging loads to prevent weld defects. This section details the principal resultant metallurgy with comparisons made to representative traditional friction stir-welded metallurgy. The resultant mechanical properties and process force analysis of the welded joints is also provided.

2.5 THE 2008 RESEARCH SUMMARY

The research results generated from this program during the year 2008 were published in an annual progress report [43]. The most important results from that report are summarized in sections 2.5.1–2.5.6.

2.5.1 Static Strength Comparison of Discontinuous Friction Stir-Welded Stiffened Panels [44]

Recent advancements in FSW technology have potential for applications in aerospace structures. FSSWs have been found to be much stronger than rivets in the same material thickness, while maintaining the discontinuous crack growth path preferred by aircraft designers. In this study, panels with discontinuous welds were prepared identically to previously investigated friction stir-welded and riveted panels. The structures under study were subscale flat, stiffened panels. The panels were fabricated with two hat-section stiffeners. The sheet was 0.04-inch thick. The AA2024-T3, and the stiffeners were AA7075-T6 spaced on 8.0-inch centers, which is representative of a transport fuselage design. The 2′ x 2′ stiffened panels were statically tested in diagonal tension. The FSSW panel failed at 35.8 kips and the average of the three continuous FSW panels was 35.2 kips. The FSSW panel failed when a spot weld pulled through the skin, creating a hole for a crack to begin. If the processing parameters were altered to force the spot weld to fail by pulling through the stiffener, it is predicted that the panel would continue to carry a load even after several spot welds have failed. The panel would still fail when an inadequate number of spot welds remained to transfer the load from the skin to the stiffener, but at a higher load than was achieved with this test. From this and the prior work, FSSW was shown to be nearly twice as strong as an equivalent riveted joint in static testing. In a stiffened panel, continuous and discontinuous friction stir-welded panels react nearly the same since the strength of a stiffened panel is mainly in the skin and not in the joint. In either case, both continuous and discontinuous friction stir welds (including FSSW) were shown to be better than an equivalent riveted structure. Several factors influence the strength of discontinuous FSW stiffened panels, and the panels can be tailored to meet strength requirements. A large shear area of the joint connecting the stiffener with the sheet

corresponds to a strong panel. At the expense of panel strength (compared to a continuous weld), gaps may be introduced to allow the weld path to cross stiffeners transverse to the weld path or to allow for additional fixtures to support the weld. However, the placement of weld gaps must be kept to a minimum if their location corresponds with higher-stress areas of the panel. The start and end points can act as stress risers in critical areas and, subsequently, initiate failure at lower overall loads. FSSW panels can also be tailored. The gap between spot welds can be altered and can cause a spot weld to fail. In this experiment, the spot welds failed by pulling through the sheet. By changing the processing parameters, the spot weld failure could be forced to pull out of the stiffener, leaving the sheet intact. The stiffener carries significantly less load than the sheet, and could better withstand a spot weld pullout. By forcing the failure into the stiffener, it was shown that the spot-welded panels would be able to carry an even higher load.

2.5.2 Property Variation of Friction Stir Butt Welds [38]

FSW is a novel joining technique that relies on localized forging and extrusion around a rotating pin tool to create a solid-state joint. The purpose of this study was to demonstrate different FSW fixed-pin tools to create a sound butt-welded joint between two plates. Specifically, the study includes an evaluation of the transverse joint tensile strength of 0.250-inch-thick friction stir butt-welded AA2024-T351 aluminum plate using six different FSW fixed-pin tool designs. Welds were performed on the NIAR MTS ISTIR PDS FSW machine at WSU. It was found that the FSW process was capable of creating a sound defect-free joint for a wide variety of accepted FSW pin tool designs. When proper care was taken to develop a given tools processing window using statistical-based design of experiments (DOE) techniques, a given joint strength performance allowable was met through a variety of different tool designs. Therefore, it was concluded that such designs can be used to produce a sound friction stir-welded joint in 0.250-inch AA2024-T351, which is also in reasonable agreement with the majority of the reported results for AA2024-T3 in a variety of thicknesses. Consequently, this study shows that different combinations of pin tools, rotational speeds, and other parameters may be sufficiently controlled to yield similar material mechanical properties.

2.5.3 Fatigue Crack Growth in Integrally Stiffened Panels Joined Using FSW and Swept FSSW [45]

Fatigue crack growth rates in an AA2024-T3 sheet joined to AA7075-T6 stiffeners by FSW were compared with rates measured in panels joined with rivets and in unstiffened parent material panels. Friction stir panels were prepared with both continuous FSW and swept FSSW. Fatigue cracks in edge crack panels with continuous FSW joints tended to grow into the parent material away from the stiffeners. This behavior was attributed to the reduced stress levels corresponding to the increased thickness of continuous FSW joints and the support of the attached stiffener. Fatigue cracks in edge crack panels followed the joint line in panels made with discrete fasteners (both rivets and swept FSSW joints). The measured crack growth rates in riveted panels grew at an increasing rate as the crack approached the riveted joints. In contrast, crack growth rates in panels joined with FSSW decreased at a diminishing rate as the crack approached the swept spot weld joints. Test results indicated that the swept FSSW process produced favorable residual stresses that inhibited fatigue crack growth along the joint line. By testing stress-relieved panels with stretcher leveling (1.5% tensile strain), it was concluded that a beneficial residual stress field

was produced around swept joints. It was also concluded that the pad-up effect, resulting from mechanically forming discrete integral joints between the sheet and stiffener (i.e., integral fasteners) contributes to the observed lowered crack growth rates in FSSW panels to a lesser extent than does the residual stress effect. Conversely, it appeared that the pad-up effect associated with continuous FSW joints imposed a sufficient stiffening effect to reduce the stress level adjacent to the joint and, in turn, caused the crack to turn away from the stiffener into higher stress areas. Therefore, the observed reduced crack growth rates along continuous FSW lap joints holds potential for overriding any possible harmful effects from, for example, the presence of a continuous heat-affected zone (HAZ). In summary, swept FSSW joints and continuous FSW joints provide effective methods for reducing the stress concentration associated with the drilled holes required for installing conventional fasteners.

2.5.4 Factors Affecting the Properties of Swept Friction Stir Spot Welds [46]

In this study, the factors involved in producing a swept friction stir spot weld are investigated to determine their effect on mechanical properties and weld joint morphology. The essential variables involved in producing linear friction stir welds, namely tool rotation speed, travel speed, and plunge depth, are also significant variables in producing swept FSSW. In addition to these variables, placement of the advancing side, spot diameter, lead angle, and start/stop location can also be influential. A DOE approach was used to investigate the effect of each variable based on unguided lap shear tensile strength and the examination of the metallographic cross sections in 0.040-inch (1-mm)-thick AA7075 and AA2024 aluminum alloys. Simple plunge and retract (basic) FSSW has been successfully implemented in a number of industrial applications. The significant factors are limited to tool design, spindle speed, tool holding time (dwell), and plunge depth. Variations in the any of these factors can have a substantial effect on the lap shear strength and should be considered in development. In swept FSSW, there are significant interactions between spindle speed, travel speed (feed rate), load control, and tangential lead angle. When considering dissimilar alloy joints, such as AA7075-T6/AA2024-T3, it appeared the retreating side, being located on the edge of the weld, produced joints with higher lap shear strength. However, in similar alloy welds, the advancing side on the outside will yield slightly higher joint strengths. Placing the advancing side on the outside tends to produce stronger joints in both swept FSSW, which may be expected based on published linear FSW lap joint results [47]. In both similar and dissimilar alloy joints, using load control versus position control does not appear to significantly affect the average tensile strength. However, there seems to be less variability in the results when using load control. Load control can also be used to overcome slight variations in sheet thickness, surface condition, etc. The use of load control may simplify equipment and feedback requirements making it more feasible for industrial implementation. The plunge location appears to only be significant in the AA2024-T3/AA2024-T3 joint. The AA7075-T6/AA2024-T3 welds show no substantial improvement by plunging on the edge; however, it is probable that variations in the tool could lead to advantages in a peripheral plunge. As the thickness of the material increased, the decreased cycle time of a peripheral plunge became more important in precipitation strengthened alloys. Overall, swept FSSW showed an improvement in static mechanical properties in an unguided lap shear coupon configuration. Potential advantages in fatigue and cross-tension tensile properties existed due to the desirable nugget morphology and tailorability of the technique (spot weld size and shape).

2.5.5 An Investigation of the Effects of Tool Design and Welding Parameters on Fatigue Life in Friction Stir-Welded AA2024-T3 [48]

While FSW has been under extensive development in the aerospace industry for more than a decade, there is still the need to understand its fatigue properties for critical structure. Based on the scatter of data in the literature and the inherent variability of fatigue tests in general, the expected fatigue life is difficult to predict. In previous work, an examination of welds produced in different aluminum alloys by tools with various shoulders revealed that surface roughness and metal deformation in the uppermost layers of welds can be greatly influenced by shoulder design. Furthermore, a weld that has been optimized for UTS may not necessarily guarantee satisfactory fatigue life performance, since fatigue life is more dependent on yield strength than ultimate strength. It has also been observed that variations in welding parameters can influence fatigue performance of a friction stir-welded joint. To better understand the fatigue performance of friction stir-welded joints, six different tool designs were used to make butt joints in .250-inch (6.35-mm) A2024-T3 using a DOE analysis over a wide range of welding parameters. One fatigue coupon per panel was tested at a single stress level, which was nominally chosen for around 10^5 cycles to discriminate between tools and processes. The weld tracks of all welds were sanded flush to a surface finish of better than 125 micro-inches R_a (roughness average). However, subsurface defects like surface galling and a lack of penetration were not removed. The purpose of the DOE was to establish that each tool had a sufficiently developed parameter window to make comparisons between tools and to investigate the differences in weld schedules optimized for UTS versus those optimized for fatigue. Two of the tools used a Wiper shoulder design [42], with one shoulder scaled down 25% from the other. In each case, the two tools produced results in fatigue, indicating that they were statistically comparable to parent material properties. While the average fatigue life of each tool was lower than the average of the parent material, a number of individual friction stir-welded coupons outperformed parent material and failed outside the friction stir-welded zone. It was also found, as expected, that surface defects such as a LOP or surface galling had a significant effect on fatigue life, while UTS did not. These results are primarily attributed to sensitivity of fatigue to surface effects and the insensitivity of yield strength to welding parameters. The fatigue life of a friction stir-welded joint was more influenced by surface effects than any microstructural variations brought on by hotter, versus colder, processing parameters, and when post-weld surface preparation was equivalent to parent material preparation, similar fatigue life performance was achieved. This study also demonstrated the potential for eliminating expensive post-weld mechanical processing of the weld track when certain shoulder designs like the Wiper are used.

2.5.6 Effects of Weld Design and Welding Parameters on Swept FSSW in Thin-Gage Aluminum [49]

In many cases, friction stir spot welds were found to be much stronger than rivets in the same material thickness. Preliminary studies have shown that, in a single spot weld lap shear test, FSSW can be up to 250% stronger than rivets for comparable joint diameters. Additionally, dissimilar materials are readily joined via FSSW with excellent mechanical properties. With processing times as low as 1 to 2 seconds per spot weld and increased reliability, FSSW is an attractive alternative to existing joining techniques, such as riveting and resistance spot welding. Plunge or poke FSSW have already shown benefits and gained implementation in the automotive industry [68]. Along

with poke FSSW, refill FSSW has shown excellent potential to leave a mechanically sound joint while leaving a nearly flush surface through the use of an opposing pin and shoulder. Swept FSSW has been shown by TWI and WSU to have mechanical properties exceeding simple plunge and retract FSSW. In this study, the factors involved in producing a swept FSSW were investigated to determine their effect on mechanical properties and weld joint morphology. A DOE approach was used to investigate the effect of welding parameters on unguided lap shear tensile strength, weld morphology, and microhardness in 0.040-inch (1-mm) AA7075 and AA2024 aluminum alloys. The majority of the results were from the AA2024-T3 to AA2024-T3 alloy combination. The data generated in this study are important to increase implementation to applications that can benefit from this highly tailorable technique.

The results of this work will also be important as a basis for understanding spot-to-spot weld interactions as a function of spacing. Swept FSSW discrete joints exhibit characteristics similar to an isotropic joint. Because it was not investigated in this study, a possibility still exists that the joint produced with the OctaSpot pattern may show a greater sensitivity to the orientation as the thickness of the sheet material increases; however, in thinner gages it did not appear to be significant. It may also be possible to overcome any thickness effects through variations of the swept FSSW, such as a peripheral plunge or elliptical. By examining the microhardness contours of the micrographs, it can be concluded that the area affected by the welding process is asymmetrical because of the travel of the pin. The spot weld has a softened area similar to the HAZ in linear friction stir weld specimens. A secondary softened area appears in all the weld microhardness maps located at the outer edge of the shoulder diameter, apparently due to additional thermal softening rather than the compressive residual stress resulting from the processing of the material. The Containment Psi™ spot welds have the lowest microhardness minimums, tensile strength, and forging loads. The other tools produced welds with higher tensile strengths and higher microhardness minimums in comparison, but again, at the cost of increased forging loads. The microhardness contour map cannot be used alone to evaluate the strength and quality of a weld, but it has been shown to be an effective tool for understanding friction stir spot welds.

2.6 THE 2009 RESEARCH SUMMARY

The 2009 research results generated from this program were published in an annual progress report [16]. A summary of the most important results presented in that report are summarized in sections 2.6.1 through 2.6.8.

2.6.1 Corrosion in 2XXX-T8 Aluminum Alloys [50]

An apparent trend in AA2XXX-T8 aluminum alloys possessing excellent as-welded exfoliation corrosion resistance in the weld zone compared to the parent material was observed. To better evaluate this trend, friction stir welds were produced in 0.125-inch (3.2-mm) AA2024-T81, 0.080-inch (2-mm) AA2219-T87, and 0.153-inch (3.9-mm) AA2198-T851 (Al-Cu-Li) material, then tested in a standard and modified ASTM G34 exfoliation environment. Unlike welding in the T3 or T4 tempers, where the weld zone can become anodic to the parent metal and exhibit preferential corrosion, when welded in the T8 starting temper the weld zone was found to be relatively cathodic compared to the parent material, and exhibited only mild evidence of corrosion.

Therefore, it was concluded that the excellent exfoliation resistance of the AA2024-T81 weld zone in as-welded condition was not just a phenomenon that was restricted to this alloy and temper but, in a broader sense, was displayed by other 2XXX-T8 alloys (i.e., AA2219-T87 and the Al-Li alloy AA2198-T851) as well. This behavior was believed to be a bulk-material phenomenon and to be generally insensitive to weld tool design and material thickness. Therefore this work suggests that this broader trend is expected with the majority of the alloys in this family; however, as results may vary with specific alloys because of the presence of various additional alloy elements, verification of these results for other AA2XXX alloys of interest should be performed.

2.6.2 Correlation Between Ultrasonic Phased Array and Feedback Force Analysis of Friction Stir Welds [51]

Ultrasonic phased array is a powerful nondestructive test and is well known for its capability to detect different kinds of FSW indications and defects. A new, process-based nondestructive test technique developed at the South Dakota School of Mines and Technology is the FSW Analysis Software, designed to analyze any specified section of the weld in real time (with a slight computation time delay). With this software, a trained operator or inspector can detect where potential flaws may exist. The purpose of this study was to determine if all the defects found using ultrasonic-phased array inspection could be identified by the software data analysis program. By correlating this software with an ultrasonic-phased array inspection, the time and expense associated with 100% inspection of parts could be significantly reduced. The ultimate goal for this research was to support the development of real-time quality control to minimize the cost of inspection through statistical process control methods. Based on the results of this study, it was concluded that there is a strong correlation between phased array analyses from different facilities. A promising correlation between the phased array and the software analysis was shown, but further investigation is required to better evaluate the reliability of the correlation. Also, a quality-control correlation analysis for lap weld configurations will be conducted in future work.

2.6.3 The Distribution and Flow of Nickel Powder and Carbon Nanotubes Mixed in an Aluminum Matrix via FSW [52]

As a low-temperature, solid-state welding process, FSW can be used to make composite materials. However, to produce a tailored composite, the distribution and flow of reinforcement must be known. Nickel and carbon nanotubes (CNT) were mixed in an AA2024-T3 aluminum alloy by FSW. The final position of the powder after welding was characterized. The nickel powder welded with the parameters used in this experiment was found to create a well-distributed composite when the groove was 0.050-inch (1.27-mm) deep. When the groove was deeper, the nickel particles tended to stay agglomerated just below the surface. CNTs welded into the alloy reacted differently; for a 0.050-inch (1.27-mm) deep groove, the CNTs aligned from the top-advancing side to the mid-advancing side of the weld. With deeper grooves, the CNTs would agglomerate just below the surface, in the middle, and loop around following the material flow lines. This research was done to develop a baseline for future FSW composites. Future composite welds will have tailored physical and mechanical properties that will provide more versatility of FSW.

2.6.4 Development of an End Effector for FSSW [53]

A specialized clamping fixture was designed and manufactured to quickly make friction stir spot welds by applying a consistent clamping force and to provide positional feedback of the workpiece surface. The fixture was designed to attach to the MTS FSW machine in the AJ&P Lab. The scope of this project included component analysis, manufacturing, final product tests, and the formation of a conceptual design capable of producing both poke spot welds and swept spot welds. Based on unguided lap shear tensile data, the end effector slightly outperformed the welds made with conventional clamping and decreased the standard deviation by 60%. Metallurgic comparison of macros created with the end effector contained no significant differences than those made without. Using the end effector greatly reduced the required time for setup and also simplified the FSSW process. This equipment could be adapted for use on robotic platforms as well.

2.6.5 Fatigue of Swept Friction Stir Spot Welds in Thin-Sheet AA2024 Aluminum [54]

An investigation was conducted to evaluate the performance of swept FSSW in fatigue applications in the 2xxx series, thin-gage aluminum. Swept FSSW differs from plunge and retract or refill FSSW. During metallographic inspection, it was observed that a benefit of swept FSSW was the ability to virtually eliminate hooking the faying surface up into the top sheet of a FSSW joint. Fatigue characteristics were determined using the National Aerospace Standard, Metric (NASM) 1312-21 specification [55]. A DOE approach, using a Box-Behnken design, was taken to determine the processing parameters to be used for this study and aided in the tool selection. A Counterflow tool probe design [56] was chosen based on the static tensile strength and weld joint morphology. The significant parameters were the tool rotation speed, travel speed around the spot, forge load or z-force, and tangential lead angle. Statically, the Counterflow tool produced an average UTS of 1148 lb (5.1 kN) with a standard deviation of 56 lb (0.2 kN) in a single spot weld unguided lap shear configuration. This was based on an average of 60 tensile specimens. The low standard deviation indicated a large processing window. This provided further support for reduced variability in swept FSSW. The overall results of this study showed that sufficient static tensile strengths can be achieved with a relatively wide array of tool designs.

2.6.6 Evaluation of Swept Friction Stir Spot Welding in Al 2219-T6 [57]

The effects of swept FSSW on tensile strength and fatigue life were investigated in 0.100-inch (2.5-mm)-thick AL 2219-T62 material with a faying surface gasket compound. The top sheet was chromic-acid anodized and the bottom sheet was sulfuric-acid anodized. A polyurethane-based nonsetting and nonhardening gasket compound was placed at the faying surface. The first round of tests involved exploratory bounding of the process windows for three tools. The bounding spots were evaluated through macroscopic inspection of spot cross sections. Coupons were pulled to failure in a single-spot, unguided lap shear configuration. Weld parameters for each tool varied in a Box-Behnken DOE. Coupons were also produced for limited fatigue tests from the three best welding parameters for each tool. The coupons were made in the 100% load transfer configuration per the NASM 1312-21 specification. A single tool was then chosen based on the previous tensile and fatigue results. Another set of DOEs was performed to evaluated tensile strength and fatigue life. These DOEs again used the NASM 1312-21 100% load transfer coupons. Selected FSSW coupons were then compared to riveted coupons at equal fatigue load levels. MS20426E5-7 flush

countersink rivets were used in this experiment. The FSSW coupons were able to outperform the riveted coupons in tensile strength and in fatigue life at high load levels. At lower load levels, FSSW coupon results were comparable to riveted coupons.

2.6.7 Corrosion and Fatigue Evaluation of Swept FSSW Through Sealants and Surface Treatments [58]

The capability of welding through sealants and surface treatments with swept FSSW was demonstrated in thin-gage AA2024-T3 aluminum alloy. The aluminum sheets had a sealant applied and were pretreated with various surface coatings. The uncured sealants were applied to the faying surface of the test coupons shortly before joining. Tests were also performed on bare sheets in the untreated condition. Corrosion tests were performed through alternate immersion in a 3.5% salt solution. The coupons were evaluated through metallography and residual strength tests. Fatigue tests were performed per the NASM 1312-21 specification. S-N data were collected for five load levels for each sample type. Riveted data were also collected using this method. Both sealants were successful in preventing ingress of solution to the faying surface in this test. The PLV 6032 sealant only had slight penetration of the solution. The PR-1432 GP sealant completely prevented solution from entering the faying surface. The surface treatments also provided protection against corrosion. The Alodine and clad fared much better than the bare surfaces. The chromic acid anodized (CAA) surfaces were also better than bare surfaces at preventing a corrosion attack. The exposed top-surface area of the FSSW, where the tool displaced the surface treatments, would likely need to be treated after welding because this untreated area was the most vulnerable to corrosion attack. Attack was also noticeable on the anvil side of the coupons in the HAZ beneath the stir zone and also needed an additional protection scheme, such as primer and paint, applied after welding. The coupons with surface treatments were effective in limiting the decrease in strength from corrosion tests. The CAA had only a small decrease in average strength, while the clad and Alodine showed higher strengths in the corroded coupons. There were not enough points, however, for this difference to be statistically relevant. In this experiment, the results indicated that the sealants and surface treatments had little influence on the fatigue characteristics of FSSW. Also, while the FSSW fatigue results fell slightly below the riveted coupons, additional work was underway to better understand the fatigue performance of these joints. Work in this area is important to support increased implementation of FSSW in production applications as a replacement for other discrete fastening methods, such as riveting and resistance spot welding.

2.6.8 Low Z-Force FSSW—Conventional Tool and Process Development Approach [59]

An investigation was conducted to develop low, normal load (Z-force) friction stir spot welds using conventional tooling and to process development approaches. Low Z-forces can be achieved by studying the relationship between pin tool features, geometries, processing parameters, and the resultant strengths of coupons produced by FSSW. Effects of geometrical changes of pin tool design, including shoulder diameter and probe features, on joint properties in 0.040-inch (1-mm)-thick AA2024-T3 Al alloy were evaluated. Weld tools included the Psi™, Counterflow [56], and Trivex™ tools. A DOE approach was used to investigate the effects of process parameters, which included spindle speed, plunge depth, plunge rate, plunge load, travel rate, and tilt angle. The program's goal to maintain the ultimate shear strength tested in tension of unguided lap shear coupons was achieved while reducing the normal force required for producing a sound joint. In

addition to single-spot unguided lap shear tests, the performance of low Z-force FSSW joints was evaluated by optical metallographic cross-section analyses, which were correlated with process parameters, process forces, UTS, and pin tool designs. Conversely, a position-control weld program cannot be controlled to repeatably produce low Z-force FSSW. This is due to the sudden increase in normal force when the tool shoulder comes into contact with the material.

Each possible solution was tried individually with a hybrid weld program without success. However, the solution using a fully load-control weld program provided a significant reduction in Z-force and maintained FSSW quality. The reduction of shoulder diameter significantly reduced the required Z-force while simultaneously maintaining good mechanical properties. The combination of pin tool design coupled with a low Z-force weld program and appropriate process parameters created a sound FSSW. Mechanical properties of low Z-force FSSW were investigated using unguided single spot lap shear. Statistical analysis software (Statgraphics®) was used to correlate the UTS of the lap shear coupons with process parameters. The faying surface interface and the weld nugget quality were also investigated using cross-sectional metallography to correlate process parameters and pin tool designs. These low Z-force FSSW results indicated that it was possible to produce sound FSSW joints within the force capability range of a typical articulated robot. Since the automotive and aerospace industries are moving toward automation to improve production and quality control simultaneously, the investigation of low Z-force FSSW will accelerate and bridge the implementation of FSSW for articulated robots in those industries.

2.7 THE 2010 RESEARCH SUMMARY

The 2010 research results generated from this program were published in an annual progress report [60]. A summary of the most important results presented in that report are summarized in sections 2.7.1 through 2.7.6.

2.7.1 The e-NDE for Friction Stir Processes [61]

A powerful new FSW e-NDE technique, which is based on process monitoring, shows promise for increasing the accuracy and precision of POD analyses compared to conventional nondestructive evaluation (NDE) inspection techniques. The new technique is based primarily on monitoring the F_y (transverse) force feedback signal, which was previously correlated with defect formation. Force feedback monitoring (as an e-NDE near real-time inspection technique) potentially eliminates the need for secondary inspection operations like x-ray and ultrasonic inspection steps. In terms of establishing standards and specifications for friction stir technologies, this e-NDE technique will greatly facilitate the establishment of performance-based specifications for FSW that will ultimately become the basis of developing design data for FSW joints in multiple structures made from multiple alloys and product forms. The ability to monitor and correlate F_y force feedback signals to the occurrence of defect formations provides a major opportunity to actively and adaptively control FSW operations in production. This unique process-monitoring tool will form the basis of a powerful e-NDE technique that will greatly reduce inspection costs, in terms of time, resources, accuracy, and quality. Because of its evaluation capability, process monitoring of F_y (transverse) feedback forces provided a viable alternative or complement to conventional NDE techniques. It can also conceivably be developed to monitor tool wear, optimize the design and performance of FSW tools, and compete different tooling design concepts.

2.7.2 Advancements in Robotic FSW and FSSW

Lower capital cost and increased range of motion make robotic systems a feasible option for FSW. This also may increase the opportunities of FSW and FSSW beyond the ability of the gantry systems. However, robotic systems are not as rigid or capable of exerting forces typical of purpose-built friction stir machines. Therefore, a comparison study was conducted on an MTS ISTIR PDS gantry system and an ABB IRB 7600 robot to understand the strengths and weaknesses of each system. For the comparison, multiple tools and materials were used for plunge spot, swept spots, and linear weldings. Evaluation of the mechanical tests and metallurgical analyses were obtained from coupons produced with these two welding platforms.

As a case study, initial development was also performed using the Kawasaki ZZX200S FSSW robotic system for producing an unpressurized aircraft door. The materials and components were provided by Hawker Beechcraft. The development work was based on DOE methodology. Through this program, weld-processing parameters were identified that produced very good joint strengths between the dissimilar metal door components. Specifically, unguided lap shear strengths of over 900 lbf per spot were attained. For comparison, the minimum design allowable in MMPDS for resistance spot welding in material of this strength and thickness is 316 lbf per spot. This could mean fewer joints would be required in production or the door may receive more corrective forming in the field, if needed, without experiencing a failure. As part of this program, two senior design projects were sponsored:

1. Fall 2009 Senior Design Projects (ME 662)—FSW End-Effector: A clamping end effector for FSSW on a Kawasaki ZZX200S robot was designed and fabricated. An analysis to determine how to keep the anvil cool during the welding process was also completed. The design was compatible with the current Kawasaki FSW end effector, which is able to apply a known and controllable fixturing pressure on the parts to be welded in the immediate vicinity of the robot-produced FSSW. The current end effector was capable of creating a friction stir spot weld, but without a pressure foot to supply localized clamping, the welds that were created were irregular. The specifications for the pressure foot clamping end effector were that it should be able to provide 100 to 600 lbf of clamping. For it to be effective, the design had to be small enough to weld close to a flange and be equipped with a cooled-backing anvil system.

2. Spring 2010 Senior Design Projects (ME 662)—Aluminum Aircraft Door Robotic FSSW Tooling Fixture: The AJ&P Lab Kawasaki robot is equipped with a C-frame-type end effector for performing friction stir spot welds. To demonstrate the capability of welding a nonpressurized light aircraft cabin door, a tooling fixture was designed. It is capable of holding the door in the correct position without significant movement under welding loads. It also is designed to accommodate access for the robotic C-frame end effector of the Kawasaki robot. A design was engineered to build the FSSW tooling fixture for the light-aluminum, aircraft cabin door.

2.7.3 Retractable Pin Tool Swept FSSW [62]

Swept FSSW is a variation of FSSW used in the production of lap joints. In contrast to conventional plunge and retract spot welding, the swept FSSW tool is programmed to travel along a closed circumscribed path immediately following the initial plunge. The swept FSSW advantages over the conventional plunge-type FSSW include a larger joint shear area and the minimization of hooking defects. This allows swept FSSW to be stronger than both conventional FSSW joints and mechanical fasteners, such as rivets. A disadvantage of creating a FSSW joint with a fixed probe tool (FPT) is the exit hole that is left in the joint. A potential method for removing the exit hole is to use a retractable probe tool (RPT) in which the probe depth is programmable and may be retracted completely from the workpiece during the welding operation. In this study, the relative advantages and disadvantages of using RPT technology versus FPT technology in swept FSSW were examined by comparing the lap shear strength and fatigue life of joints produced by both technologies. The lap joints tested in this study were made between a 0.040-inch (1-mm)-thick AA7075 top sheet and a 0.040-inch (1-mm)-thick AA2024 bottom sheet.

2.7.4 Weld Tool Database for Friction Stir Technology Perishable Tools

As the FSW technology gains use in a wide range of industrial applications, the need for a well-structured tool database increases. In industry, it is very important to know what kind of weld tool and material combinations work best in terms of mechanical strength and metallurgical quality of the joint and what processing window is good for each combination. To address all issues, the current research program was assigned to create a web-based tool database system that can provide clients and laboratory researchers with easy-to-access and up-to-date tool information. As of this writing, the weld tool database and the administrator web pages were successfully created along with data security features.

2.7.5 The FSW and FSSW Standards and Specifications Coordination [63]

FSW is an emergent joining technology that is being incorporated in a variety of aerospace structural applications to reduce part count, manufacturing cycle times, material buy-to-fly ratios, environmental impacts, etc. Though it has been in use since the early 1990s, industrywide specifications and standards are still lacking. Consequently, applications are typically developed on a case-by-case basis, requiring greater effort in terms of testing and validation when compared to applications based on traditional fasteners and joints. Methodologies for developing standards and specifications are needed to ensure the safe and consistent implementation of this technology. Therefore, coordination with specification organizations has been initiated to establish material standards and specifications for friction-stirred materials and joints.

2.7.6 Effects of Tool Design and FSW Parameters on Weld Morphology in Aluminum Alloys [64]

FSW is a complex thermomechanical process that produces wrought microstructure with microstructural gradients in grain size, grain orientation, dislocation density, and precipitate distribution. The type and degree of microstructural modification is a function of the particular alloy chosen, its initial temper, the tool design and corresponding weld process parameter window,

and other variables like material thickness, size, and fixturing. Since the microstructural changes produced can dramatically affect resultant mechanical performance and corrosion response, a thorough understanding of the variables involved in those changes is needed. A DOE approach was used to study the effects of weld parameter selection on the microstructural changes wrought by FSW with two different sizes of the same FSW tool design. A combination of microhardness mapping and electrical conductivity testing was used to investigate potential differences. The importance of these factors and the means for characterizing them for developing standards and specifications are also discussed. In this study, it was demonstrated that a range of possible hardness and electrical conductivity properties from FSW precipitation strengthened aluminum alloys, specifically AA2024-T3, using two different-sized tools and process parameters. In one case, a weld stir zone (nugget) with an aggressively overaged microstructure and low microhardness was produced. This result suggests that the peak temperature in the stir zone was below the solidus temperature of the alloy and, consequently, a dramatic difference in weld microstructure resulted. A joint with the least degree of variation in hardness and conductivity was produced using a tool with a smaller, 0.60-inch (15-mm) shoulder and high processing speeds. In this case, welds with high post-weld hardness and strength were produced, having almost no sign of a HAZ and a weld nugget that apparently reached full solution temperature. While influenced by tool design, the resulting gradients and distribution of hardness and conducting are principally a function of the thermal process to which the material is subjected. Therefore, these results are not constrained to a particular tool or process condition or to this alloy. A DOE approach in process development can reveal where these boundaries are so that stable processes can be identified. Furthermore, electrical conductivity tests can readily identify these overaged regions when present. While this experiment looked only at a single aluminum alloy (AA2024-T351), the principles laid out have implications for all precipitation-strengthened aluminum alloys. For instance, research literature has also shown that in AA7050-T7451, very cold welds can produce soft, overaged nuggets that are unresponsive to further aging treatments. The findings presented in this report have further implications for understanding variations in corrosion response within similar alloy/temper combinations, but using different tool designs and process parameters. It is also an important step toward developing the necessary standards and specifications required for maturing the FSW process for industry applications.

3. DEVELOPMENT OF DESIGN DATA FOR FSW AND FSSW

Consistent and standardized methodologies for developing industry-based design data are needed to more efficiently and consistently design products with FSW and FSSW. Therefore, emphasis was placed on developing a model for establishing design properties data for joints produced in aluminum alloys by friction stir-related technologies.

3.1 PROCESS VARIATION FORMULATION

An understanding of the parameters controlling the varibility of FSW is crucial in the development of an approach to account for different weld tools and corresponding process parameters that may be used in producing a given component. Based on the data available (from experience and the open literature), it may be shown that widely varying tool designs have been used to make sound joints with independently developed process windows in virtually all aluminum alloys. FSW may be viewed as a supplemental, locally applied, thermomechanical processing operation superimposed over the parent material thermomechanical processing history. It does not change bulk chemistry (no filler typically added), nor does it involve recasting the alloy (no bulk solid/liquid phase transformation). Joint properties are observed to be typically increased in work-hardened, non-heat-treatable alloys (e.g., Al 5xxx in the unhardened condition) as a result of grain refinement in the stir zone (a.k.a. weld nugget). In precipitation strengthened aluminum alloys, joint properties are typically decreased as a result of overaging in the HAZ adjacent to the joint. Friction stir technologies, such as FSW, FSSW, and friction stir processing (FSP), rely on the efficient application of basic metalworking principles in a localized manner. That is, the underlying mechanisms of these processes involve thermal and mechanical process elements. Therefore, in this study, friction stir technologies are treated specifically as localized metalworking operations.

3.1.1 Thermal Components of FSW

The thermal process elements or components of FSW are typically controlled indirectly (i.e., passively) through the process variables that most strongly influence them, namely mechanical factors, such as spindle speed, travel speed, and the applied weld tool axial force. Through the influence of these indirect means, thermal energy is generated during FSW by forcing a rotating, nonconsumable metalworking tool into the joint line between components to be joined. Once stable processing conditions are established locally, the weld tool is then forcibly translated or advanced along the joint line to form a consolidated unit.

The energy for conveying material from the advancing to the retreating side of the weld tool is supplied by the FSW machine's torque and compressive forces as applied to the workpiece through the specialized, nonconsumable metalworking tool. The actual energy imparted to the workpiece by the machine is converted into heat through mechanical stirring and frictional shearing interaction between the nonconsumable tool and workpiece. This heat, which is generated in a local, but traveling, work zone can be viewed conceptually as flowing away from the work zone along three generalized heat sink paths (or conduits).

- Path 1: The Spindle Path—including the metalworking (welding) tool, tool holder, spindle, and machine frame.
- Path 2: The Workpiece Path—the workpiece, fixture, machine bed, machine frame, clamps, connecting structure, etc.
- Path 3: The Surroundings Path—the atmosphere, applied materials (coolants, gases, etc.).

Ideally, the distribution of heat flow away from the localized work zone will remain stable without either a substantial buildup of heat or a substantial loss of energy as the weld progresses. The level of heat buildup or loss may shift due to, for example, a local change in the thermal mass of the part or fixture (e.g., at a stiffener or with an increase or decrease in section thickness). It also may result from traveling at a rate faster than heat can be dissipated along the three paths collectively.

In practice, the proportion of heat that flows along each of these heat sink paths at any given time can vary widely. Many factors influence the relative heat flux along each path. For example, in path 2 (the workpiece path), the flux of heat away from the local work zone is first regulated by the thermal conductivity and heat capacity of the workpiece and is then regulated by these same properties of the fixturing and supporting components (e.g., the backing bar). For regularly shaped parts, where the effective thermal mass cross section does not vary over the length of the part, a greater probability exists that the process will remain stable throughout the duration of the FSW process. In contrast, in irregularly shaped parts or setups, which vary in thermal mass along the direction of the weld (i.e., variations in the joint cross section), joint properties can vary substantially as a result of the changing thermal environment (heat sink) in and around the local work zone if not properly accounted for and addressed.

Edge effects also have the potential for contributing to joint property variation. For example, as the FSW process progresses toward the end of a workpiece, the heat generated in the part tends to build up near the end of the part where there is a decreasing amount of material available to contain the heat generated by the advancing tool. Potential approaches for maintaining a consistent thermal environment as the local work zone nears the end of a part may include changing process parameters to lessen the heat input into the joint line in the close-out region of the joint.

Rather than attempting to precisely regulate heat flow during FSW, application development work is typically based on a phenomenological approach in which process parameters are developed for each unique setup and welding system [14]. Bounding welds are usually conducted first to identify a suitable process window limit. Then experimental design techniques (e.g., Statistical Process Control and DOE) are used to refine the process window for optimizing selected joint properties. If changes are made to any of the three general thermal conduits in the system, the process output (e.g., joint material properties) should be checked to determine what impact, if any, there may have been as a result of the change. This approach is often justified where a thorough analysis of the setup is not warranted or deemed tractable given the available program resources.

The actual thermal efficiency of a given FSW process, and the gradients associated with it, may never be well understood or directly controllable. As such, attempting to establish repeatable processes through a single rigid process specification (e.g., fixing the setup, tool, process parameters, or weld system) for all applications is not deemed necessary or even appropriate..

3.1.2 Mechanical Components of FSW

Unlike the thermal components of the FSW process, the mechanical components are typically controlled directly through the FSW machine capabilities and controls, the selection of the metalworking tool and fixture designs, the setting of processing speeds and feeds, etc. Because process controls can be set directly through machine settings and tool designs, defining a process specification around machine controls may seem to be a straightforward approach for establishing design data for FSW. The steep gradients introduced by FSW may mean that small variations in input (independent) variables (e.g., speed, feed, load, and tool design) can lead to relatively large variations in local response variables (e.g., thermal gradients, residual stresses, and transverse tensile properties). However, bulk properties may not be affected by these local transients.

Therefore, to establish usable databases for FSW design data, an understanding of potential sources of variation is required and robust methods for managing these inherent variations must be developed. For example, once the basic FSW machine is selected, an unlimited number of metalworking (weld) tools may be used with it. Literally hundreds of combinations of geometric features on weld tools are in use today throughout various industries that use FSW. Shoulder-design considerations alone include a multitude of factors to be established, such as its basic shape (concave, convex, flat, etc.) and the optimum ratio between the shoulder diameter and the probe. All of these individual parameters need be controlled within the general global requirements, which could be covered in a generic performance specification.

The effect of shoulder and probe features combined with weld parameters on the friction stir weld is complex, as shown in figure 3. Thermomechanical energy is introduced into the material as the probe effectively forges material from the leading edge to the area behind the probe, filling in a void that forms there [65]. This forms the nugget through the complex flow of material around the probe. The shoulder rotation on the surface causes frictional energy and the material adjacent to the weld is heated, which forms the HAZ. The thermomechanically affected zone (TMAZ) is the result of mechanical forces experienced at the edge of the stir zone as the probe moves through the material, and the heat that flows through the area as the nugget is formed.

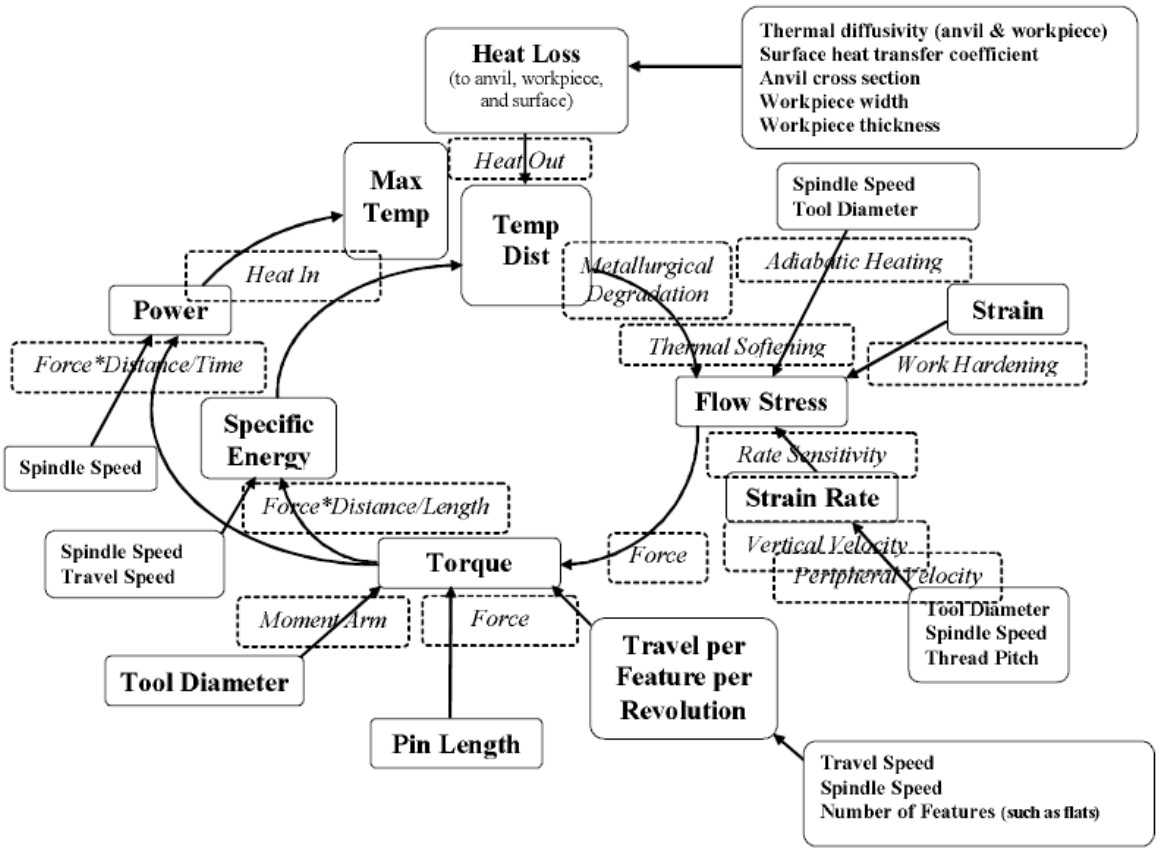

Figure 3. The complex effect of tool design and weld parameters on friction stir welds [66]

There is not one single tooling solution for all joints, not even for a specific joint. In general, many different tools may be used to produce the required engineering properties for a given application as long as a controlled optimized process window is established for each tool on a tool-by-tool basis [63]. Further, some tools may be more sensitive to tool wear and variations in the manufacture of weld tool features in terms of how they affect the data population generated. Therefore, while it may be determined how tool design affects joint properties, ultimately it is more important to determine what level of control is needed for a given tool to ensure consistent joint properties over the life of the tool, as well as between setups, part configurations, suppliers, etc.

Alloy and workpiece dimensions all come into play when selecting appropriate tool features and combinations of features. While it may be straightforward to control processing parameters, such as spindle and travel speeds, attempting to control all of the factors that go into the process is not so straightforward. Different alloys also react differently to the possible combinations of features. There are numerous patents covering weld tool features. Therefore, attempting to establish process specifications by fixing tool designs will not lead to the desired outcome of a controlled process. Specifications must be data- and results-driven. The e-NDE technique featured in section 5 of this report will greatly facilitate the establishment of performance-based specifications for FSW and may become the basis for developing design data for FSW joints in numerous structures made from multiple alloys and product forms.

3.2 MULTIPATH INDEPENDENCE

Based on experience and the open literature, FSW has a sufficiently flexible process window that allows all aluminum alloys to be joined with a wide variety of weld tool designs [3, 4, 38, and 48]. Therefore, it was hypothesized that for aluminums:

- An unspecified number of tool designs can be used to make equally sound joints with independently developed process windows.
- Any advantage one tool may have over another is expected to be evident primarily in terms of productivity (e.g., welding and processing speeds).

Additional observations support the tractability of a multipath approach. For example, FSW is an additional thermomechanical-processing operation that does not change bulk chemistry (filler metal typically is not added) and it does not involve recasting the alloy (bulk solid or liquid-phase transformation does not typically occur). Joint properties are observed to be related to parent material mechanical properties (e.g., strength). They usually are increased in work-hardened, non-heat-treatable alloys (e.g., Al 5xxx) via grain refinement in the dynamically recrystallized zone (i.e., the weld nugget). In precipitation-strengthened Al alloys, joint properties normally decrease as a result of overaging in the HAZ adjacent to the joint. Therefore, the process is expected to be relatively independent of the process for a given alloy system.

To explain, consider an aluminum sheet product such as an aircraft aluminum alloy (e.g., AA2024-T3), which may be produced as a sheet product on either a continuous rolling line or in a batch facility; or it may be formed into a limitless number of extruded and forged shapes either at a primary mill or a secondary supplier. Both forms of sheet product may be sold to the same industry specification because the specification does not call out, for example, the type of rolling stands or the other mechanical equipment used to thermomechanically process the material. These parameters need to be controlled at the local level to cover the unique requirements of each manufacturer.

3.3 INTEGRAL FASTENER FORMULATION

The integral fastener approach involves developing FSSW similar to installed fastener systems [45]. Individual spots are viewed as conventional fasteners (e.g., rivets) with the exception that parent material is used to form the fastener. Like installed fasteners, discrete integral fasteners are mechanically installed in place by a metalworking process (i.e., FSSW). In both static and dynamic tests, properly designed FSSW joints are proving superior to rivets. Further, they are also expected to be the most straightforward friction stir-related technology to qualify for inclusion in handbooks because they are the most like mechanical fasteners (e.g., discrete). This initiative is expected to provide the supporting groundwork for establishing industry specification for discrete, discontinuous, and continuous friction stir joints.

The purpose of evaluating friction stir spots as integral fasteners is to qualify them with existing procedures established for qualifying conventional style fasteners (e.g., new alloys). Of primary interest are the developed procedures maintained in the MMPDS handbook, formerly MIL-HDBK-5.

Viewing FSSW as discrete integral fasteners is practical for several reasons. FSSW is a thermomechanical operation that uses the parent material to form the fastener. Like most mechanical fasteners, FSSW spots (integral fasteners) are installed through mechanical means. FSSW is repeatable and quick, and the resulting joint properties can be tailored to be far superior to any other discrete fastener systems in sheet metal. There is more latitude with their shape (e.g., diameter-to-thickness ratio and aspect ratio) and function in structure. Also, as discrete joints, they can be analyzed as being similar and familiar to conventional fasteners.

The integral fastener initiative is directed at generating design data that will be available industrywide. Most of the data needed for industry specification development are either proprietary to individual companies or nonexistent. This program was established to work toward building clean, internally consistent data sets (as opposed to attempting to piece together inconsistent and incomplete data sets derived from the open literature). These data sets will then be used for supporting industry specifications and preparing tables of design data for inclusion in the industry-supported handbooks. Associated with this work is the identification of essential and nonessential process variables and acceptance criteria, etc.

A number of different forms of FSSW have been developed, including a simple plunge or poke spot-welding process patented by Mazda Motor Corporation [68], a refill process developed by Gesellschaft zur Förderdrung der Kernenergie in Schiffbau und Schiffstechnik [69], a swing spot-welding process developed by Hitachi America, Ltd. [70], and a circular spot pattern introduced by TWI in Great Britain [71]. Although unique, each of these FSSW technologies produces a similar discrete joint. In all cases, parent material is locally stirred thermomechanically with specially designed metalworking tools to form a metallurgical bond between two or more components in a lap joint configuration. As such, the various forms of FSSW are referred to collectively as integral fasteners.

4. MULTIPATH MANUFACTURING AND MMPDS ROUND-ROBIN

FSW can be used to make welds in metals that are traditionally difficult to weld with other methods, such as 7XXX series aluminums [72]. The aircraft industry is interested in FSW because it lessens the weight where a FSW is used. FSSW can be used as integral fasteners that can cut weight by eliminating mechanical fasteners. Another attractive aspect of FSSW is that it is adaptable to robotics applications. This makes FSSW very appealing to both the aerospace and automotive industries. Because of the ergonomic factors associated with installation of mechanical fasteners and the increased speed of making spot welds, the robotics applications could be beneficial to many industries.

Because of the localized nature of FSW and FSSW processes, gradients in mechanical and material properties are produced. The gradients can be separated into microstructural regions: the nugget, the TMAZ, and the HAZ. The strength of the joint is related to the material properties of the parent material and is dependent on the final microstructure in these weld regions [75]. The approximate location of the different areas of a friction stir weld is shown in figure 4, superimposed on a macrographic cross-section of the joint. Also, this figure shows the microhardness contour map, which indicates the softened area associated with the HAZ.

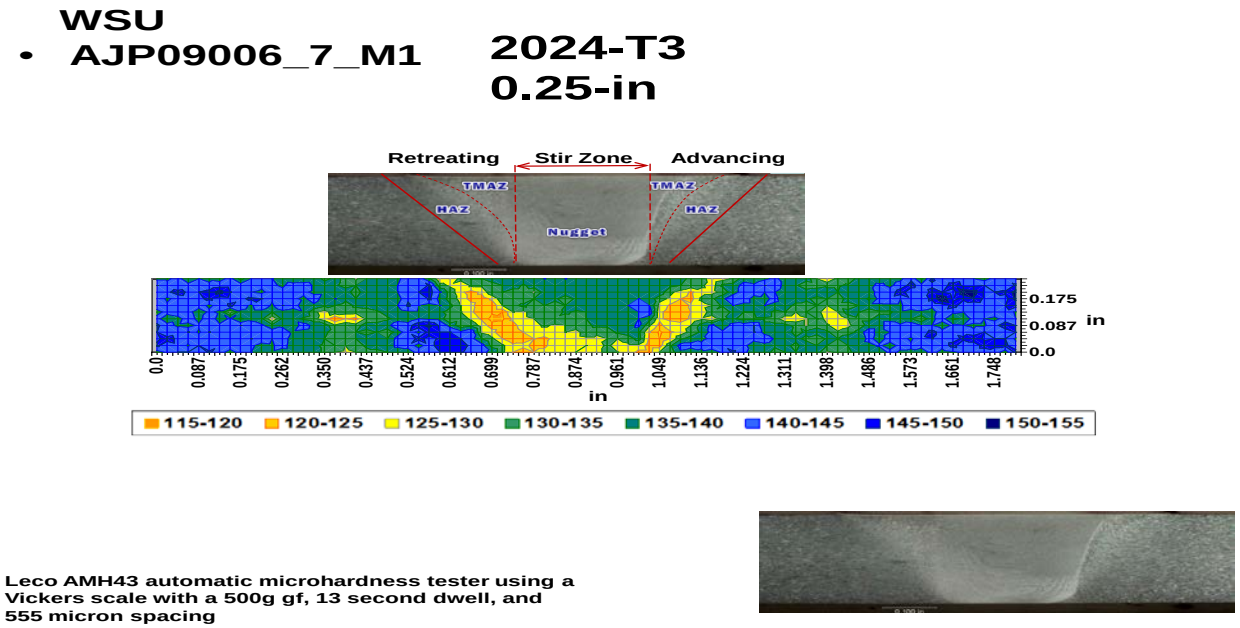

Figure 4. Cross section of a weld specimen and corresponding microstructural microhardness contour map

Because it is a relatively new technology, the material and joint standards and specifications are still in development, which would provide industry with minimum deliverables for friction stir-welded joints. Although industry specifications are being developed, material and joint property specifications would provide performance requirements, property minimums, acceptance criteria, and deliverables that would make it possible for any industry to develop programs that could consistently produce sound friction stir welds with acceptable strength and performance.

The purpose of this study was to determine if performance limits and design allowables data can be generated for FSW and to investigate the effect of various tool designs on the microstructure of friction stir butt welds. The design allowables data would provide a basis for determining minimum performance levels that would be statistically derived based on the MMPDS protocols and possibly HDBK-17 protocols for industry use in developing process controls and procedures supported by developing industry standards.

The tool design determines the weld parameters that can be used to produce a strong weld without defects as a function of the flow of material around the probe and frictional forces produced during the welding process. Because there are so many combinations possible for shoulder and pin features of tool designs that could be used to produce a sound friction stir weld, industry-wide controls based on the weld tool features would be difficult to define. Given the thermal element of the process, consistent results cannot be guaranteed within any given precision. An alternative would be to develop a robust path and protocols that are independent of weld tool design. In other words, an outcome-based approach would be a practical alternative. The development of global parameters created a means for individual manufacturers to demonstrate their unique equipment yield results that met those required global parameters. With this in mind, a DOE approach was used to choose appropriate weld parameter windows over a wide range of parameters for each tool to be used in the study.

To demonstrate path independence in producing a sound FSW joint, it was hypothesized that for aluminums:

- An unspecified number of tool designs could be used to make equally sound joints with independently developed process windows.
- Any advantage one tool may have over another is expected to be evident, primarily in terms of productivity (e.g., welding and processing speeds)

The study was set up in two phases. Phase I of the study was to look at path independence with respect to the tool design and weld parameters for 0.25-inch-thick AA2024-T3. This study was completed at WSU.

Phase II was a round-robin coordinated study that examined the ability of independent facilities to produce a sound weld within the process controls and procedures of that facility and to evaluate site-to-site variability. This phase of the study was performed with four MMPDS members (Airbus, Aluminum Company of Canada (Alcan), Lockheed Martin (LM), and WSU) as part of the Emerging Technologies Working Group (appendix A). WSU, Westmoreland Mechanical Testing & Research, Inc., and Battelle also participated in providing and analyzing test results. The results reflected the ability to use the outcome-based approach to create standards and specifications for FSW. In addition to the alloy used in Phase I, AA2198-T8 sheet was included in Phase II. This third generation Al-Lithium material has received a lot of interest from the aviation industry as a material that can both decrease density and increase strength [73].

4.1 EXPERIMENTAL PROCEDURE

4.1.1 Phase I

Cessna Aircraft provided 4′ x 12′ plates of 0.25″ AA2024-T351 bare material in three heat lots for the welds to be made for Phase I. The composition of each heat lot is shown in table 1. Material from each heat lot was used to make welds with each weld tool design (see table 2). All welds were made on an MTS ISTIR PDS 5-axis motion, 7-axis force monitoring FSW machine on an anvil made of 4130 steel. Top clamps were applied normally to 0.50 inch by 1.00 inch steel bars positioned 2.0″ from the joint line on each side to apply 1200 lbf per foot to secure the piece during welding. The edges were secured using set screws tightened to apply approximately 200 lbf against steel bars on each side. They were spaced 4.00″ apart with four bars per plate. The fixtures are shown in figure 5.

Table 1. Heat lot designations, material composition, and tensile strengths for materials tested [74]

0.250 - AA2024-T351 Material	Tensile Strength (ksi)	Composition (wt %)								
		Si	Fe	Cu	Mn	Mg	Cr	Zn	Ti	Al
Lot 480-021	LT: 68.3	0.08	0.17	4.6	0.63	1.5	0.01	0.11	0.03	Bal.
Lot 360456A8	LT: 69.8	0.09	0.24	4.65	0.57	1.41	0.01	0.23	0.01	Bal.
Lot 740-581	LT: 67.9	0.07	0.16	4.6	0.64	1.5	0.01	0.06	0.03	Bal.
A-basis allowable	LT: 64									
B-basis allowable	LT: 66									

Table 2. Phase I welds listed by heat lot material used to produce each weld shown in table 1

	Weld Tool Design (Figure 6)					
Heat Lots	WSU26	WSU27	WSU33	WSU37	WSU38	WSU45
480-021	26_2	27_11	33_6	37_6	38_1	45_6
	26_3	27_12	33_7	37_7	38_2	45_7
	26_4	27_13	33_8	37_8	38_3	45_8
	26_5	27_14	33_9	37_10	38_4	45_9
	26_6	27_15	33_10	37_11	38_5	45_10
		27_16				
		27_18				
360456A8	26_7	27_6	33_1	37_1	38_16	45_2
	26_8	27_7	33_2	37_2	38_17	45_3
	26_9	27_8	33_3	37_3	38_18	45_4
	26_10	27_9	33_4	37_4	38_19	45_5
	26_11	27_10	33_5	37_5		
	26_12					
	26_13					
740-581	26_14	27_1	33_11	37_12	38_11	45_11
	26_15	27_2	33_12	37_13	38_12	45_12
	26_16	27_3	33_13	37_14	38_13	45_13
	26_17	27_4	33_14	37_15	38_14	45_14
	26_18	27_5	33_15	37_16	38_15	45_15
			33_16	37_17		45_16
			33_17	37_18		45_17

Phase I was performed in two stages. In Stage 1, the tools were chosen and initial weld parameters for each tool were identified. Six fixed-probe weld tool designs were considered for Phase I of the study (shown in figure 6). The base probe lengths were from 0.229–0.247 inch and the base probe diameters were between 0.275 and 0.400 inch. The tool bodies were made from Maraging 300 alloy and the probes from MP159® alloy. The shoulder diameters were 0.60 to 1.00 inch. Bead-on-plate screening welds were performed in position control to determine the weld parameters, including travel speed (weld inches per minute [ipm]), spindle speed (weld rpm), and forge load (measured in lbf), where welds without observable defects could be made with each tool.

Figure 5. The FSW fixture used in the NIAR AJ&P Lab at WSU [74]

Metallographic samples were taken from each weld and mounted in epoxy resin. The samples were then polished to a 0.050-micron finish using Buehler EcoMet® polishers to inspect for weld defects that affect the strength of the weld. After etching the specimens with Keller's solution, micrographs were made using an Olympus SZ61® stereomicroscope and the PaxCam digital microscope camera and image-management system (PAX-it Image Analysis Software, Version 7.1). The micrographs were inspected for voids and lack of penetration. The shoulder-side surface of the welds was inspected for surface galling and flash.

Figure 6. The FSW weld design tool used in WSU path independence study [34, 37]

In Stage 2 of Phase I, weld parameter windows were identified by looking at the weld condition data from Stage 1. The identified parameter ranges were entered into Statgraphics and a test matrix for a central star composite 2^3 + star design DOE was generated. Material from each heat lot provided by the suppliers was used to make welds with each tool. The tensile results were used to identify the parameters to include in the study. To eliminate more variability, the process windows could have been refined and optimized further by running a DOE using only the best weld parameters from the first DOE. However, by using the data from this stage, a level of variability could be retained to reflect possible site-to-site variability in industry when calculating the allowables. The parameter windows for Phase I are documented in figure 7 and the parameters for each weld with parameters in the process windows for Phase I are documented in table 3.

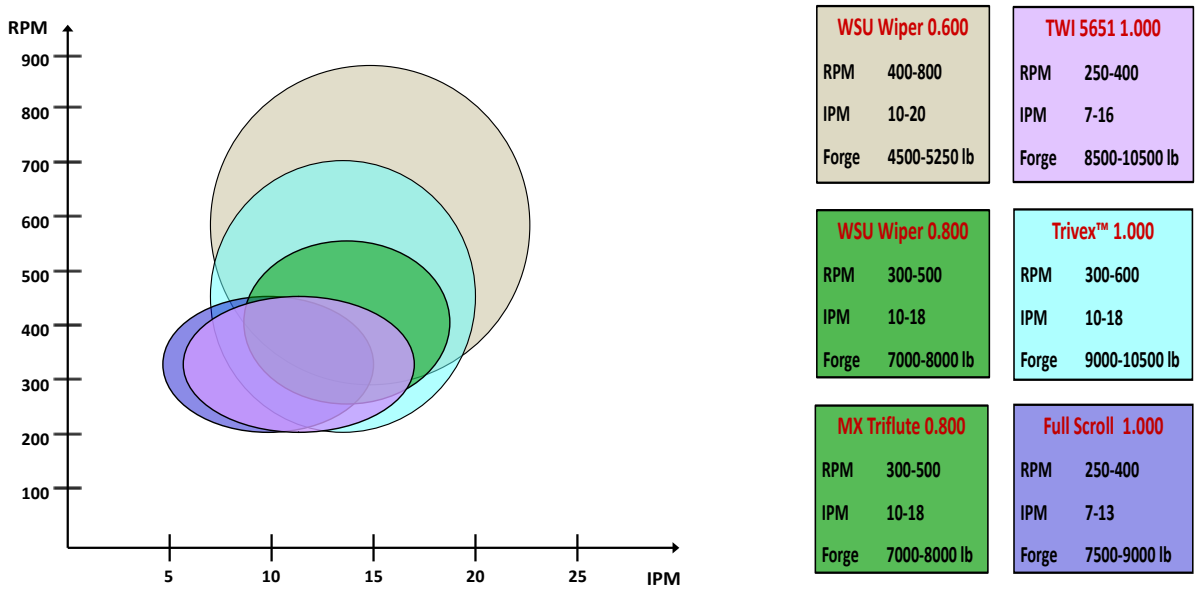

Figure 7. The FSW process windows for multipath study tools (figure 6) developed in the DOE for stage 2 of Phase I [75]

Each of the plates provided by Cessna was cut and machined into 4″ x 12″ plates with parallel longitudinal edges for welding. The bottom edges were given a slight chamfer of 0.020 inch and lightly sanded on the top surface with 180-grit sandpaper to remove the oxide layer. The panels were then wiped with methyl ethyl ketone to remove any surface contaminants, debris, or oils from handling, etc. Butt welds were made under load control using parameters within the process windows that had been identified. Each welded plate was marked and cut to have three metallographic specimens for microscopy and three tensile specimens meeting ASTM E8 specifications. An example of the cut plan is shown in figure 8.

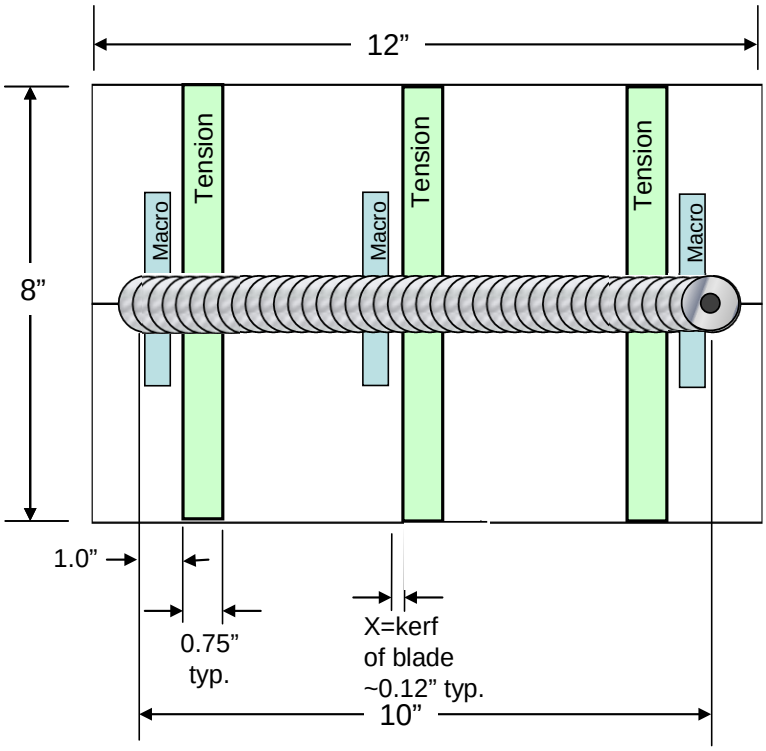

Figure 8. Cut plan for welded panels [74]

This study included tensile tests, full-field microhardness tests, and conductivity tests. Conductivity tests can be used to determine the final microstructure of the welded material because a high-purity Al matrix has the highest conductivity. Precipitates are too big to affect conductivity and solute atoms decrease conductivity [76]. Tensile tests of the coupons were performed on a 22-kip MTS 810 load frame. All tests were performed after at least 100 hours of natural aging time to allow the welds adequate time to stabilize before testing. A clip-on MTS axial extensometer was used to obtain strain data to calculate stress. Microhardness tests in accordance with ASTM E384 were performed on selected specimens on a LECO® AMH43 automatic microhardness tester using a Vickers scale with a 500 grams-force, 13-second dwell, and 555-micron spacing.

Electrical conductivity tests conforming to ASTM E1004-09 were performed on the specimens that were microhardness tested. This was accomplished using a Hocking AutoSigma 3000DL Electrical Conductivity Meter with a GE Inspection Technologies model 47P002 500-kHz, 0.300-inch (8-mm)-diameter probe. Each conductivity chart is the average result of three sets of readings every 1/16 inch in the transverse direction across the weld with the readings taken in the direction from the advancing side to the retreating side. The precision of the measurements is limited by the size of the conductivity probe. Each reading is an average of an 0.300-inch (8-mm)-diameter area but does produce an accurate representation of average conductivity across the weld. In table 3, the parameters used to make each weld in Phases I and II are documented. The tools in shaded cells are those that were optimized in Phase I.

Table 3. The AA2024-T3 FSW process parameters developed in Phases I and II by Weld Label

Phase I Specimen		Spindle Speed (rpm)	Travel Speed (ipm)	Forge Load (lb)		Phase I Specimen		Spindle Speed (rpm)	Travel Speed (ipm)	Forge Load (lb)		Phase II Round Robin Specimen	Spindle Speed (rpm)	Travel Speed (ipm)	Forge Load (lb)
Large Wiper WSU 26	26_3	300	10	7000		**Tri-flute** WSU 27	27_3	400	13	7500		Airbus_1B_LL	700	8	2023
	26_4	400	13	7500			27_4	500	16	7000		Airbus_2B_HL	900	8	2023
	26_5	500	16	7000			27_5	500	10	8000		Airbus_3B_HH	900	16	2023
	26_6	500	10	8000			27_6	300	16	7000		Airbus_4B_LCP	700	12	2023
	26_7	232	13	7500			27_7	500	16	8000		Airbus_5B_MPM	800	10	2023
	26_8	400	18	7500			27_8	300	10	8000					
	26_9	400	13	6659			27_10	500	10	7000		ALCAN_133_HL	600	20	5620
	26_10	568	13	7500			27_11	232	13	7500		ALCAN_134_LL	500	20	5171
	26_11	400	13	8340			27_12	400	18	7500		ALCAN_135_LH	500	24	5845
	26_12	400	8	7500			27_13	400	13	6659		ALCAN_136_HH	600	24	5620
	26_13	400	13	7500			27_14	568	13	7500		ALCAN_153_LH	500	10	7868
	26_14	300	16	7000			27_15	400	13	8340		ALCAN_154_HH	600	10	7644
	26_15	500	16	8000			27_16	400	8	7500		ALCAN_155_HL	600	8	6969
	26_16	300	10	8000			27_18	400	13	7500		ALCAN_156_LL	500	8	7194
	26_17	400	13	7500											
	26_18	500	10	7000											
Small Wiper WSU 45	45_1	800	20	4500		**Scroll** WSU 33	33_1	400	13	7500		LM_0.125A_LL	300	7	3450
	45_2	600	15	4875			33_2	250	13	9000		LM_0.125B_LH	300	9	3450
	45_4	800	10	5250			33_4	400	7	9000		LM_0.125C_HL	350	7	3450
	45_5	400	10	4500			33_6	250	7	9000		LM_0.125D_HH	350	9	3450
	45_6	400	10	5250			33_7	325	10	8250		LM_0.25A_LL	325	8	6500
	45_9	600	15	9875			33_12	451.13	10	8250		LM_0.25B_LH	325	10	6500
	45_10	400	20	4500			33_13	198.87	7	8250		LM_0.25C_HL	375	8	6500
	45_11	300	15	5505			33_14	325	4.95	8250		LM_0.25D_HH	375	10	6500
	45_12	600	23.4	4875			33_17	325	15.05	8250					
	45_14	600	15	4875											
	45_15	600	6.6	4875											
	45_16	900	15	4875		**TWI 5657** WSU 37	37_1	400	16	8500		WSU_3_HH	650	18	4875
	45_17	300	10	4875			37_2	325	11.5	9500		WSU_4_LL	550	12	4875
Trivex WSU 38	38_2	325	11.5	9500			37_4	400	7	10500		WSU_5_LH	550	18	4875
	38_5	600	10	10500			37_6	250	7	10500		WSU_6_CP	600	15	4875
	38_11	300	10	10500			37_11	250	16	8500		WSU_7_HL	650	12	4875
	38_12	450	14	9750			37_12	200	11.5	9500		WSU_27_LL	550	12	3750
	38_13	300	18	9000			37_14	325	19.07	9500		WSU_28_LH	550	18	3750
	38_17	450	7.27	9750			37_17	325	4	9500		WSU_29_HH	700	18	3750
	38_19	450	20.77	9750			37_18	451	11.5	9500		WSU_30_HL	700	12	3750

4.1.2 Phase II

In Phase II of the study, four sites were identified to make the welds. Welds were made by WSU, Alcan, Lockheed Martin (LM), Michoud Operations, and Airbus. The AA2024-T3 0.250-inch, AA2024-T3 0.125-inch, and AA2198-T8 0.150-inch material to be welded was supplied by Aluminum Company of America (ALCOA), Alcan, and Kaiser Aluminum. The maximum composition-by-weight percent of the materials provided can be found in table 4.

Table 4. Phase II material compositions and corresponding tensile strength

Material	Tensile Strength (ksi)	Composition (wt %) max. (Ref. [75] and SAE AMS 4412)												
												Other		
		Si	Fe	Cu	Mn	Mg	Cr	Zn	Ti	Ag	Zr	Li	Ea.	Tot.	Al
2024-T3	LT:70.2	0.5	0.5	3.8-4.9	0.3-0.9	1.2-1.8	0.1	0.25	0.15	--	--	--	0.05	0.15	Balance
2198-T8	LT:79.8 TL:78.0	0.08	0.1	2.9-3.5	0.5	0.25-0.8	--	0.35	0.1	0.1-0.5	0.04-0.18	0.8-1.1	0.05	0.15	Balance

Each site was instructed to produce four strong welds with their own tools of the AA2024-T3 0.125- and 0.250-inch material and four strong welds of AA2198-T8 0.150-inch material. They produced a weld from each corner of their weld parameter windows (rpm vs. ipm) according to the American Welding Society (AWS) D17.3 [77] (draft) and their own internal process specifications. A schematic representing the general weld parameters used is shown in figure 9. The panels from Alcan and LM were cut and tested in the NIAR AJ&P Lab at WSU as described in Phase I. The panels from WSU and Airbus were sent to Westmoreland Mechanical Testing & Research for independent tensile and shear tests.

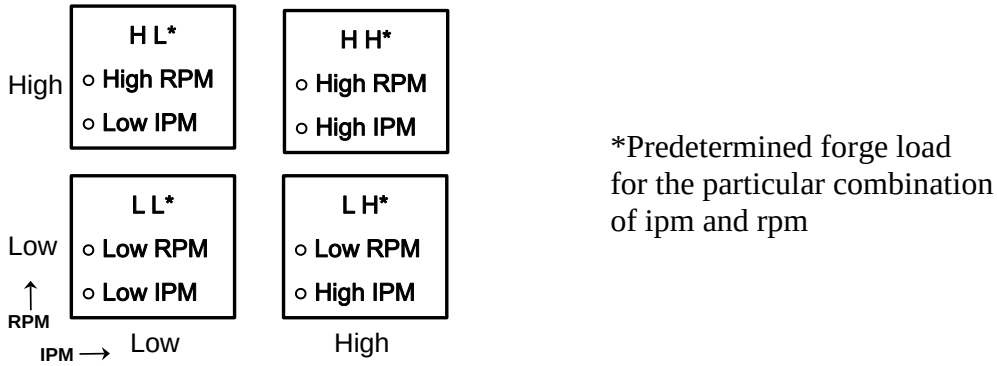

Figure 9. Phase II process parameter designations and relative process windows [78]

The tool design chosen to make the 0.150-inch AA2198-T8 material welds in Phase II had a 0.500-inch Wiper shoulder design [42] and a 0.145-inch-long, threaded probe with twisted flats. The probe had a 0.160 inch diameter at the shoulder. The welds in the AA2024-T3 0.125-inch material were made with a 0.800-inch shoulder tool with a 0.120-inch-long threaded probe with flats. This probe had a 0.225-inch diameter at the shoulder. The Wiper with a 0.600-inch shoulder was used in Phase I. It was also used to make the Phase II AA2024-T3 0.250-inch welds.

Figure 10 shows the tools used to produce the 0.150-inch AA2198-T8 and 0.125-inch AA2024-T3 material welds. The tool in figure 10(a) had a 0.147-inch-long probe and twisted flats, and was used for the AA2198-T8 material. The tool in figure 10(b) had flats with a 0.120-inch-long probe and was used for the AA2024-T3 0.125-inch material. The weld parameters used to produce the AA2198-T8 material welds are listed in table 5.

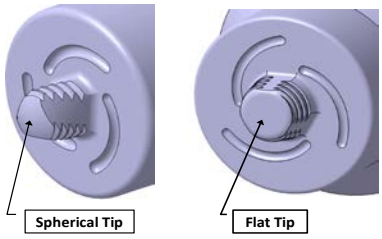

(a) (b)

Figure 10. Phase II tool designs had a wiper shoulder design [42] with a) a threaded probe with twisted flats and b) a threaded probe with straight flats

Table 5. The FSW process parameters for AA2198-T8 welds in Phase II

Phase II Round Robin Specimen	Spindle Speed (rpm)	Travel Speed (ipm)	Forge Load (lb)		Phase II Round Robin Specimen	Spindle Speed (rpm)	Travel Speed (ipm)	Forge Load (lb)
ALCAN _84_LL	800	12	2810		WSU_01	900	10	2100
ALCAN_85_HL	900	12	2698		WSU_02	900	5	2000
ALCAN_86_HH	900	16	2585		WSU_04	900	5	1700
ALCAN_88_LH	800	16	3035		WSU_05	1200	5	1500
LM_29_LL	375	15	3300		WSU_06	900	10	1900
LM_31_LH	375	17	3300		WSU_08	600	10	2100
LM_33_HL	425	15	3300		WSU_09	900	15	2000
LM_35_HH	425	17	3300		WSU_10	1200	15	1900
					WSU_11	1200	10	1800
Airbus_1_HH	1600	24	1911		WSU_12	600	15	2100
Airbus_2_LH	1200	24	1911		WSU_14_LL	900	10	2100
Airbus_3_HL	1200	16	1911		WSU_15_LH	900	15	2000
Airbus_4_LL	800	16	1911		WSU_16_HH	1200	15	1900
Airbus_5_CP	1200	20	1911		WSU_17_HL	1200	10	1800

4.2 EXPERIMENTAL DATA

4.2.1 Phase I

The tensile coupons from each Phase I welded panel were tested per ASTM E8. The average UTS from the welds for each tool can be seen in figure 11. The average UTS from welds produced by three of the tools was between 90.7% and 91.6% of the parent material strength. The other three had average UTS values of 76.4% to 85.5% of the parent material strength. The tensile results were lower for the 1.00-inch shoulder tools compared to the others.

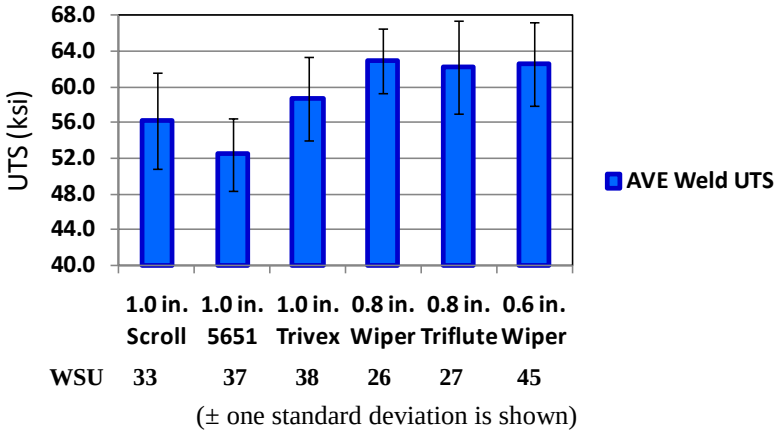

Figure 11. Average UTS of all welds made with the Phase I tools [43, 74]

There were three tensile coupons tested for each Phase I weld. The average UTS data obtained from the tensile tests were entered into the Design-Expert® 6.0.6 software. Response surfaces for each tool were generated (see figure 12). The response surfaces were based on a central star composite design: 2^3 + star [74]. Since there was a plateau in the response surfaces on three of the tools, their parameters were considered optimized. The plateau is highlighted by the blue circled areas. Three of the tools were not considered optimized because there was no plateau on those response surfaces (see figure 12). The red arrows on these three surfaces indicate the direction in which the UTS values increased where optimized parameters could possibly be identified. Two of the tools that were not optimized showed promise of being optimized. However, the MTS welding machine did not have the torque at the low spindle speeds required to make welds at the indicated parameters. The third tool, the TWI 5651, would possibly require feature modifications to be optimized. It was decided to exclude the tools that were not optimized from the study and continue with the remaining three and their optimized parameters.

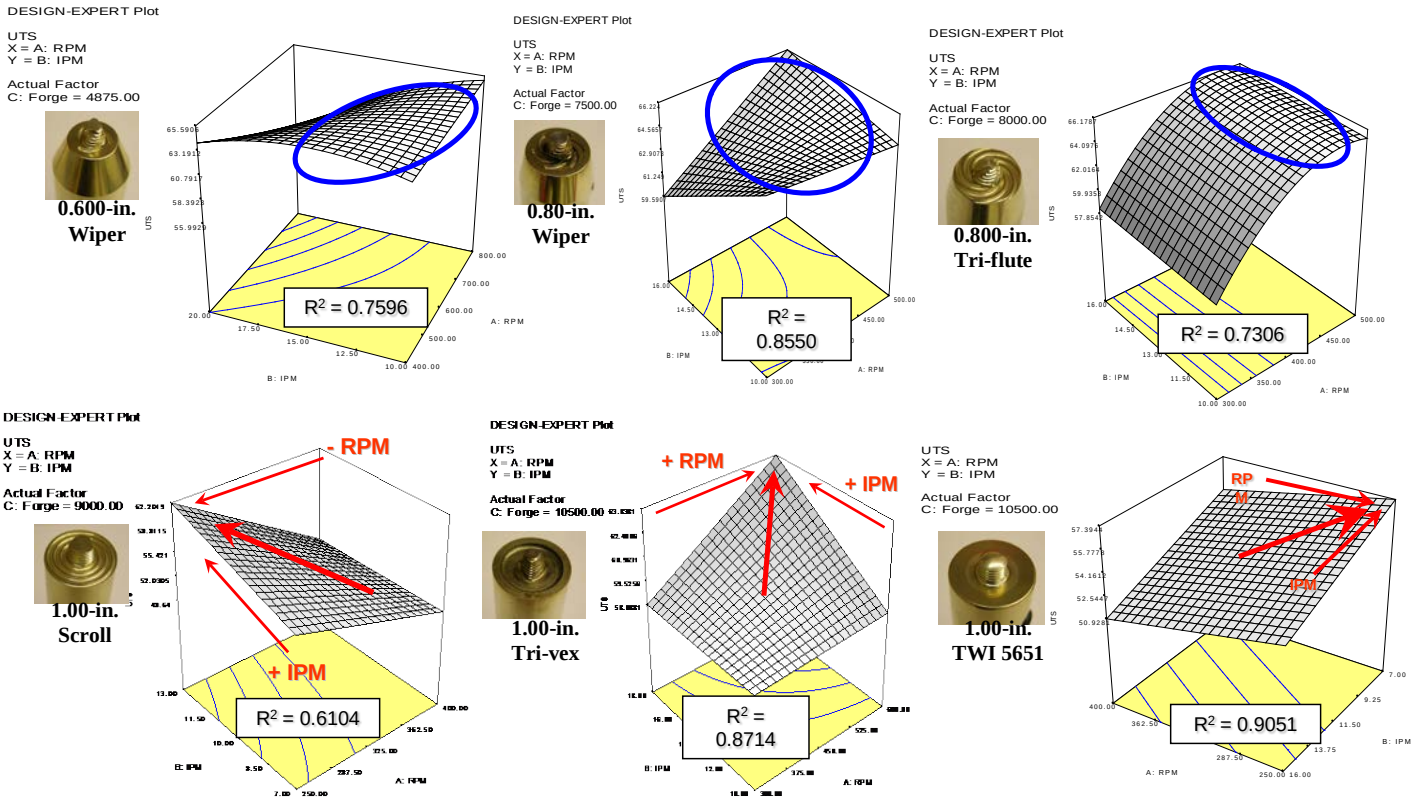

Figure 12. The UTS response surfaces with optimized FSW process parameter windows from design-expert software [74]

As the tools with higher UTS values were optimized with stable welding parameters, the data from their welds should be comparable based on the path independence hypothesis. This was confirmed using the methods outlined in the MMPDS, Section 9.5.3.1 through 9.5.3.3. The data for the study parameters for the remaining tools were used to compute design allowables according to the MMPDS Section 9.2.4.1 [35, 74]. The tensile data are shown in figure 13 with the T_{99} and T_{90} values that were calculated.

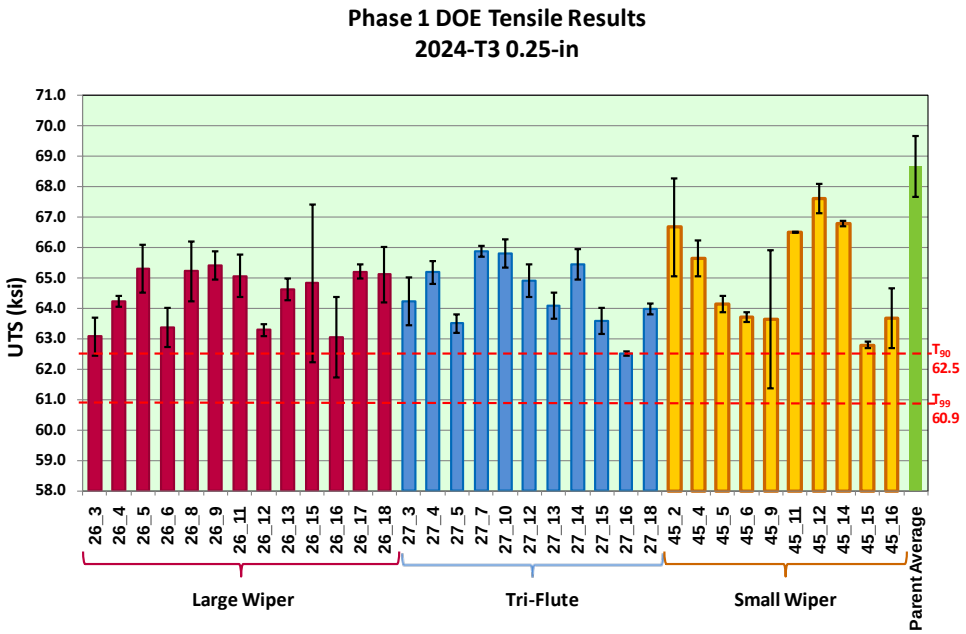

(Error bars represent ± one standard deviation)

Figure 13. Average UTS values for phase I AA2024-T3 FSW shown with the computed T_{99} and T_{90} per MMPDS, Section 9.5.3

4.2.2 Phase II

In Phase II, there were 30 AA2024-T3 welds produced. All AA2024-T3 tensile test data from all three sites for Phase II were sent to Battelle for independent evaluation. Alcan and LM produced four welds of AA2024-T3 0.250-inch material and four welds of 0.125-inch AA2024-T3. Airbus did not produce any AA2024-T3 0.250-inch material welds, but did produce an extra AA2024-T3 0.125-inch weld with central parameters from their parameter window. Therefore, Airbus produced five welds of 0.125-inch AA2024-T3 material. WSU produced an extra 0.250-inch weld using the center-point parameters of the process window, which means WSU produced five welds of AA2024-T3 0.250-inch material and four welds of 0.125-inch AA2024-T3. Therefore, 30 total welds of AA2024-T3 material and five tensile specimens from each weld were evaluated by Battelle. The average UTS for each AA2024-T3 material weld produced in Phase II is shown in figure 14, with the design allowable T_{90} and T_{99} values calculated from the Phase I AA2024-T3 weld tensile test data. It shows that all the Phase II data are above the T_{99} value, and all except three of the values are above the T_{90} value.

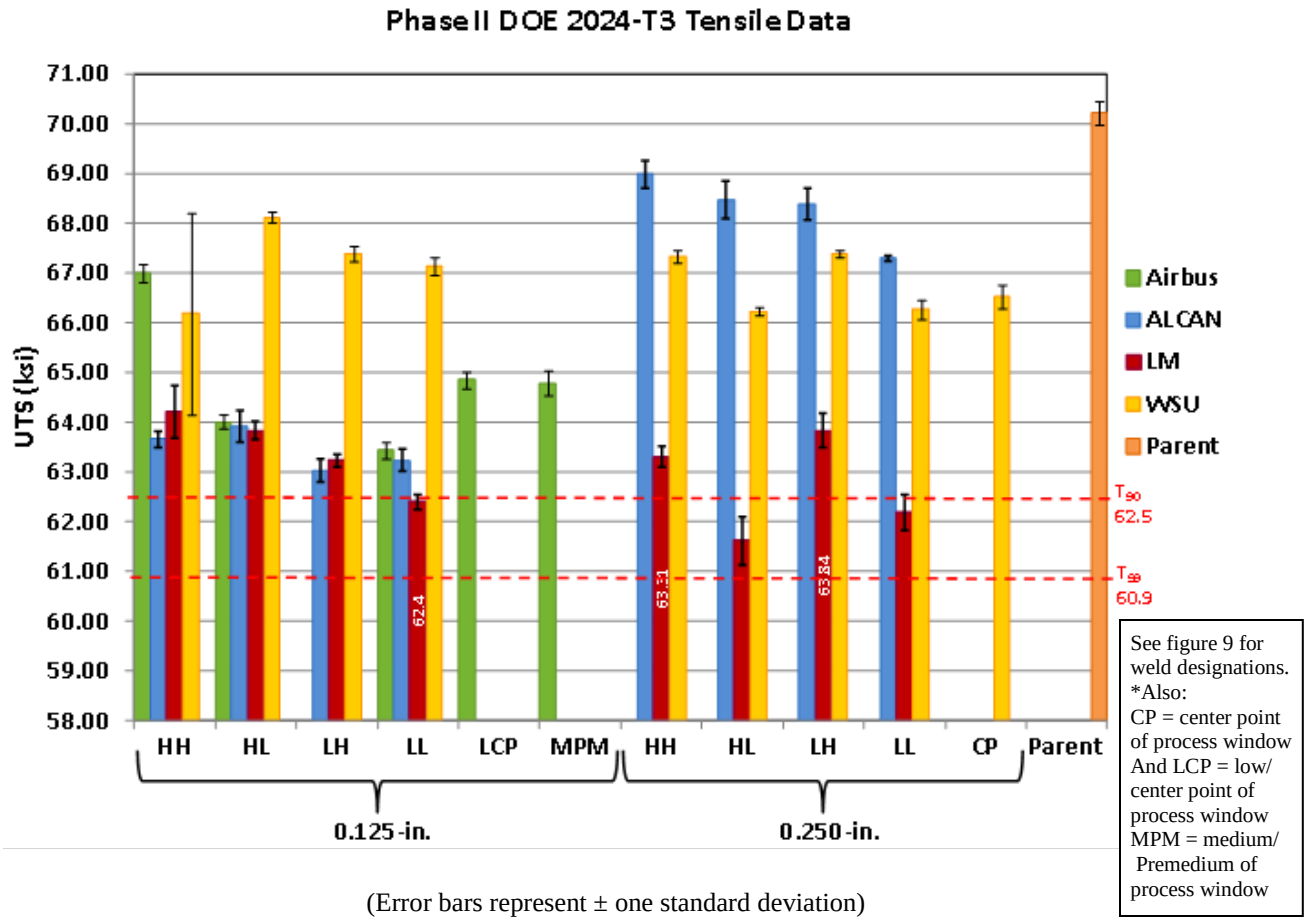

(Error bars represent ± one standard deviation)

Figure 14. Average UTS for Phase II AA2024-T3 FSW welds produced by ALCAN, LM, WSU, and Airbus

4.2.3 Microhardness

The results of the microhardness tests on selected AA2024-T3 material specimens from Phases I and II can be found in table 6 with UTS values for each weld. Microhardness tests were performed using a Vickers hardness (HV) scale, 500-grams-force load, and a 13-second dwell time. The nominal value for HV for AA2024-T3 is considered to be 137 HV [79]. The reported results for the microhardness tests reflect the lowest value (minimum) for hardness in the hardness data for each microhardness test. The microhardness minimum ranged from 103-126 HV/500 for Phase I and 110-132 HV/500 for Phase II. The process windows in Phase I included parameter ranges as wide as possible where welds without visible defects could still be produced. This would retain more variation in the Phase I weld UTS values, which was meant to reflect the site-to-site variation that could occur. The optimized welds of Phase II had higher UTS values than the welds that were retained in Phase I. Only 19% of the UTS values for the welds were above 66 ksi in Phase I, and 53% were above 66 ksi in Phase II. Since microhardness is an indication of the weld strength, this would explain why the microhardness minimums were higher for Phase II than Phase I. Also, the higher UTS values in Phase II could mean that the site-to-site variation was much less than expected.

Table 6. The UTS values and full-field microhardness test data of selected AA2024-T3 welds produced for Phases I and II

Phase I Specimen		Microhardness (HV/500) Minimum	Average UTS (ksi)	Phase I Specimen		Microhardness (HV/500) Minimum	Average UTS (ksi)		Phase II Round Robin Specimen	Microhardness (HV/500) Minimum	Average UTS (ksi)
Large Wiper	26_5	120	65.30	TWI 5657	37_1	113	46.02		ALCAN_133_HL	132	68.47
	26_6	115	63.36		37_2	111	53.89		ALCAN_134_LL	126	67.30
	26_7	110	64.78		37_4	110	53.91		ALCAN_135_LH	129	68.40
	26_8	120	65.21		37_6	109	59.16		ALCAN_136_HH	128	69.00
	26_10	115	59.70		37_11	108	55.27		ALCAN_153_LH	114	63.04
	26_12	115	63.28		37_12	110	48.61		ALCAN_154_HH	117	63.67
	26_13	118	64.63		37_14	110	48.83		ALCAN_155_HL	114	63.93
	26_14	115	57.65		37_17	109	52.63		ALCAN_156_LL	112	63.24
	26_16	116	63.04		37_18	115	55.17		LM_0.125A_LL	115	62.40
									LM_0.125B_LH	116	63.24
Tri-flute	27_3	116	64.23	Trivex	38_2	117	54.68		LM_0.125C_HL	116	63.84
	27_4	121	65.19		38_5	114	54.31		LM_0.125D_HH	116	64.22
	27_5	117	63.50		38_11	110	56.52		LM_0.25A_LL	110	62.20
	27_6	114	57.40		38_12	115	56.55		LM_0.25B_LH	113	63.84
	27_8	114	61.15		38_13	110	51.76		LM_0.25C_HL	112	61.63
	27_1	109	44.02		38_17	113	64.31		LM_0.25D_HH	113	63.31
	27_12	120	64.92		38_19	116	64.08		WSU_3_HH	123	67.34
	27_14	121	65.44						WSU_4_LL	120	66.28
	27_16	111	62.52						WSU_5_LH	122	67.40
Scroll	33_1	116	55.31	Small Wiper	45_1	126	54.23		WSU_6_CP	122	66.54
	33_2	111	63.30		45_4	117	65.64		WSU_7_HL	118	66.24
	33_4	106	48.83		45_6	117	63.71		WSU_27_LL	123	67.14
	33_6	107	58.48		45_9	116	63.64		WSU_28_LH	124	67.40
	33_7	108	55.47		45_10	118	63.86		WSU_29_HH	127	66.20
	33_12	113	48.93		45_12	125	67.61		WSU_30_HL	122	68.12
	33_13	109	60.40		45_15	114	62.79		Airbus_1B_LL	116	63.44
	33_14	103	55.11		45_16	112	63.67		Airbus_2B_HL	115	64.02
	33_17	114	59.97		45_17	111	60.90		Airbus_3B_HH	124	67.00
									Airbus_4B_LCP	120	64.86
									Airbus_5B_MPM	119	64.80

For Phase II, 16 welds of AA2198-T8 material were produced. There were five tensile coupons tested from each weld. The welds had low standard deviations, but one weld had a much lower tensile strength than all the other welds. The results of tensile tests can be seen in figure 15.

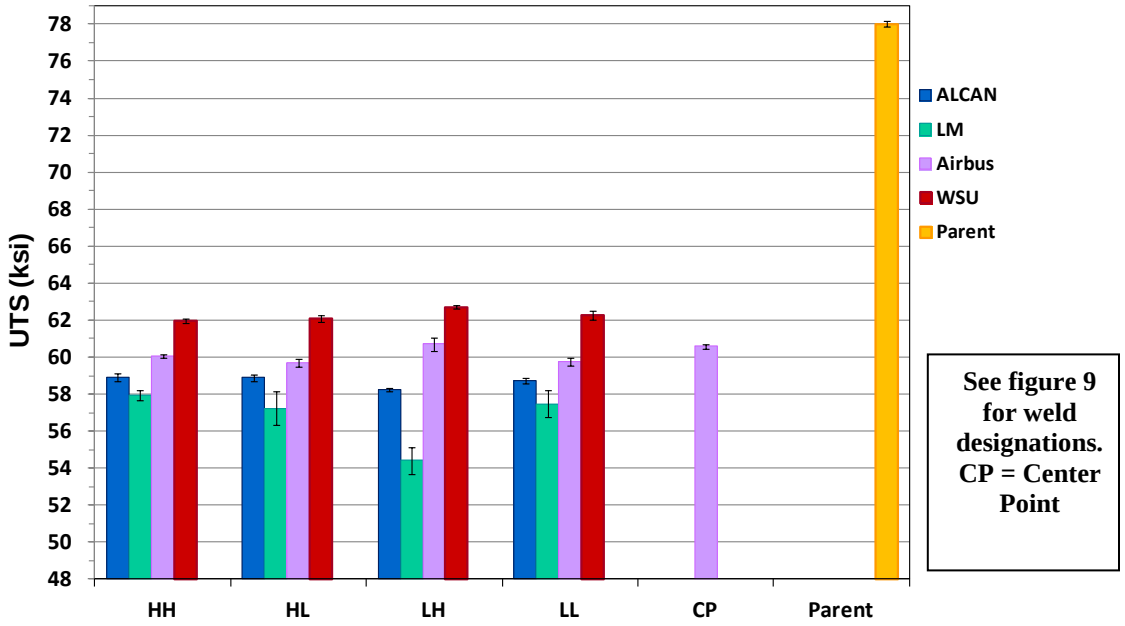

Figure 15. Average tensile strength for the Phase II AA2198-T8 material from all sites

Full-field microhardness was performed on the welds of AA2198-T8 material used for finding the process window (bounding welds) for the tool chosen as well as the welds that were to be tested for the study. Both sets of microhardness data for the WSU Phase II AA2198-T8 welds are included in table 7 along with the microhardness data for the welds produced at the other sites. The average UTS and minimum hardness values were very consistent. The minimum HV values had a range of 102-109 HV/500 for the study welds. The microhardness minimums for the bounding welds were consistently lower than the study welds. Microhardness tests were done on parent material for the AA2198-T8 material. The average HV for the AA2198-T8 material provided by the supplier was 166.7 HV/500.

In table 7, the WSU data include the bounding welds, 1-12, as well as the study welds, 14-17.

Table 7. Phase II AA2198-T8 FSW UTS and microhardness data

Phase II Round Robin Specimen	Microhardness (HV/500) Minimum	Average UTS (ksi)		Phase II Round Robin Specimen	Microhardness (HV/500) Minimum	Average UTS (ksi)
ALCAN _84_LL	102	58.73		WSU_01	97	56.20
ALCAN_85_HL	102	58.89		WSU_02	98	55.50
ALCAN_86_HH	103	58.91		WSU_04	69	55.43
ALCAN_88_LH	104	58.23		WSU_05	65	57.40
LM_29_LL	104	57.48		WSU_06	94	56.90
LM_31_LH	102	54.42		WSU_08	96	53.97
LM_33_HL	104	57.24		WSU_09	97	55.97
LM_35_HH	104	57.92		WSU_10	97	57.30
				WSU_11	92	56.93
Airbus_1_HH	104	60.06		WSU_12	94	49.35
Airbus_2_LH	106	60.70		WSU_14_LL	107	62.10
Airbus_3_HL	105	59.70		WSU_15_LH	109	61.98
Airbus_4_LL	104	59.74		WSU_16_HH	108	62.72
Airbus_5_CP	105	60.58		WSU_17_HL	107	62.26

4.3 DISCUSSION

Following the completion of Phases I and II, a separate analysis of the compiled data was conducted [80]. The Phase I AA2024-T3 welds were evaluated to determine if the UTS values fit a normal distribution. The frequency histogram and normal probability plot for the data are shown in figures 16 (a and b). The data were observed to be adequately represented by a normal distribution. A simple regression was performed in Statgraphics. The residual plot from the data regression shows that six data points have residuals between two and three standard deviations. The studentized residual plot is shown in figure 17. This does not separate the data according to weld parameters or the different tools. When the simple regression analysis was performed on the

weld data separately for each tool, the large Wiper welds had two data points with residuals greater than two standard deviations but less than three. The small Wiper welds had only one data point with a residual greater than two standard deviations but less than three. The Tri-flute™ welds had no residuals greater than two standard deviations. Data points that fall outside three standard deviations of the mean value are considered to be outliers. Those that fall between two and three standard deviations are considered to be suspect. Based on these criteria, no outliers of a 5% significance level were identified.

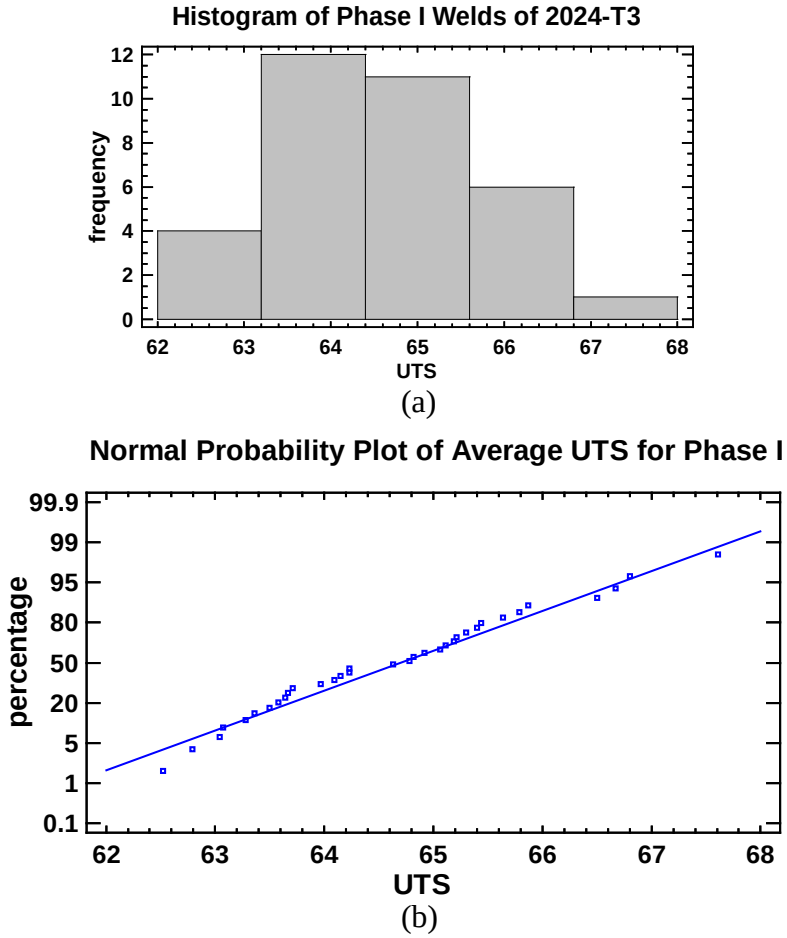

Figure 16. a) Histogram of the average UTS for retained Phase I AA2024-T3 welds and b) normal probability plot for Phase I weld UTS values

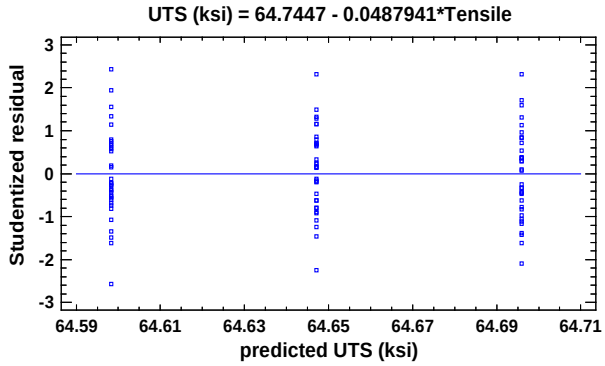

Figure 17. The studentized residual plot of all Phase I tensile data grouped according to location in the weld panel

A multiple-sample comparison of the AA2024-T3 weld data, grouped according to the location of the tensile coupon in the weld joint line, did not indicate any significant outliers and there were no significant differences in the means of the data sets as shown in figure 18. The average tensile strength for the welds was analyzed using a multiple regression with blocking for weld parameters, heat lot, and tool. The model is shown in figure 19. The R^2 for the model was 49.6 percent. A distribution analysis yielded the residual plot shown in figure 20. There were three studentized residuals greater than two standard deviations and one had a studentized residual more than three standard deviations. This data point residual was within 3.5 standard deviations. In this case, a value less than 3.5 was considered suspect and a value greater than 3.5 was considered an outlier. Therefore, an outlier test was performed using both the Grubb's test and Dixon's test. Using these tests, no significant outliers were found at a 5% significance level, so it was concluded that no outliers were identified. (Note: The data point in question is not considered an outlier.)

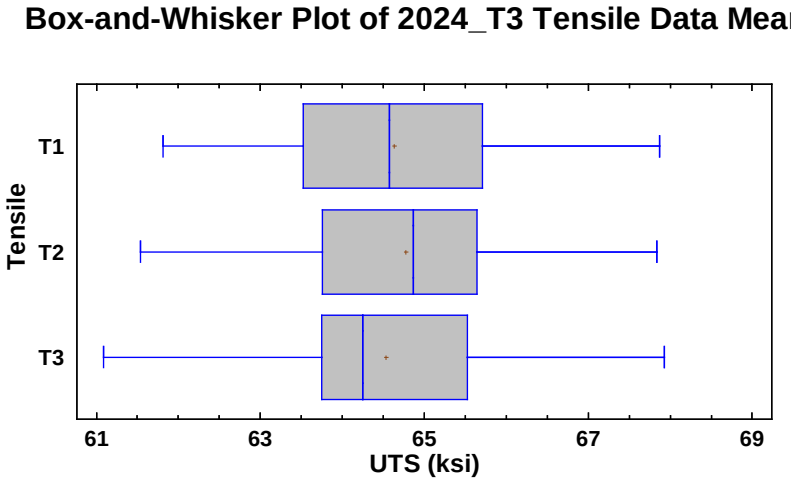

Figure 18. Box-and-Whisker plot from statgraphics analysis multiple sample comparison of Phase I UTS data grouped according to location of tensile coupon in weld joint line

Multiple Regression - Average UTS

Dependent variable: Average UTS (ksi)
Independent variables:
Forge Load
BLOCK (TOOL)
Heat Lot
Spindle Speed (rpm)
Travel Speed (ipm)

		Standard	*T*	
Parameter	Estimate	Error	Statistic	*P*-Value
CONSTANT	63.1065	2.3406	26.9617	0.0000
Forge Load	-0.000233786	0.000231546	-1.00967	0.3213
BLOCK	-0.18797	0.360238	-0.521794	0.6059
Heat Lot	-0.0868712	0.212759	-0.408308	0.6862
Spindle Speed	0.001278	0.00168455	0.758661	0.4544
Travel Speed	0.234423	0.0505268	4.63957	0.0001

Analysis of Variance

Source	Sum of Squares	*Df*	Mean Square	*F*-Ratio	*P*-Value
Model	25.298	5	5.0596	5.51	0.0012
Residual	25.7029	28	0.917961		
Total (Corr.)	51.0009	33			

R^2 = 49.6031 percent
R^2 (adjusted for d.f.) = 40.6036 percent
T = tensile test data
Standard Error of Est. = 0.958103
Mean absolute error = 0.679445
Durbin-Watson statistic = 1.70719 (P = 0.1097)
Lag 1 residual autocorrelation = 0.0484521

Figure 19. Multiple regression analysis results for Phase I average tensile test data

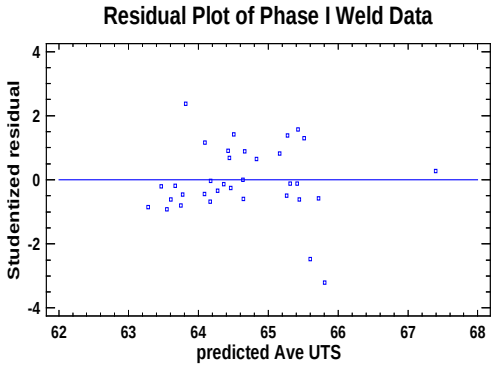

Figure 20. Studentized residual plot from multiple regression analysis of average tensile strength of welds

Data for FSW AA2024-T3 material weld tensile strength values reported in literature are shown in table 8. Much of the data are above the computed T_{90} and T_{99} design allowable values calculated in Phase I for AA2024-T3 material. The table shows the data average agrees with the T_{90} value. Although not conclusive, this collection of independent data sets, which have been taken from the literature, tend to support the path-independence hypothesis. A total of 60% of the reported data

in table 8 falls above the calculated T_{90} value of 62.5 ksi from the phase I data and 70% is above the calculated T_{99} value of 60.9 ksi. The reported values are from various thicknesses of material produced at different sites using different equipment with various tools and weld parameters; the amount of agreement between the reported data was good with a 4.9 ksi standard deviation. The degree that the tool parameters were optimized for the welds associated with the reported data is unknown, but the welds that are below the T_{90} and T_{99} values could possibly be brought up to within the T_{90} and T_{99} range, if optimized.

Table 8. Tensile results reported in literature for FSW welds of AA2024-T3 sheet and plate [38]

Material Thickness	Ultimate Tensile Strength	Weld Elongation (%)
0.040 in. (1 mm)	58.9 ksi (406 MPa)	6.0
0.064 in. (1.6 mm)	66.9 ksi (461 MPa)	11
0.080 in. (2 mm)	64.7 ksi (446 MPa)	13.0
0.080 in. (2 mm)	64 ksi (441 MPa)	16.3
0.090 in. (2.25 mm)	53 ksi (366 MPa)	- -
0.100 in. (2.5 mm)	71.1 ksi (490 MPa)	17
0.125 in. (3.2 mm)	63.5 ksi (438 MPa)	12.2
0.l60 in. (4 mm)	62.7 ksi (432 MPa)	7.6
0.200 in. (5 mm)	59.5 ksi (410 MPa)	5.1
0.250 in. (6.35 mm)	60.9 ksi (420 MPa)	--
Average	62.5 ksi (431 MPa)	11
Standard Deviation	4.90 ksi (33.8 MPa)	4.5

All the AA2024-T3 material weld data from Phase II are above the calculated T_{90} allowable in Phase I, except for three data points. Those data points are below the T_{90} value of 62.5 ksi, but above the T_{99} value of 60.9 ksi. The standard deviation of two of the values indicates that the difference between the weld average UTS and the T_{90} value may not be significant. Out of the 64 welds in AA2024-T3 from both Phases I and II, there are only three welds with an average UTS that fall below the T_{90} value of 62.5 ksi. Of the three, two have an average UTS value of 62.2-62.4 ksi, which possibly could have been improved. All the UTS values for the AA2024-T3 welds for Phases I and II are above the T_{99} value of 60.5 ksi. The average UTS for 46.6% of the welds from Phase II was ≥66 ksi, which is 94% of the minimum parent material tensile strength of 70 ksi [79]. All the UTS values for the AA2024-T3 welds from Phases I and II are at least 88% of the minimum tensile strength of the parent material. The average UTS value for the parent material tested in Phase I was found experimentally to be 68.6 ksi and 70.2 ksi for Phase II.

The weld data from Phase II, which was analyzed by Battelle, included 150 tensile test results from the 30 welds produced in AA2024-T3 at the four sites and 65 tensile test results from 13 welds in AA2198-T8.[1] The parameter ranges for all Phase II AA2024-T3 and AA2198-T8 material welds are shown in table 9. The weld parameter windows are shown in figure 21. The variables of the data considered in Battelle's analysis were supplier, tool, parameter set, and material thickness. The stated primary focus of the analysis was to test the tensile data variation within subgroups and primary FSW groups [77]. The coefficient of site-to-site variation in UTS for AA2024-T3 0.125-inch material was found to be 3.24%. For AA2024-T3 0.250-inch material, the variation in UTS was 2.99%.

Table 9. Phase II weld parameter ranges used by round-robin sites when welding AA2424-T3 and AA2198-T8 material

Parameter	Range
Travel Speed (in/min)	5–24
Rotational Speed (rpm)	300–1600
Plunge Force (lbf)	1500–7868

[1] The Alcan 2198-T8 material welds were inadvertently not provided to Battelle for analysis and therefore are absent from the Battelle analysis.

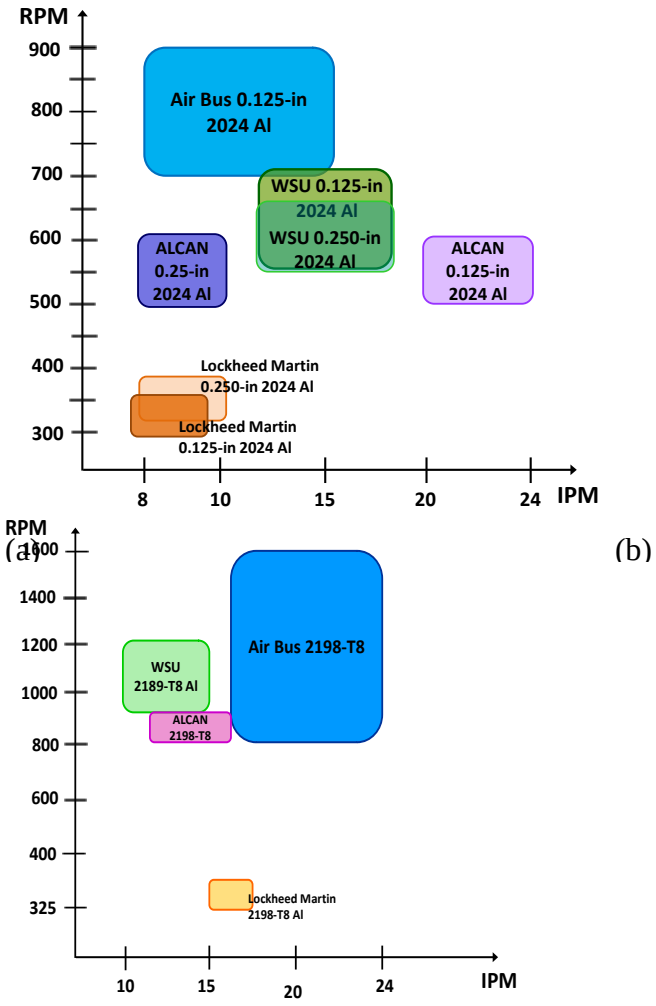

Figure 21. Weld parameter windows for participating sites for listed aluminum alloy and material thickness

The Battelle data analyses showed the coefficient of variation for each weld was less than 1% for UTS, and comparing weld-to-weld variation in UTS when grouped by site, ranged from 1.00% to 1.92%. From Battelle's data analyses, it was concluded that: 1) there was not a significant data variation between each weld, 2) there was not a significant data variation between each site, and 3) site-to-site variation was higher than weld-to-weld variation. Battelle also compared the data to other current and emerging aerospace metallic material and component production technologies. These results were found to be comparable.

Shear data were also evaluated by Battelle and the analysis results are shown in table 10. The shear tests were performed at WSU on the same load frames as the tensile tests. The shear strength was good compared to the expected value of 41 ksi for the shear strength of AA2024-T3 material [76] and had a small standard deviation. The data were compared by Battelle to results obtained from other sources. The variability was comparable with many wrought products.

Table 10. Ultimate shear stress results for shear test weld specimens (analysis by Battelle) [78]

2024-*T*3		
Ultimate Shear Stress, ksi		Thickness, in.
Average	45.69	0.125
Standard Deviation	0.91	
COV	2.0%	
Average	45.08	0.25
Standard Deviation	1.01	
COV	2.2%	

COV = coefficient of variation

Tensile failure locations were evaluated for Phase II AA2024-T3 material welds. The Alcan weld numbers 86 and 88 had tensile failures in the TMAZ on the advancing side. The Alcan weld numbers 84 and 85 had failures in the nugget, which could indicate weld defects, so the micrographs were inspected. There were no visible voids or oxide lines in the micrographs of any of the Alcan welds. A small amount of flash was present at the sides of all weld tracks. All Airbus weld tensile specimens failed at the TMAZ on the advancing side. The Airbus_3B weld had a void in the advancing side of the nugget, which is shown in figure 22, but the UTS value from the tensile test results showed this weld had the highest tensile strength of the Airbus welds. All WSU tensile specimens failed in the TMAZ on the retreating side, except for two from the same 0.125 weld. The T1 tensile from the WSU17_29 weld failed in the nugget, and the T4 tensile failed at the nugget/TMAZ border. The UTS values for the two tensile specimens were 64.9 and 63.4 ksi, and the remaining tensile specimens for this weld were 67.1 to 68.5 ksi. This indicates that this weld could have had defects, although none were observed when visually inspected. These two tensile values are at least as high as, or higher than, all LM tensile results and most Airbus results; they are also comparable to the Alcan 0.25-inch material tensile results. All LM AA2024-T3 material welds failed in the boundary of the HAZ and TMAZ. There were no defects noted with visual inspection.

(The red arrow indicates a void in the advancing side of the nugget)

Figure 22. Airbus_3B Weld

A normal probability plot and a frequency histogram of the average UTS values for the Phase II welds of AA2024-T3 material were plotted to check the distribution. The result is shown in figure 23. The data roughly fit a normal distribution. The Weibull analysis in figure 24 indicates that there is evidence that the data fit a Weibull distribution with 95% confidence.

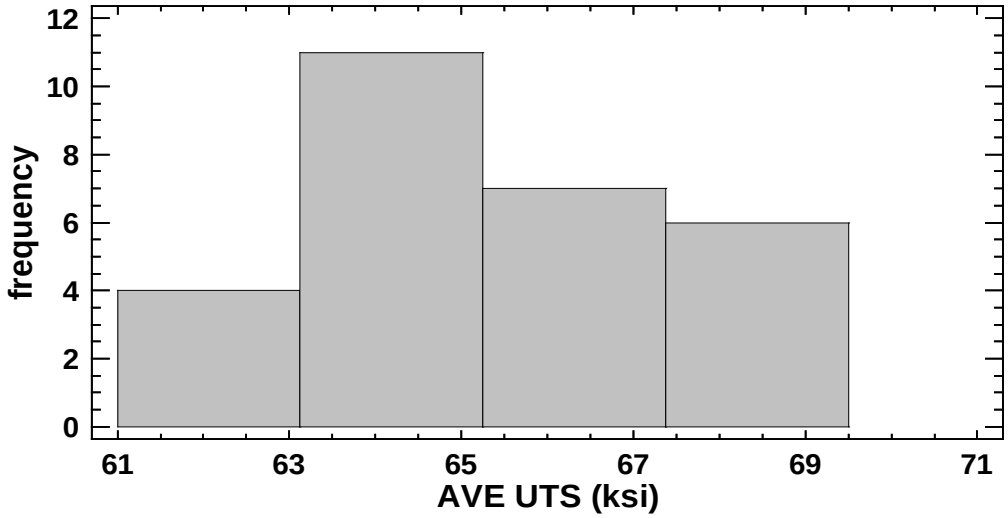

(a)

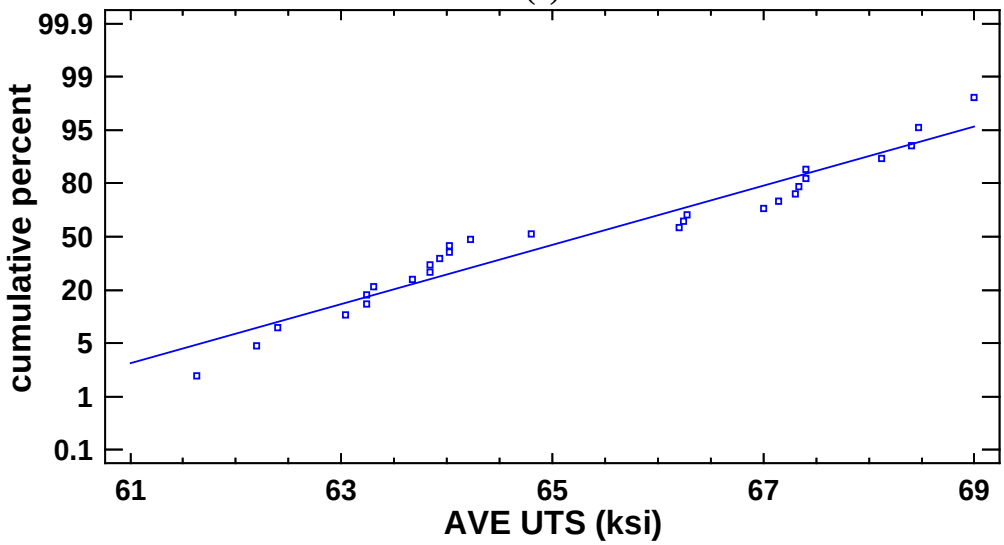

(b)

Figure 23. Statgraphics analysis of a) frequency histogram of Phase II AA2024-T3 weld tensile data and b) normal probability plot showing linearity of data

Weibull Analysis - Ave UTS
Data variable: Ave UTS
Estimation method: maximum likelihood
Sample size = 28
Number of failures = 28
Estimated shape = 33.3587
Estimated scale = 66.3258
Specified threshold = 0.0
95.0% confidence intervals
Shape: [23.1859, 42.3141]
Scale: [65.5042, 67.1577]
Goodness-of-Fit Tests for Ave UTS
Kolmogorov-Smirnov Test

	Weibull
DPLUS	0.211162
DMINUS	0.110858
DN	0.211162
P-Value	0.16471

(a)

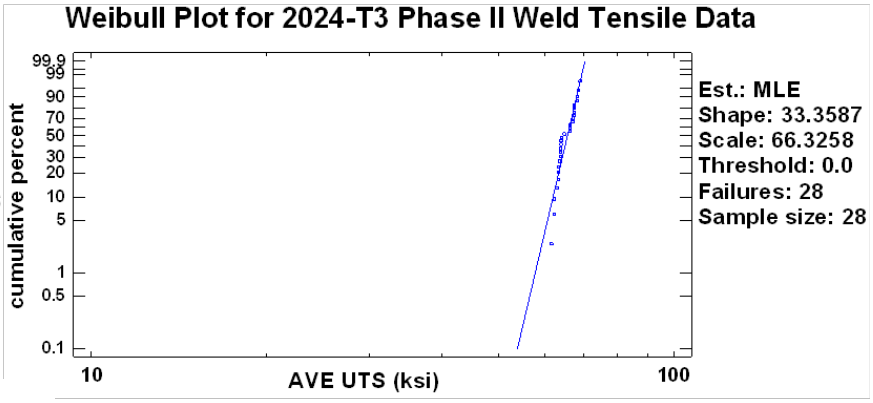

(b)

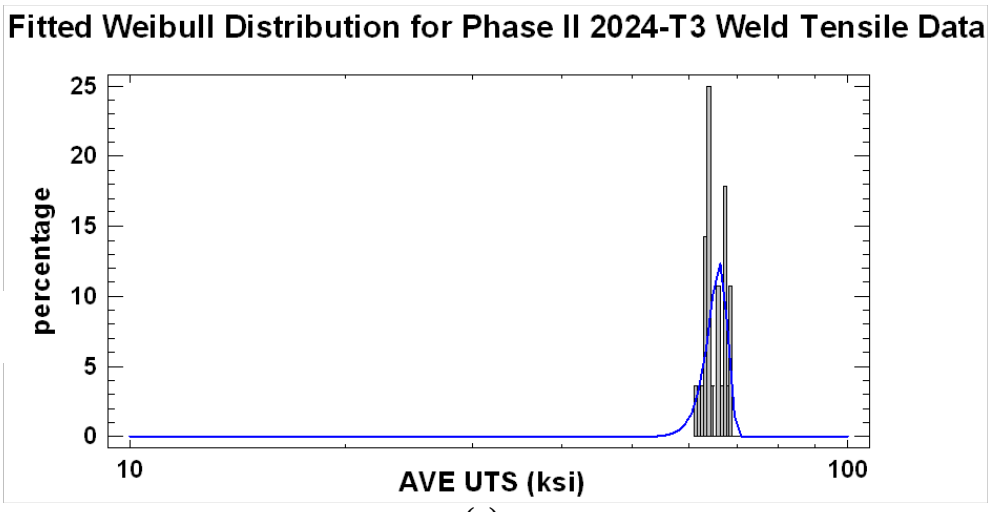

(c)

Figure 24. Statgraphics Weibull analysis of AA2024-T3 welds from Phase II: a) Statistical results, b) linearity of data, and c) comparison of data with normal distribution

The tensile data were entered into Statgraphics Centurion XVI.I and analyzed. A multiple regression analysis generated the residual plot shown in figure 25, which indicates that two studentized residuals were greater than two, but less than three, standard deviations from the mean. Therefore, these two data points were suspected of being outliers, and outlier identification tests were performed. Both the Grubb's test and Dixon's test did not identify any statistically significant outliers, so it was concluded that these two points were not significant outliers.

R^2 = 85.0722 percent
R^2 (adjusted for d.f.) = 82.4761 percent
Standard Error of Est. = 0.917595
Mean absolute error = 0.649171
Durbin-Watson statistic = 2.4167 (P=0.6866)

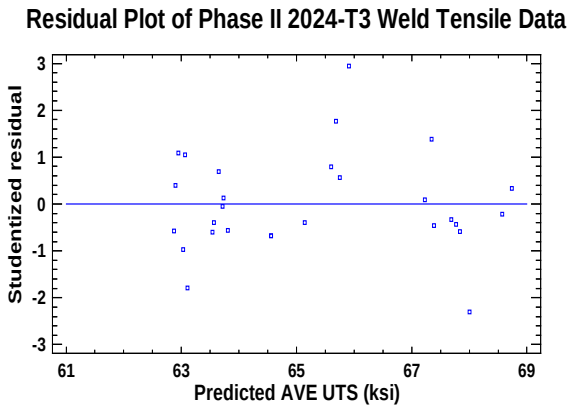

Figure 25. Statgraphics analysis studentized residuals plot of Phase II AA2024-T3 FSW tensile data

The weld data were evaluated according to the site where it was produced. The box-and-whisker plot shown in figure 26 compares the means of each site. The Airbus and Alcan data means are not statistically different from any of the other sites. The mean for the WSU data and the means for the LM data are statistically different from the other sites. The model for the box-and-whisker plot and some of the results are shown in figure 27.

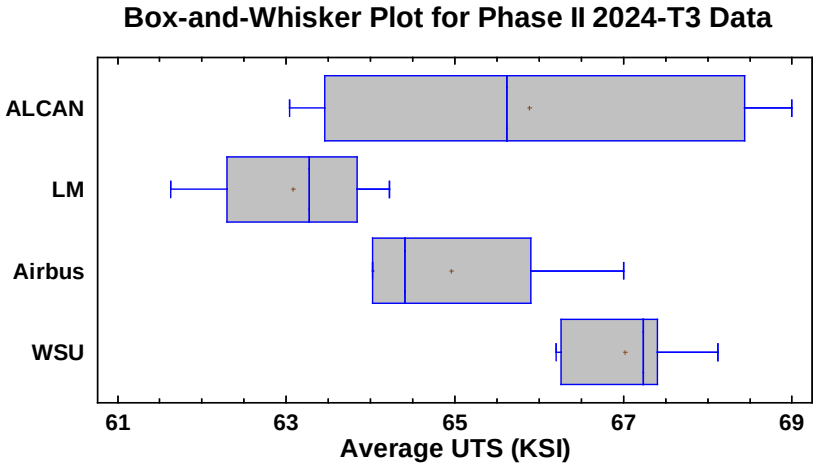

Figure 26. Statgraphics analysis Box-and-Whisker plot from a multiple-sample comparison of data from each site

The variance check shown in figure 27 indicates there was a statistically significant difference between the standard deviation of Alcan to WSU and Alcan to LM. The variability between sites was significant at a 95% confidence level, but low at 2.19 to 3.93 ksi. This analysis of variation (ANOVA) does not adjust for the hot-weld parameters versus the cold-weld parameters. Therefore, it may be possible to improve the model and decrease the variation. The data consist of only four welds of 0.25-inch AA2024-73 from three sites and four welds of 0.125-inch AA2024-T3 from four sites. Increasing the number of welds evaluated would possibly improve the statistical analysis of the data.

Multiple-Sample Comparison

Sample 1: ALCAN (AVERAGE UTS)
Sample 2: LM
Sample 3: Airbus
Sample 4: WSU
Sample 1: 8 values ranging from 63.04 to 69.0
Sample 2: 8 values ranging from 61.63 to 64.22
Sample 3: 5 values ranging from 64.02 to 67.0
Sample 4: 8 values ranging from 66.2 to 68.12

ANOVA Table

Source	Sum of Squares	*Df*	Mean Square	*F*-Ratio	*P*-Value
Between groups	66.312	3	22.104	8.14	0.0007
Within groups	65.1453	24	2.71439		
Total (Corr.)	131.457	27			

Summary Statistics

	Count	Average	Standard deviation	Coeff. of variation	Minimum	Maximum	Range
ALCAN	8	65.8813	2.63306	3.99668%	63.04	69.0	5.96
LM	8	63.085	0.915923	1.45189%	61.63	64.22	2.59
Airbus	4	64.83	1.5597	2.40583%	63.44	67.0	3.56
WSU	8	67.015	0.701407	1.04664%	66.2	68.12	1.92
Total	28	65.2561	2.20653	3.38135%	61.63	69.0	7.37

	Stnd. skewness	Stnd. kurtosis
ALCAN	0.0833122	-1.44506
LM	-0.502887	-0.683538
Airbus	1.00442	0.544954
WSU	0.0610319	-0.66987
Total	0.298234	-1.52308

Multiple Range Tests
Method: 95.0 percent LSD

	Count	Mean	Homogeneous Groups
LM	8	63.085	X
Airbus	4	64.83	XX
ALCAN	8	65.8813	XX
WSU	8	67.015	X

Table of Means with 95.0 percent LSD intervals

			Stnd. error		
	Count	*Mean*	*(pooled s)*	*Lower limit*	*Upper limit*
ALCAN	8	65.8813	0.582493	65.0312	66.7313
LM	8	63.085	0.582493	62.2349	63.9351
Airbus	4	64.83	0.82377	63.6278	66.0322
WSU	8	67.015	0.582493	66.1649	67.8651
Total	28	65.2561			

Contrast	Sig.	Difference	+/- Limits
ALCAN - LM	*	2.79625	1.70018
ALCAN - Airbus		1.05125	2.08229
ALCAN - WSU		-1.13375	1.70018
LM - Airbus		-1.745	2.08229
LM - WSU	*	-3.93	1.70018
Airbus - WSU	*	-2.185	2.08229

*** denotes a statistically significant difference.**

(a)

Variance Check

	Test	*P-Value*
Levene's	14.9226	0.000010831

Comparison	*Sigma1*	*Sigma2*	*F-Ratio*	*P-Value*
ALCAN / LM	2.63306	0.915923	8.26427	0.0124
ALCAN / Airbus	2.63306	1.5597	2.84996	0.4197
ALCAN / WSU	2.63306	0.701407	14.0923	0.0024
LM / Airbus	0.915923	1.5597	0.344854	0.2224
LM / WSU	0.915923	0.701407	1.70521	0.4981
Airbus / WSU	1.5597	0.701407	4.94473	0.0752

Kruskal-Wallis Test

	Sample Size	*Average Rank*
ALCAN	8	16.5625
LM	8	6.6875
Airbus	4	13.75
WSU	8	20.625

Test statistic = 12.1975 P-Value = 0.00673599

(b)

Figure 27. Statgraphics multiple sample comparison: a) results of analysis and b) variance check and Kruskal-Wallis

The residual plot shown in figure 28 was generated from a simple regression analysis of the Phase II AA2024-T3 tensile data, grouped according to the tensile coupon location in the weld joint line. In this evaluation, only the welds that were considered to be in the four corners of the process window were evaluated because extra welds were made using central process window parameters. One data point was noted at -2, but no other possible outliers were observed. Since this was the point for two standard deviations, it was not considered to be a concern at that time. A multiple-sample comparison with the data grouped according to tensile coupon location in the weld joint line was used to generate the box-and-whisker plot in figure 29. The analysis, which had a *P*-value of 0.996, showed the differences between the means of each group of data. A Kruskal-Wallis test, which assumes all medians are the same, shows no statistical difference between the medians of the groups with a 95% confidence. The *P*-value was 0.994.

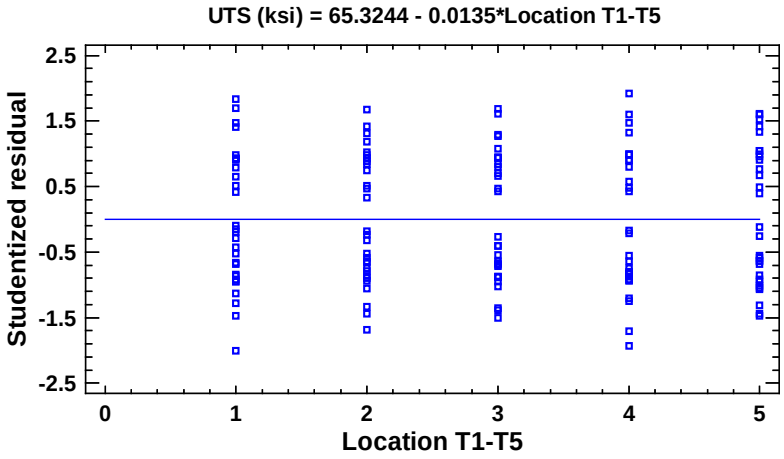

Figure 28. Residual plot for tensile data generated from a simple regression analysis of the UTS data for Phase II AA2024-T3 FSW welds

The two WSU_29 tensile coupons (*T*1 and *T*4), which had lower tensile strengths, were not outliers, but did contribute to increased variation (see figure 29) because the *T*1 and *T*4 boxes show a larger standard deviation. There is evidence that a defect-free weld is uniform in tensile strength from beginning to end.

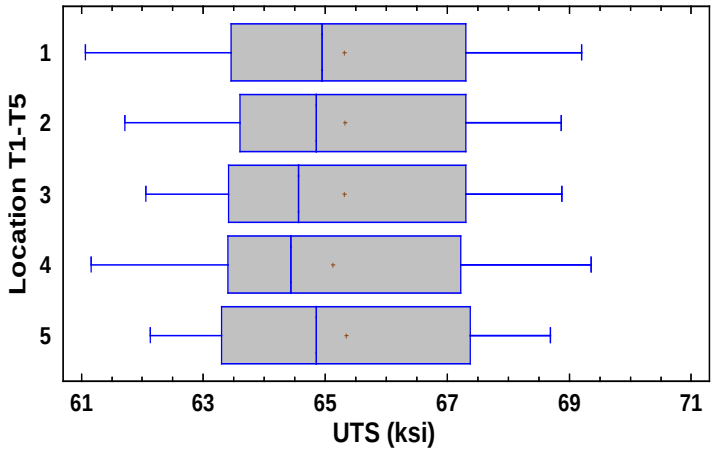

(Each group represents a location along the weld joint line)

Figure 29. Box-and-Whisker plot comparing the means of four groups of data

The welds were grouped according to the location of the weld parameters in the process window. Figure 30 shows the results of a one-way ANOVA of the welds, which were grouped according to weld parameters within the process window (The first letter, either *H* or *L*, represents the rpm, and the second letter represents the ipm.). The ANOVA table and results of a variance check are shown in figure 30(a). The *P*-value for the variance check analysis was 0.8455. This indicated no significant difference in the standard deviations between the groups of data, with a 95% confidence level. The Kruskal-Wallis test of the medians resulted in a *P*-value of 0.72675, which indicated no significant difference between the medians of the groups of data at a 95% confidence level because the *P*-value was >0.05 (see figure 30(b)). The fact that there are no outliers reinforces the conclusion that the two LM average weld tensile strengths that are below the T_{99} line are not significantly below. This also indicates the third may not be significant, especially because the tensile strength could be improved with measures to eliminate the void and joint remnant line.

Source	Sum of Squares	*Df*	Mean Square	*F*-Ratio	*P*-Value
Between groups	5.82433	3	1.94144	0.37	0.7747
Within groups	125.633	24	5.23471		
Total (Corr.)	131.457	27			

Variance Check

	Test	*P*-Value
Levene's	14.9226	0.000010831

Comparison	Sigma1	Sigma2	*F*-Ratio	*P*-Value
ALCAN/LM	2.63306	0.915923	8.26427	0.0124
ALCAN/Airbus	2.63306	1.5597	2.84996	0.4197
ALCAN/WSU	2.63306	0.701407	14.0923	0.0024
LM/Airbus	0.915923	1.5597	0.344854	0.2224
LM/WSU	0.915923	0.701407	1.70521	0.4981
Airbus/WSU	1.5597	0.701407	4.94473	0.0752

Kruskal-Wallis Test

	Sample Size	Average Rank
ALCAN	8	16.5625
LM	8	6.6875
Airbus	4	13.75
WSU	8	20.625

Test statistic = 12.1975 *P*-value = 0.00673599

ANOVA Table for Average UTS by Weld

(a)

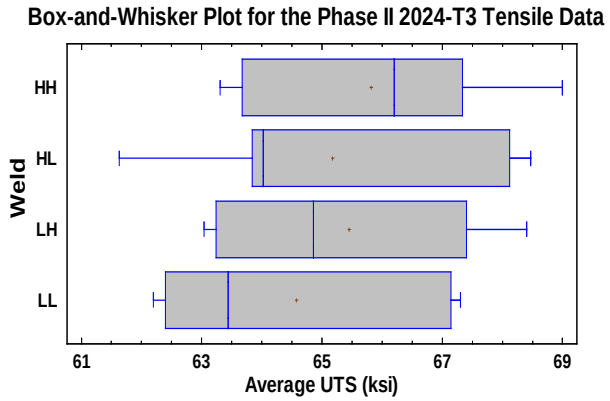

(b)

Figure 30. Analysis results of the data grouped according to the process window parameters sets: a) analysis results and b) Box-and-Whisker plot

The micrograph of an AA2024-T3 weld with the full-field microhardness contour map of the weld is shown in figure 31. The micrograph was representative of the AA2024-T3 welds. In this particular weld, the microhardness map was uniform with a hardness minimum in the root of the weld, and very little softening was associated with the HAZ/TMAZ border. Tensile tests resulted in a tensile strength of 67.3 ksi. The asymmetry of the weld could be observed with a narrow TMAZ on the advancing side; the retreating side is diffused in this area. This is secondary to the flow of material around the probe and the influence of the shoulder at the surface.

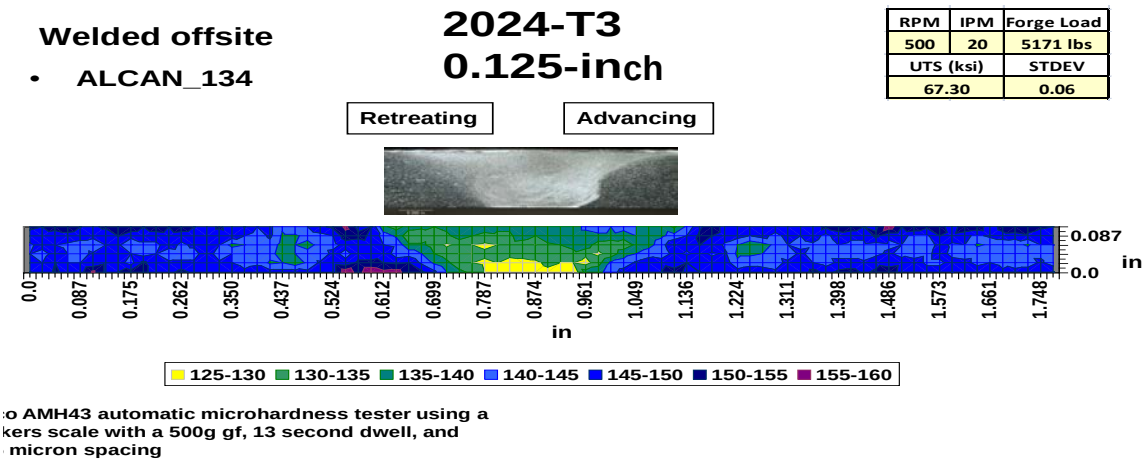

Figure 31. Micrograph of a specimen with the microhardness map from the ALCAN-134 weld in the 0.125-inch AA2024-T3 material

The microhardness map shown in figure 32 was taken from figure 4. Also shown is a graph of the average values of lines 5 through 7 (the middle three lines) of the hardness data. There are minimums associated with the HAZ at approximately 0.25 inch on both sides of zero and a maximum to the right of zero, which is in the nugget. Outside the HAZ, there is a minimum on both sides of the nugget. The hardness in the area between the HAZ and outer minimum approximately matched the base material hardness. The shoulder used to produce this weld was 0.6 inch in diameter. The beginning of the outer area of lower hardness was just outside the shoulder by ~0.10 inch, as shown by the width measurement of 0.788 inch between the lines at the inside edges. The classic *W* formed by the hardness values across the weld is evident. A study by Jones, et al. [81], examined the area between the nugget and outer minimum. Transmission electron microscopy (TEM) images obtained during the study showed that the area between the HAZ and outer minimum had a microstructure similar to the base material, but with very fine *S*-phase precipitates, which contributed to the increase in hardness in that area. TEM images indicated no *S*-phases in the outer minimum area. It was believed that the outer-minimum hardness area was due to dissolution of the fine *S*-phase particulates with the small elevation in temperature during the weld cycle.

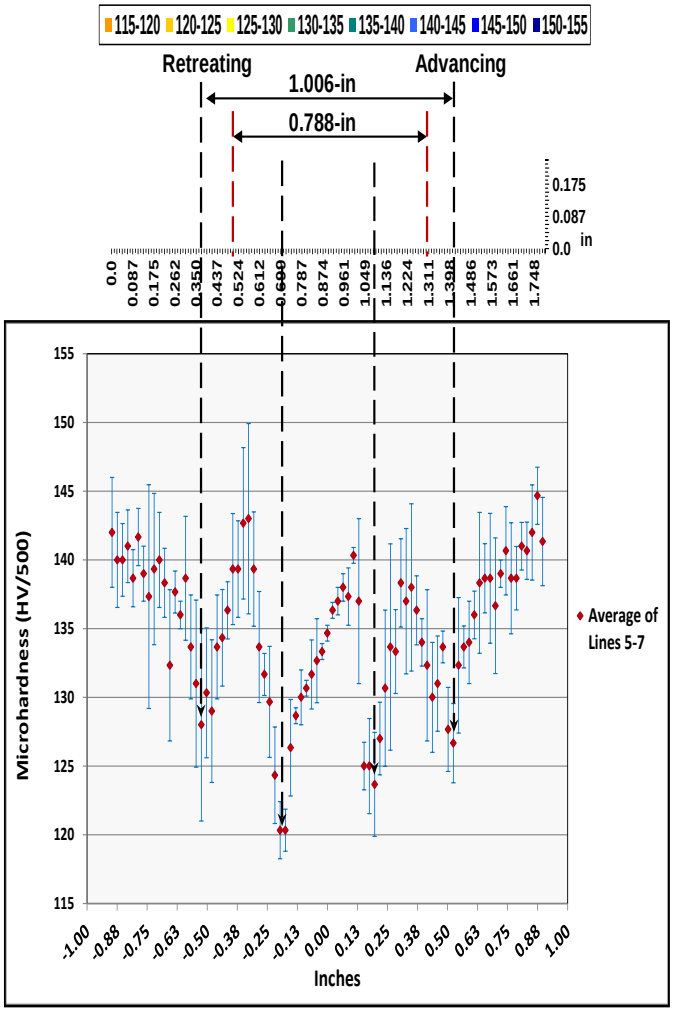

(Variation shown is ± one standard deviation.)

Figure 32. Microhardness map from figure 4 with graph average of lines 5–7 from microhardness data with minimums connected with corresponding area of microhardness map by dashed lines

The graph of the midline (line 6 of 12) from all 0.25-inch Alcan weld microhardness data and line 3 of 6 from the 0.125-inch Alcan weld microhardness data is shown in figure 33. The hardness graphs for the 0.125-inch weld data is higher than for the 0.25-inch weld data. The cause of this is not known, but it could be because of the different tool designs used for the various thicknesses of materials, or the company could have two welding machines or two anvils. Any one of these reasons could explain the difference. Still the *W*-form of the graph can be observed in the weld-zone area, and the outer minimums are present at 0.612 inch. Each of the two groups of data is close to values within their groups.

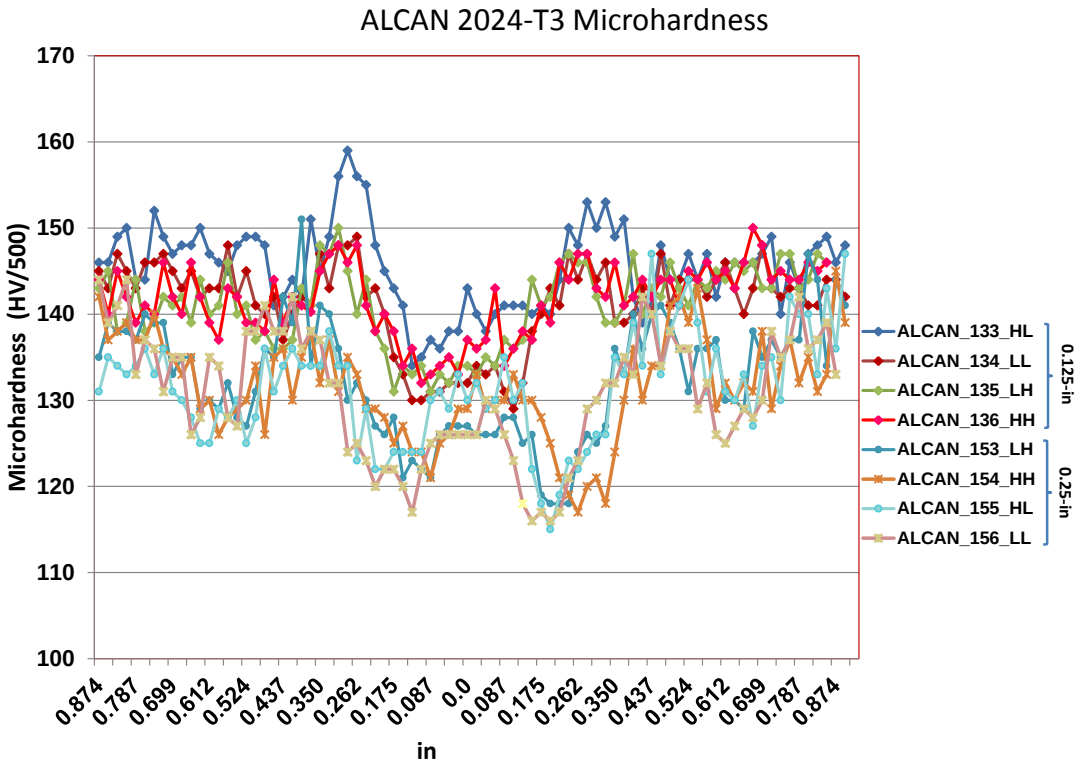

Figure 33. Graphs of middle line of microhardness data from all Alcan AA2024 welds

Because the strength of the weld depends on the final microstructure gradients in the weld, the hardness distribution is an indication of the strength of a defect-free weld. Full-field microhardness contour maps from the welds made with the 0.800-inch WSU Wiper and the 0.800-inch Tri-flute are shown in figure 34. These welds were produced using very different welding tool designs, but using the same set of weld parameters for the two sets of welds. The WSU Wiper has three scrolls on the shoulder and twisted flats on a threaded probe. The Tri-flute has six full scrolls on the shoulder and twisted grooves on the probe. The red-bordered microhardness maps in figure 34 were made with a threaded probe with flats, and the 0.800-inch WSU Wiper shoulder and others were made with the Tri-flute probe with a scrolled shoulder. The black-dashed line indicates the direction of progression from hot welds to cold welds (based on the weld pitch, i.e., the ratio of rpm to ipm).

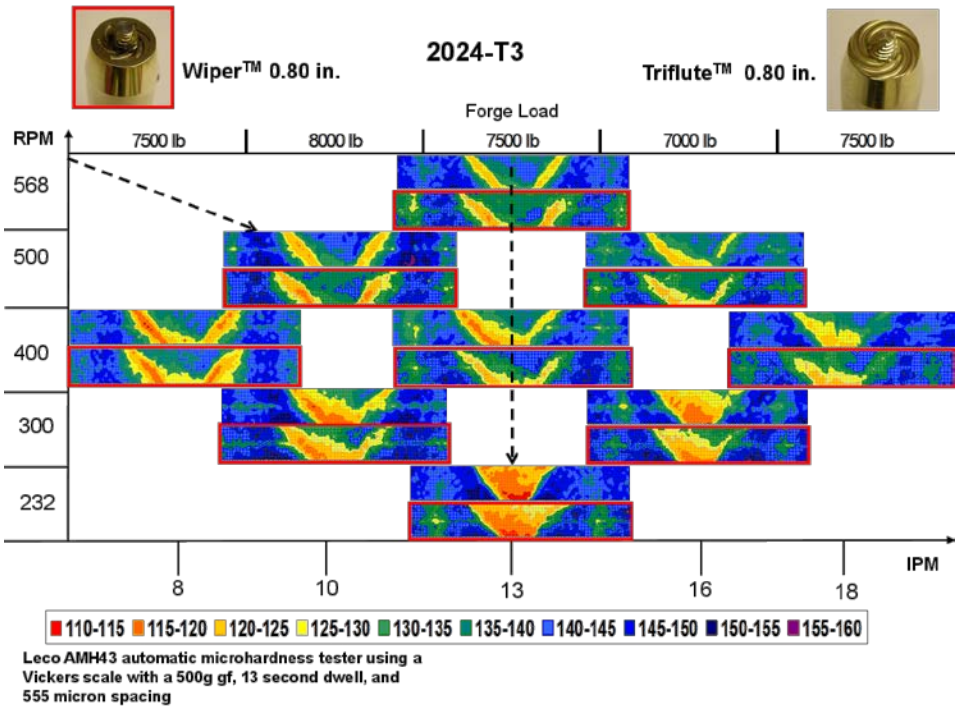

Figure 34. Weld microhardness maps for two tool designs at the same ipm and rpm

An end view of the two probes is shown in figure 35. The microhardness contour maps show the softened areas associated with the minimum hardness of the weld HAZ. These softened areas represent microstructural changes due to the thermomechanical and frictional energy introduced during the welding process.

The gradient changes shown in figure 34 indicate that the size of the HAZ/TMAZ and extent of the decrease in hardness can be, to some extent, controlled by changes in the weld parameters. The arrow indicates the direction of temperature change in the nugget, from the higher temperatures of a hot weld decreasing to the lower temperatures of a cold weld. The figure shows a thinning of the HAZ/TMAZ and a corresponding softening of the nugget. Eventually, the nugget becomes the area of minimum hardness because of overaging of the nugget material with decreased heat input. This is the progression for each forge load noted.

Changes in the gradients of the microhardness map are relatively the same from left to right and from top to bottom for each tool. In the hot welds (upper left), the temperatures reached during welding may be closer to the solidus temperature for the material, which results in a relatively wide and softened HAZ. However, the nugget exhibits a higher hardness because of the fine coherent grains that form due to dynamic recrystallization in the nugget as the tool passes along the joint line. To make a strong weld without defects it is better to avoid the extreme areas of the parameter window.

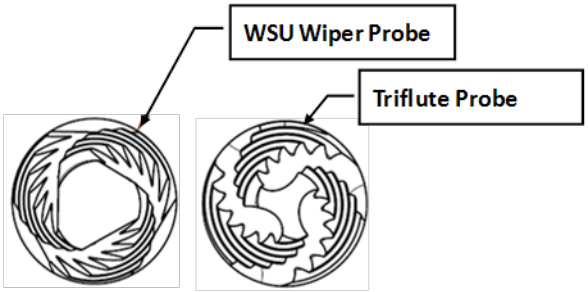

Figure 35. End view of a) twisted flats probe used with the WSU wiper tool shoulder and b) Tri-flute probe used with the full-scroll tool (see figure 6)

The TWI 5651 tool made very hot welds, as shown in figure 36, possibly due in part to the wide shoulder, resulting in a very wide HAZ and poor weld strength. This tool requires very low weld parameters (according to the predicted direction) to find the optimized parameter zone (see figure 12). It is unknown if it is possible to make a strong defect-free weld at such low rpm or ipm parameters. This tool may require adjustment to the design to make a good weld. The HAZ is very wide and the microhardness minimums are lower than with the WSU Wiper and Tri-flute tools. A duplicate weld was made with one weld parameter set, which is shown at the bottom right of figure 36. The duplicate weld and the other with the same parameters are outlined in purple. As the maps show, the gradients are the same in the repeated weld as in the original weld with the same parameters. Therefore, there is evidence that repeated parameters produce the same hardness gradients with the same tool and relatively the same hardness gradients with different tools.

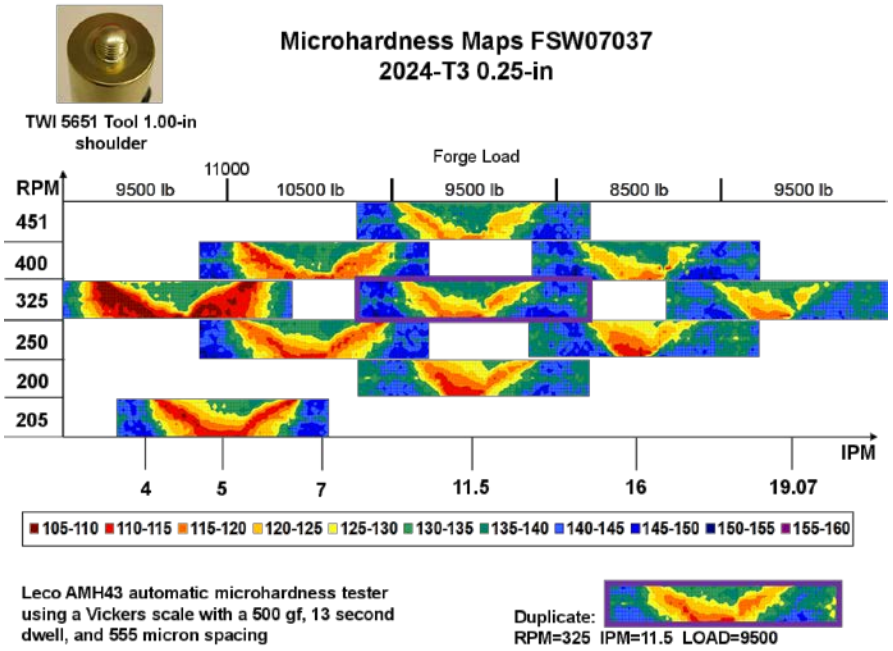

(Maps outlined in purple were made with the same weld parameters)

Figure 36. Microhardness maps for welds produced with the TWI 5651 tool

The microhardness contour maps for the welds shown in figure 37 have a fairly uniform hardness with higher minimums than the other welds (note the uniformity across these welds and the limited amount of softening). The top weld was from Phase I and was the only weld in that phase that produced a nominally uniform hardness map. Although it had higher minimum microhardness values, it had a lower tensile strength, possibly due to a weld defect. The other welds were produced in Phase II and have very high tensile strength and higher microhardness minimums. These welds are all made with parameters using the highest rpm and higher travel speeds, which are parameters at the edge of the process window. Although the welds can have higher strengths, it is possible to develop weld defects with the extreme parameters.

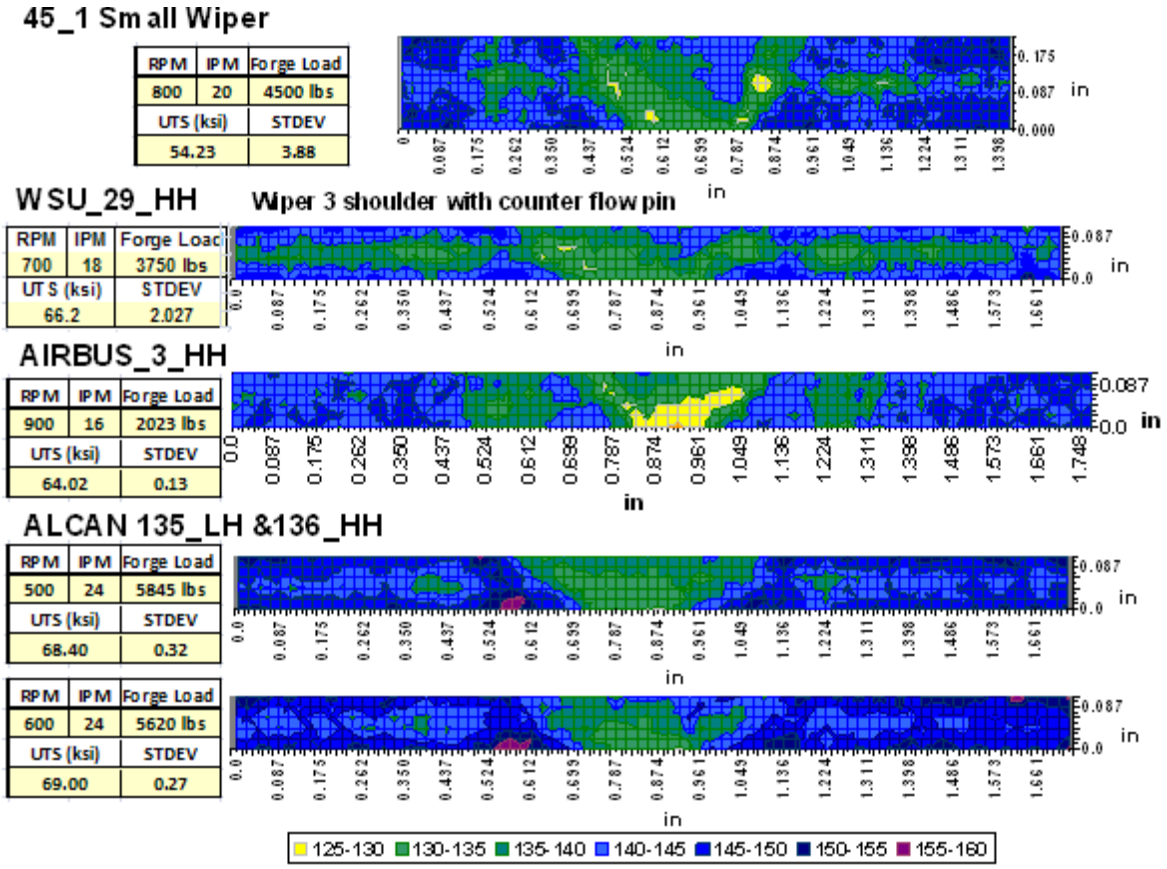

Figure 37. Microhardness maps of welds produced by WSU, Airbus, and Alcan showing very little HAZ hardness loss and similar hardness in the stir zone to parent material properties

There were 65 tensile test results from 13 welds in AA2198-T8 material welds. The failures in the tensile specimens for the majority of the AA2198-T8 material welds followed a line from the surface of the weld nugget on one side of its centerline at an approximate 45-degree angle to the root base material crossing the line of the TMAZ. Figure 38 shows the approximate line of failure of those tensile specimens. In the figure, the blue-dashed lines show the approximate site for the TMAZ, HAZ, and nugget; the black line shows the approximate line of failure for this weld. Three of the WSU15 tensile specimens failed at the TMAZ, and WSU10 and WSU11 each had one tensile failure in the nugget. All others failed from the nugget through the TMAZ to the base material, as in figure 38. The ALCAN_86 and ALCAN_88 welds each had one weld tensile that failed at the TMAZ or HAZ boundary and the rest failed from the surface through the TMAZ to the base material. Airbus_3 had two tensile specimens fail in the HAZ, and all others failed from the weld surface through the TMAZ to the base material.

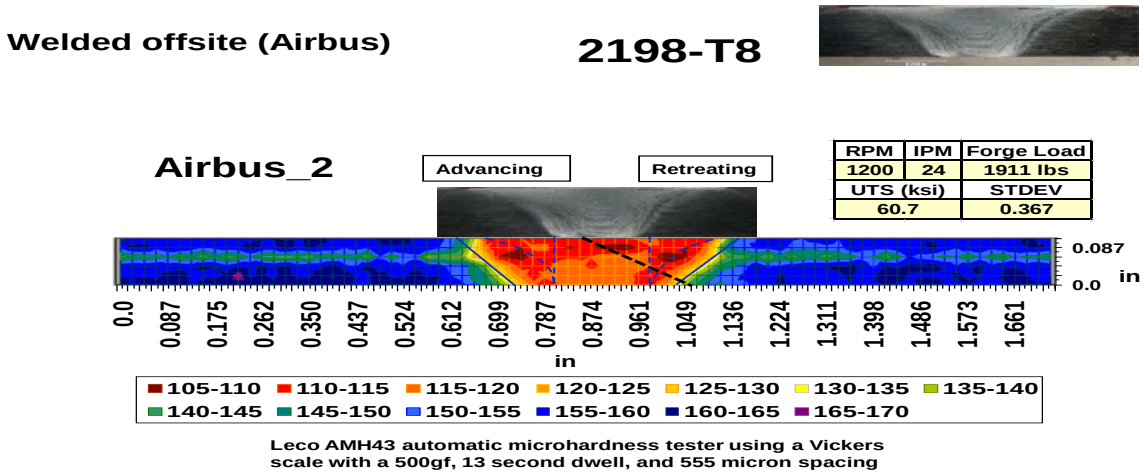

Figure 38. Metallographic specimen shown above microhardness map of AA2198-T9 weld

Most LM welds failed in the nugget, with the weld line visible at the root of the weld as if there had been a lack of penetration (LOP), but visual inspection of the welds under magnification did not show obvious LOP. The metallographic specimens were inspected at high magnification as shown in figure 43. All LM 2198-T8 welds were determined to have a remnant of the faying surface (joint line) present, which would affect the strength of the weld [82] (see figures 39(a) to 39(d)). The presence of the faying surface remnant indicates there was inadequate mixing of the material when the welds were made. A void was found in the LM_31 weld, which would explain why it had the lowest UTS value (see figures 39(e) and 39(f)). The coldest weld had the lowest tensile strength. This would indicate that adjustments to the weld parameters or adjustments to the weld tool design could improve the strength of those welds.

LM_33 (HL)

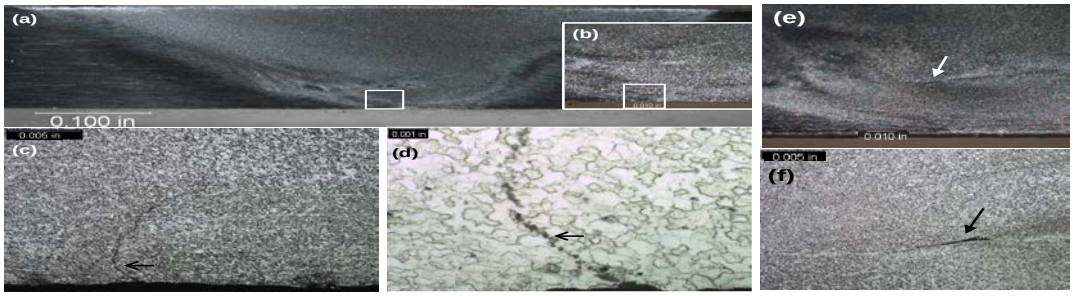

LM_31 (LH)

Figure 39. Micrograph sections of LM_33 AA2198-T8 weld: a) macrosection, b) higher magnification of section noted by square in previous view, c) further magnification of outlined section with faying surface remnant identified by arrow, d) higher magnification of faying surface, e) micrograph of LM_31 AA2198-T8 weld identifying void location, and f) higher magnification of void

The tested tensile strength for the AA2198-T8 material used in this study was 79.8 ksi. The tensile results ranged from 54.4 to 62.7 ksi. Therefore, all welds were at least 68% of the parent material strength, and 75% of the data were found to be greater than 58 ksi or 72.7% of the parent tensile strength. The average tensile strength of all welded AA2198-T8 material was 59.46 ksi, which would be 74.9% of the parent material strength; 56% of the data had average UTS values that were equal to or greater than 59.7 ksi.

Figure 40 shows a frequency histogram of the UTS values for the welds from the AA2198-T8 material, indicating how well the data from the AA2198-T8 material welds fit a normal distribution. The normal probability plot, which shows the linearity of the data, is shown in figure 40(a). The data plot is fairly linear, and the frequency histogram indicates possible normal distribution of the UTS values. A studentized residual plot, shown in figure 41, has no indication of outliers because absolute values for the standard deviations are less than 3. Data points greater than 2 are suspect. One point is at approximately 2.5 standard deviations from the mean. However, using outlier identification tests (Grubb's and Dixon's tests), no significant outliers were found; therefore, it was concluded that the point at 2.5 standard deviations was not a concern.

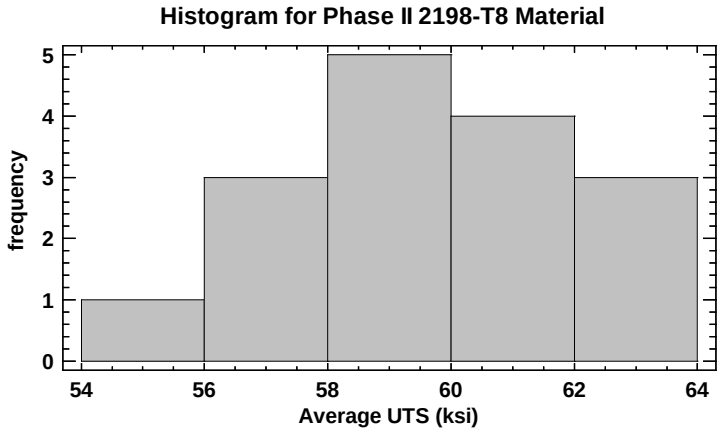

(a)

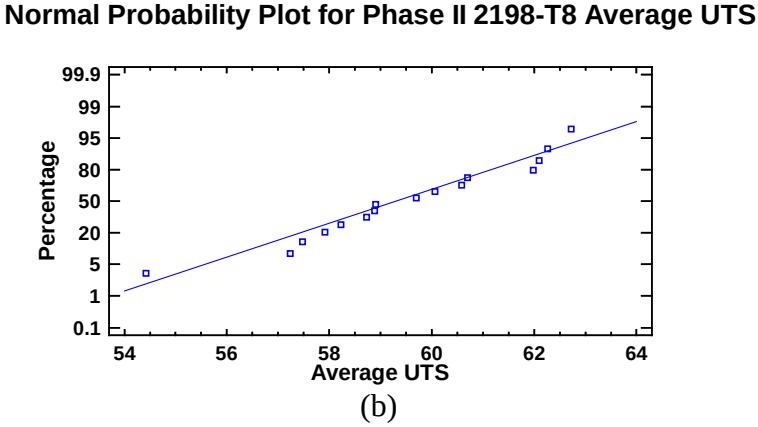

(b)

Figure 40. Normality check of Phase II AA2198-T8 weld tensile data: a) frequency histogram and b) normal probability plot

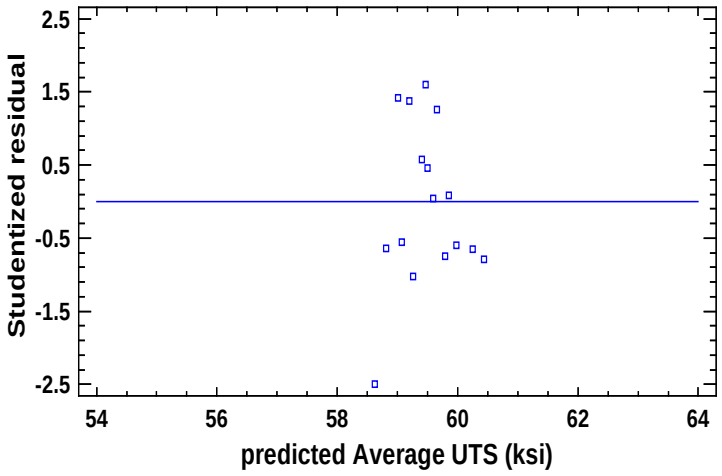

Figure 41. Residual plot for Phase II AA2198-T8 welds tensile data

A Weibull analysis is shown in figure 42. The UTS values, shown in figure 42(a) are linear and are fitted to a Weibull distribution shown in figure 42(b). The data, which show a normal distribution, were evaluated in Statgraphics. From the Weibull analysis, it was not clear if the data fit a Weibull distribution with a 95% confidence.

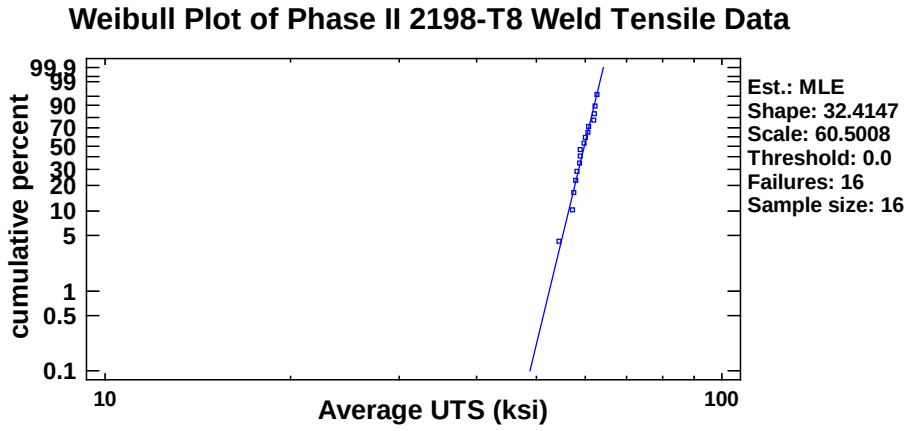

(a)

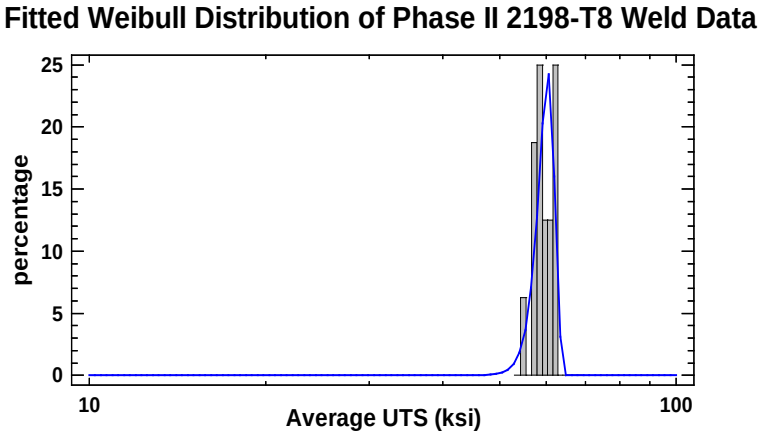

(b)

Figure 42. Weibull analysis for Phase II AA2198-T8 welds: a) plot of linearity and b) fitted Weibull plot

When the average tensile data were grouped according to the site where the welds were produced, the variation was found to be significant but low, with the highest variations at 2 to 5.5 ksi. Some of the printed results, including the box-and-whisker plot from the analysis, are shown in figure 43.

Variance Check

	Test	*P-Value*
Levene's	0.942951	0.450433

Comparison	*Sigma1*	*Sigma2*	*F-Ratio*	*P-Value*
ALCAN / Airbus	0.31707	0.465331	0.464286	0.5448
ALCAN / LM	0.31707	1.58849	0.039842	0.0252
ALCAN / WSU	0.31707	0.324294	0.955943	0.9713
Airbus / LM	0.465331	1.58849	0.0858136	0.0736
Airbus / WSU	0.465331	0.324294	2.05895	0.5682
LM / WSU	1.58849	0.324294	23.9933	0.0268

Kruskal-Wallis Test for Average UTS by Company

Company	*Sample Size*	*Average Rank*
ALCAN	4	6.5
Airbus	4	10.5
LM	4	2.5
WSU	4	14.5

Test statistic = 14.1176   P-Value = 0.0027492

Multiple Range Tests for Average UTS by Company

Method: 95.0 percent LSD

Company_1	*Count*	*Mean*	*Homogeneous Groups*
LM	4	56.765	X
ALCAN	4	58.69	X
Airbus	4	60.26	X
WSU	4	62.265	X

Contrast	*Sig.*	*Difference*	*+/- Limits*
ALCAN - Airbus	*	-1.57	1.32208
ALCAN - LM	*	1.925	1.32208
ALCAN - WSU	*	-3.575	1.32208
Airbus - LM	*	3.495	1.32208
Airbus - WSU	*	-2.005	1.32208
LM - WSU	*	-5.5	1.32208

* denotes a statistically significant difference.

(a)

Variance Check

	Test	P-Value
Levene's	0.942951	0.450433

Comparison	Sigma1	Sigma2	F-Ratio	P-Value
ALCAN / Airbus	0.31707	0.465331	0.464286	0.5448
ALCAN / LM	0.31707	1.58849	0.039842	0.0252
ALCAN / WSU	0.31707	0.324294	0.955943	0.9713
Airbus / LM	0.465331	1.58849	0.0858136	0.0736
Airbus / WSU	0.465331	0.324294	2.05895	0.5682
LM / WSU	1.58849	0.324294	23.9933	0.0268

Kruskal -Wallis Test for Average UTS by Company

Company	Sample Size	Average Rank
ALCAN	4	6.5
Airbus	4	10.5
LM	4	2.5
WSU	4	14.5

Test statistic = 14.1176 P -Value = 0.0027492

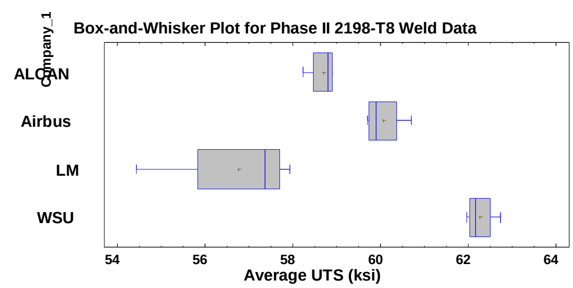

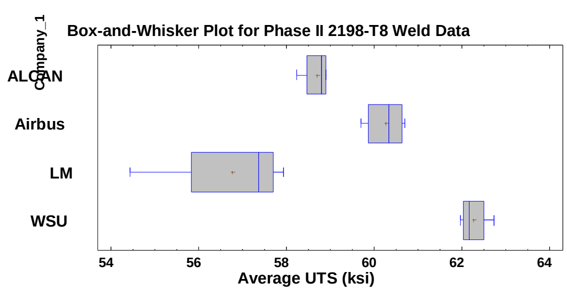

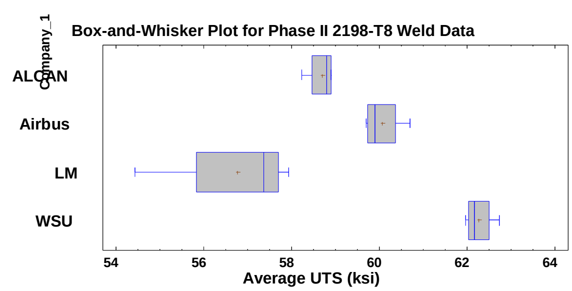

(b)

Figure 43. Statgraphics analysis: a) results and b) Box-and-Whisker plots from a multiple-sample comparison of AA2198 average tensile data, grouped according to site where the weld was produced

The welds were grouped by weld parameters HH, HL, LH, or LL and evaluated. Only the data from welds that could be considered to be in the four corners of the process windows were included. The Statgraphics multiple-sample comparison analysis results are shown in figure 44(a), and the variance check and Kruskal-Wallis test results are shown in figure 44(b). No indication of a significant difference between the means or medians for the welds was found when grouped as parameters HH, HL, LH, and LL. The box-and-whisker plot from the analysis is shown in figure 44(c). The variation of the average UTS is larger between sites than between welds, as shown in the box-and whisker plot of figures 43 and 44.

ANOVA Table

Source	Sum of Squares	*Df*	Mean Square	*F*-Ratio	*P*-Value
Between groups	1.13348	3	0.377827	0.09	0.9637
Within groups	45.8593	11	4.16903		
Total (Corr.)	46.9928	14			

(a)

Variance Check

	Test	*P-Value*
Levene's	0.581739	0.638204

Comparison	*Sigma1*	*Sigma2*	*F-Ratio*	*P-Value*
HH / HL	2.07191	2.09247	0.98045	0.9874
HH / LH	2.07191	3.32804	0.387585	0.4569
HH / LL	2.07191	1.95706	1.12082	0.9275
HL / LH	2.09247	3.32804	0.395314	0.4660
HL / LL	2.09247	1.95706	1.14316	0.9150
LH / LL	3.32804	1.95706	2.89179	0.4064

Kruskal-Wallis Test

	Sample Size	*Average Rank*
HH	4	9.75
HL	4	8.25
LH	4	7.75
LL	4	8.25

Test statistic = 0.397059 P-Value = 0.940849

(b)

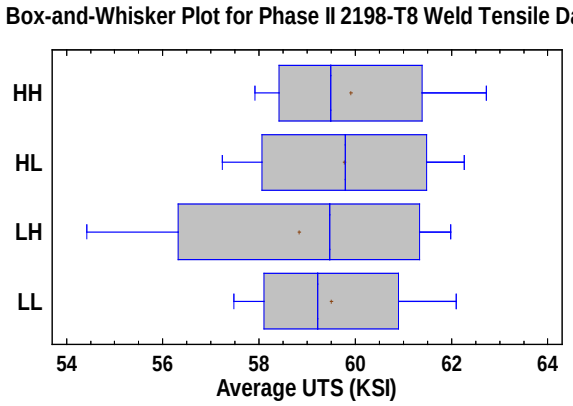

(c)

Figure 44. Average UTS values for welds analyzed with a multiple sample comparison: a) ANOVA table, b) Kruskal-Wallis test of medians, and c) Box-and-Whisker plot for means of UTS data sets

A Statgraphics multiple-sample comparison with the AA2198 tensile data grouped according to the location of the tensile specimen in the weld joint line is shown in figure 45. The variation check and Kruskal-Wallis test are shown in figure 45(a). The box-and whisker plot from the analysis shown in figure 45(b) indicates that the standard deviations for the means of the data groups are not significant. There were two points more than two standard deviations from the means. These points were from the LH weld produced at the LM site. The LH weld had the lowest average tensile strength at 54.42 ksi. This was the LM_31 weld with the void in it. Because the only weld with significantly different tensile results was the LH weld, there is significant evidence that a defect-free weld is uniform in tensile strength from beginning to end.

Variance Check

	Test	*P-Value*
Levene's	0.215241	0.929204

Comparison	*Sigma1*	*Sigma2*	*F-Ratio*	*P-Value*
T1 / T2	1.96989	2.3792	0.685524	0.4618
T1 / T3	1.96989	2.1623	0.829951	0.7140
T1 / T4	1.96989	2.22766	0.781958	0.6300
T1 / T5	1.96989	2.35274	0.701026	0.4885
T2 / T3	2.3792	2.1623	1.21068	0.7160
T2 / T4	2.3792	2.22766	1.14067	0.8021
T2 / T5	2.3792	2.35274	1.02261	0.9660
T3 / T4	2.1623	2.22766	0.942173	0.9097
T3 / T5	2.1623	2.35274	0.844659	0.7480
T4 / T5	2.22766	2.35274	0.8965	0.8352

Kruskal-Wallis Test for UTS by Location

Location	*Sample Size*	*Average Rank*
T1	16	40.375
T2	15	38.6333
T3	15	36.9667
T4	15	37.8
T5	15	38.6

Test statistic = 0.203764 P-Value = 0.995149

(a)

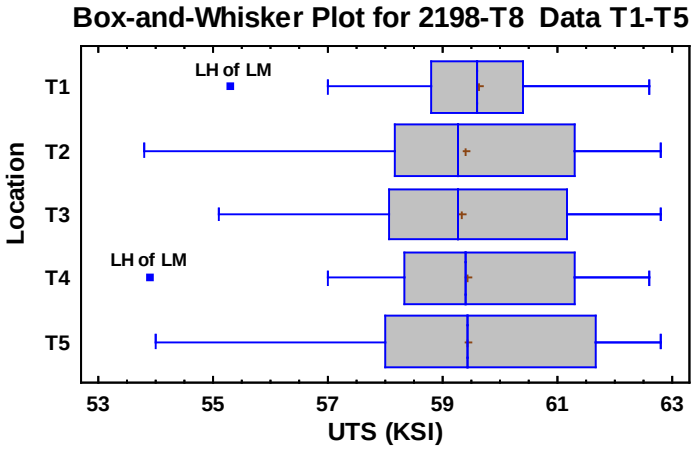

(b)

Figure 45. a) Statgraphics multiple-sample comparison analysis variance check with data grouped according to tensile specimen location in the weld joint line and b) Box-and-Whisker plot of means of the average UTS

Figure 46 shows the microhardness maps of the highest tensile strength welds in AA2198-T8 by site. The nugget is softer in the AA2198-T8 welds than in the AA2024-T3 welds. The average hardness of the nugget of the AA2198 welds was found to be approximately 68.6% of the base material hardness. The microhardness contour maps did not have the same relative changes in microhardness for the different microstructural areas of the weld, but there were only four welds for each site, so the changes may have been more distinguishable if there were more welds with parameters from each process window.

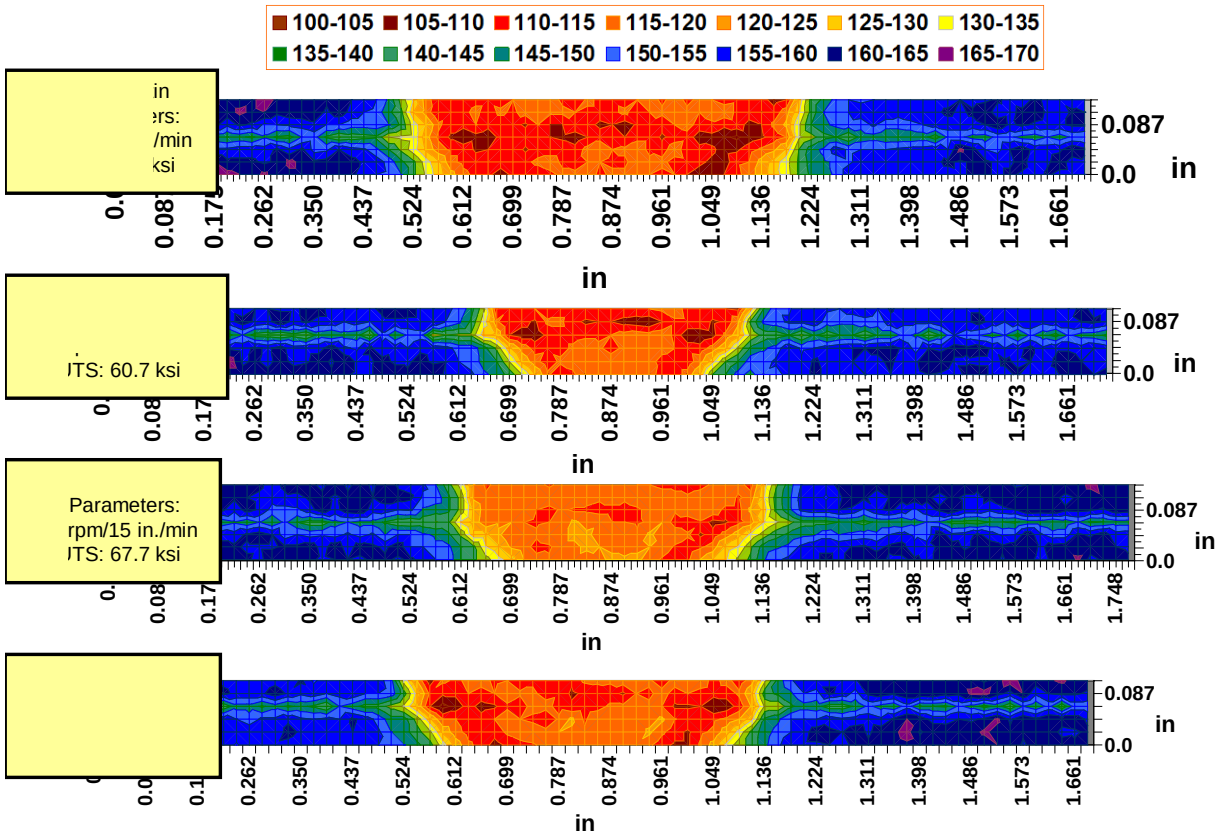

Figure 46. Microhardness maps for AA2198-T8 welds from each site that had the highest UTS values

The microstructural areas of the AA2198-T8 material welds can be more readily identified by comparing the microhardness contour map to the metallography of the weld cross section, as shown in figure 47. During FSW, dissolution of the T_1 phase (which contains Li) occurs. Since it is this phase that provides a significant proportion of the strengthening in the parent material, the weld zone must not be overheated to ensure the retention of acceptable properties. The extent to which the T_1 phase precipitates depends on thermal exposure [73]. It is believed that this is the mechanism that has the main effect on the weld zone hardness and strength in AA2198-T8 material.

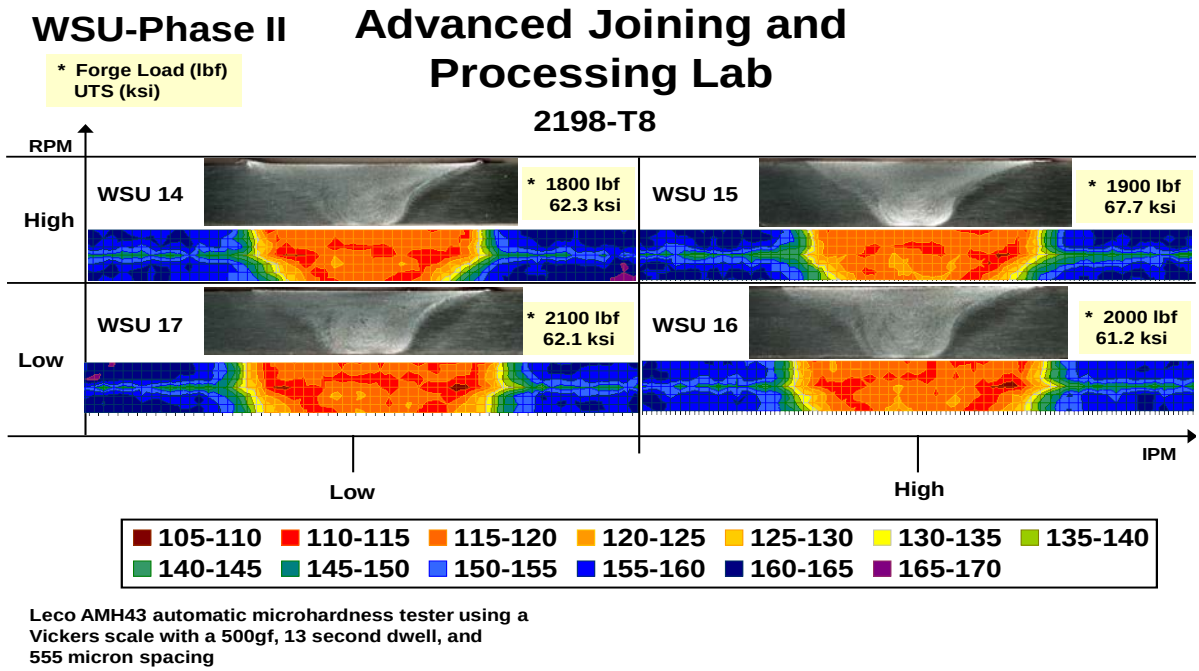

Figure 47. Full-field microhardness contour maps shown with the corresponding metallographic cross-sections of WSU AA2198-T8 welds

The centerline graphs for all WSU AA2198 welds are shown in figure 48 (WSU Centerline Graphs of welds and Micrograph of WSU_17 Weld) with the micrograph of the WSU_17 weld. The approximate location of the microstructural areas is labeled on the micrograph. The hardness measurements through the weld zone shown in figure 48 are not significantly different for all the WSU welds.

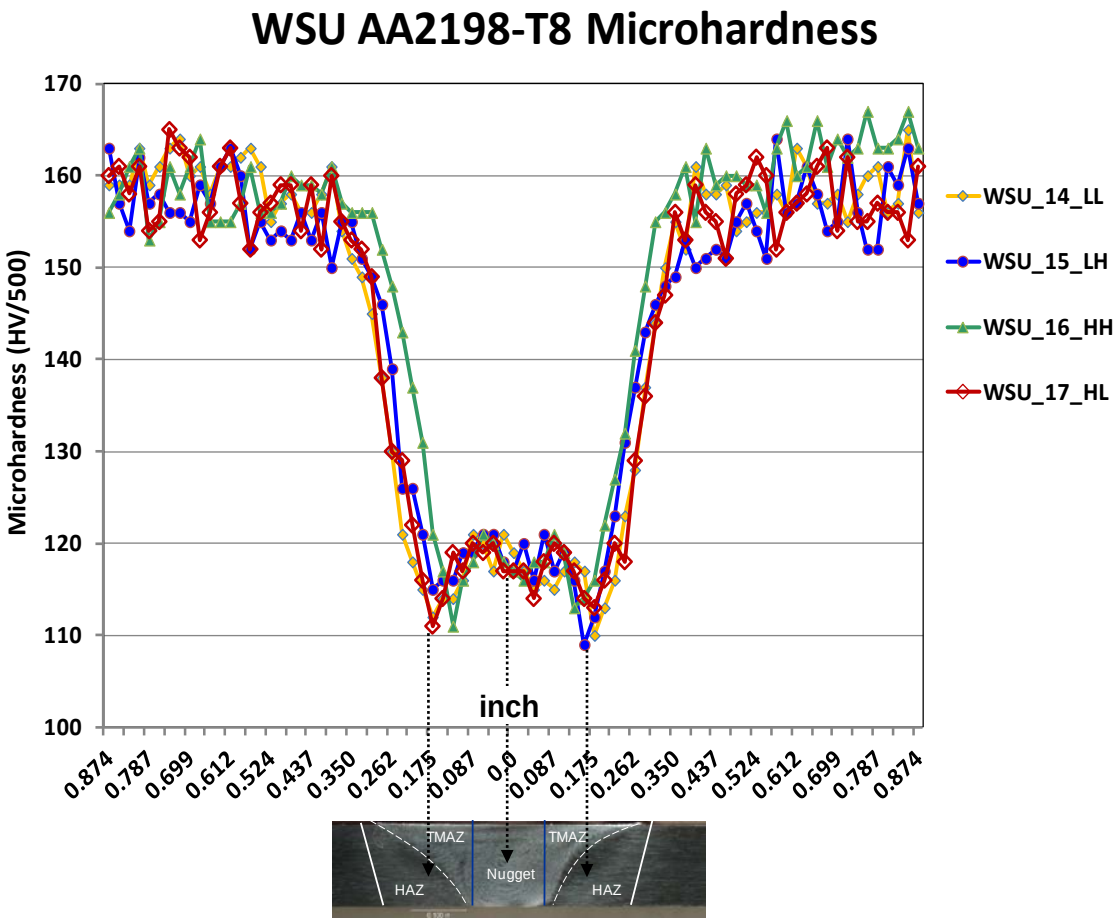

Figure 48. The WSU centerline graphs and the micrograph of WSU_17 welds

The minimum hardness measurements associated with the HAZ is shown at approximately 0.175 inch on both sides with an elevation associated with the nugget. There are no outer minimums observed in the AA2198 weld hardness maps. The centerline graphs of all the welds from the four sites are shown in figure 49. There is no significant difference in the hardness for any of the welds.

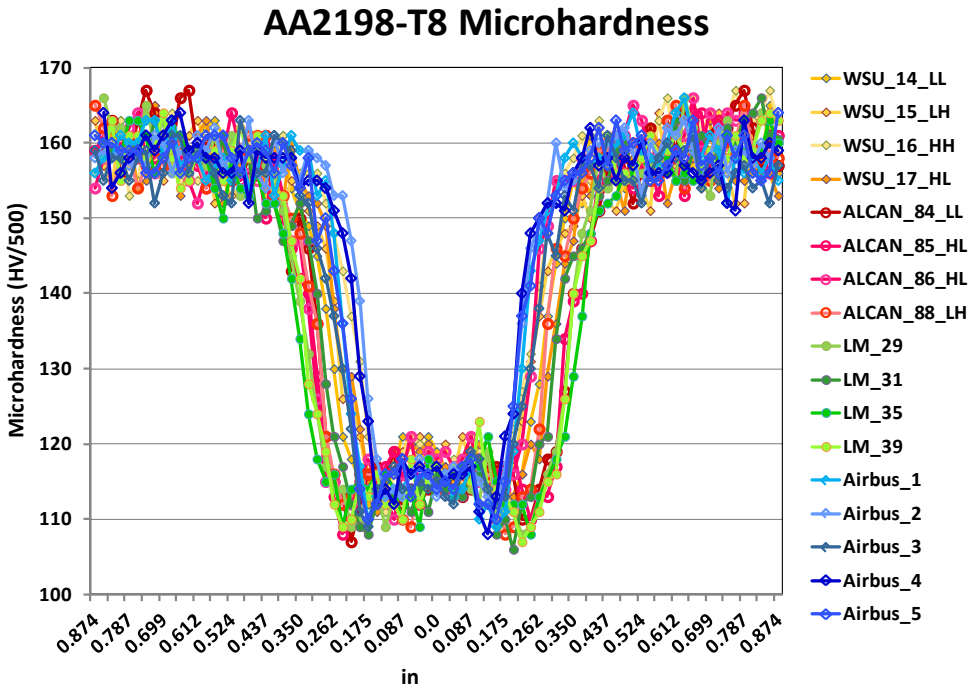

Figure 49. Microhardness data from the centerline of each weld of Phase II AA2198

Bounding welds were produced to determine the process window for the tool used to make the WSU AA2198-T8 welds. When the microhardness maps for the bounding welds (see figure 50) were compared to the microhardness results shown in figure 49, a significant difference in the minimum hardness values was noticed. The study welds had the same parameters as the WSU_1, WSU_9, WSU_10, and WSU_11 bounding welds, and the welds were produced with the same tool on the same machine; therefore, the microhardness results should be the same. The tensile results were also lower for each bounding weld compared to the corresponding study weld (see table 7). There were several possible explanations for this. It could have been due to the tensile specimen configuration differences between the coupon used by WSU and the one used by Westmoreland (see figure 51). Westmoreland also used a higher strain rate for testing. The differences in test results could have also been due to different load frames or operators. Another possibility is that the difference in UTS and hardness values were due to natural aging of the weld material. To investigate this, tensile specimens were made from leftover WSU study weld material and LM weld material in the configuration used by each site. There was a limited supply of leftover material from the study welds and no leftover material for the bounding welds, but the specimens tested for microhardness were available.

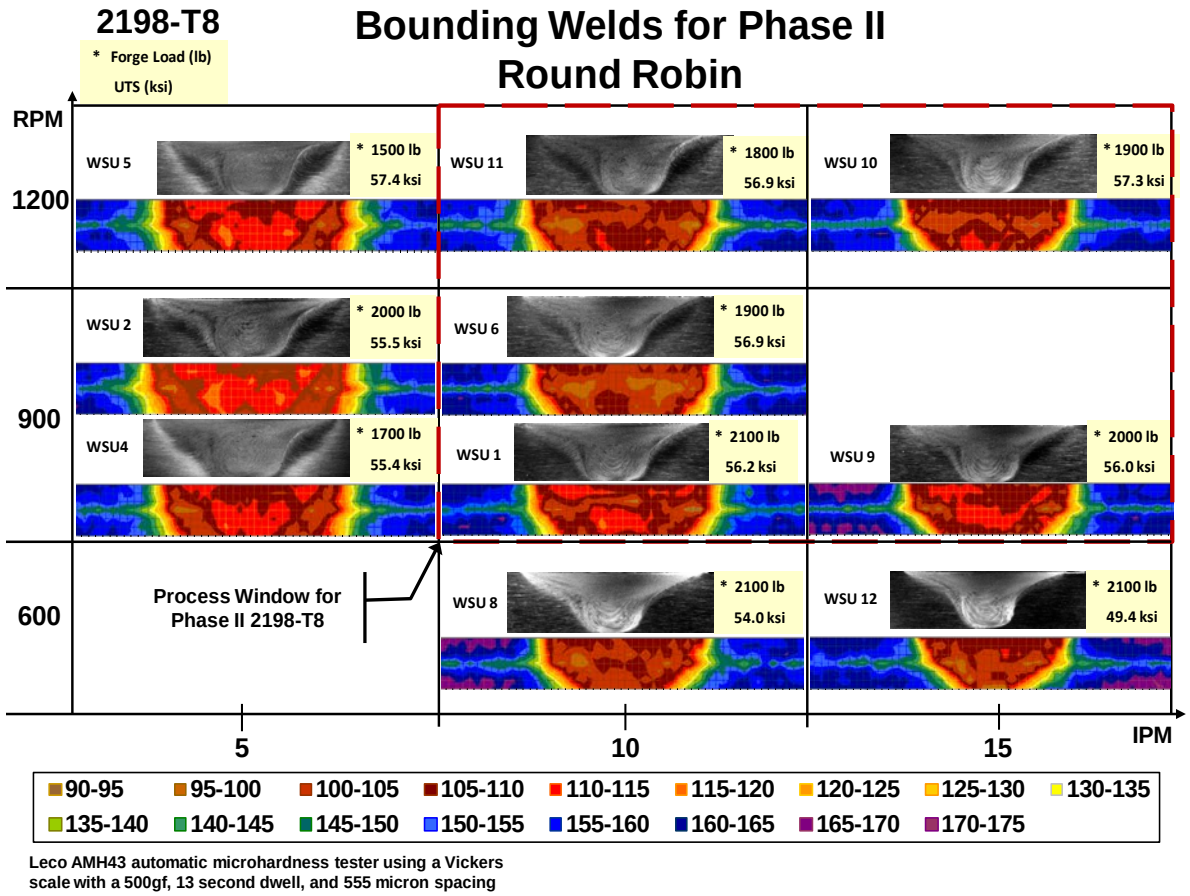

Figure 50. Full-field microhardness contour maps for WSU bounding welds that were microhardness tested within 40 days of welding

The configuration shown in figure 51(b) was used to test the LM welds at WSU; therefore, retesting with the LM tensile coupon would show if the tensile strength had changed since the welds were first tested. Tests using the tensile coupon configuration shown in figure 51(a) would indicate any difference due to the coupon configurations when compared to the first tensile test results. The coupon configuration shown in figure 51(a) was used previously by Westmoreland to test the WSU study welds. Therefore, tests using the WSU weld coupon configuration (figure 51(a)) would indicate if there was any change in tensile strength since the welds were first tested by Westmoreland, and tests using the configuration in figure 51(b) would indicate differences due to the coupon configuration when compared to the previous results. Some tensile specimens were tested with the Westmoreland rate and some with the WSU rate. Microhardness tests were repeated on the bounding weld specimens tested previously.

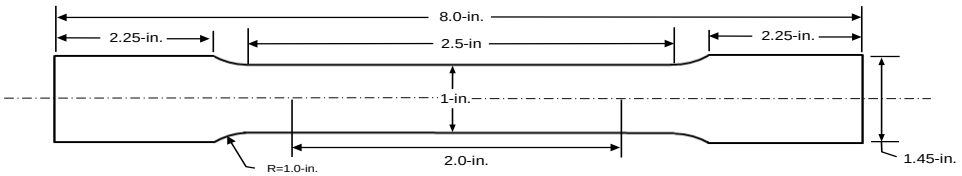

(a)

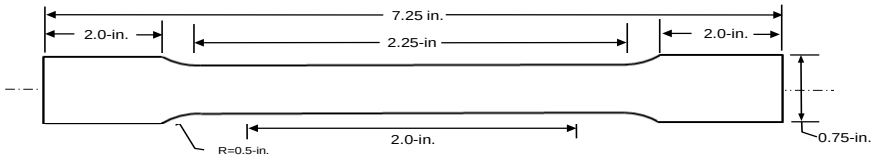

(b)

Figure 51. Configurations for tensile specimens used for tensile tests of FSW: a) ASTM E8 configuration used by Westmoreland for tensile tests and b) ASTM E8 configuration used by WSU

Tensile tests were performed at WSU on July 28, 2008, after 100 hours of natural aging of the bounding welds, and were retested again almost 3 years later. Because the WSU study welds had to be packaged, shipped to Westmoreland, and then cut up by Westmoreland before they could be tested, those welds were not tested until June 25, 2009, which was 11 months after they were welded. The tensile retest results are shown in table 11. The control tensile tests checked for changes in tensile strength from the original tensile tests. There was no significant change in the UTS values for the tensile retest results performed at WSU compared to the original test results from Westmoreland. Therefore, there is evidence that the different tensile test results were not due to the different test sites (equipment or operators), configurations, or strain rates.

Table 11. Results of tensile retesting of AA2198-T8 weld material to investigate the cause of differences in test results (for coupon configurations, see figure 51)

Weld Number	Tensile	Width	Thickness	2% Yield	UTS (ksi)	% Elongation	Configuration and Test Rate	Original Avg. UTS (ksi)	Original Stdev
AJP09005_ALCAN_2198_85	T1	0.999	0.127	44.1	60.7	5.70	Their tensile (a) – their rate	58.9	0.18
	T2	0.998	0.127	44.6	61.3	6.16	Their tensile (a) – their rate		
	T3	0.501	0.128	42.4	59.4	6.68	Our tensile (b) – their rate		
	T4	0.498	0.127	43.6	61.0	6.68	Our tensile (b) – their rate		
	T5	0.504	0.126	43.1	60.9	6.91	CONTROL tensile (b) – our rate		
AJP09005_LM_2198_31	T1	0.503	0.152	42.9	54.6	2.87	CONTROL tensile (b) – our rate	54.4	0.72
	T2	0.497	0.152	42.7	54.6	2.88	CONTROL tensile (b) – our rate		
	T3	1.001	0.152	44.0	52.5	2.27	Their tensile (a) – their rate		
	T4	0.988	0.152	43.6	55.2	3.00	Their tensile (a) – their rate		
	T5	1.001	0.152	43.4	53.0	2.64	Their tensile (a) – their rate		
AJP08020_17	T1	0.501	0.148	43.5	60.6	6.37	Our tensile (b) – their rate	62.3	0.2
	T2	0.499	0.148	43.5	60.9	6.11	Our tensile (b) – their rate		
	T3	0.505	0.148	44.4	61.6	6.10	Our tensile (b) – their rate		
	T4	0.998	0.148	46.2	62.7	5.26	CONTROL tensile (a) – their rate		

Their = Westmoreland
Our = WSU

For comparison, the full-field microhardness contour maps from retesting the AA2198-T8 bounding weld metallographic specimens are shown in figure 52 with the previous microhardness contour maps from testing the same specimens. The microhardness full-field contour maps of the WSU bounding welds are observed to be much like the study weld results (see figures 47 and 50). The minimum hardness values for the bounding welds are 105 to 108 HV/500, which is close to the 107 to 109 HV/500 range for the study welds. The original range of the hardness minimums for the bounding welds was 92.2 to 97.3 HV/500.

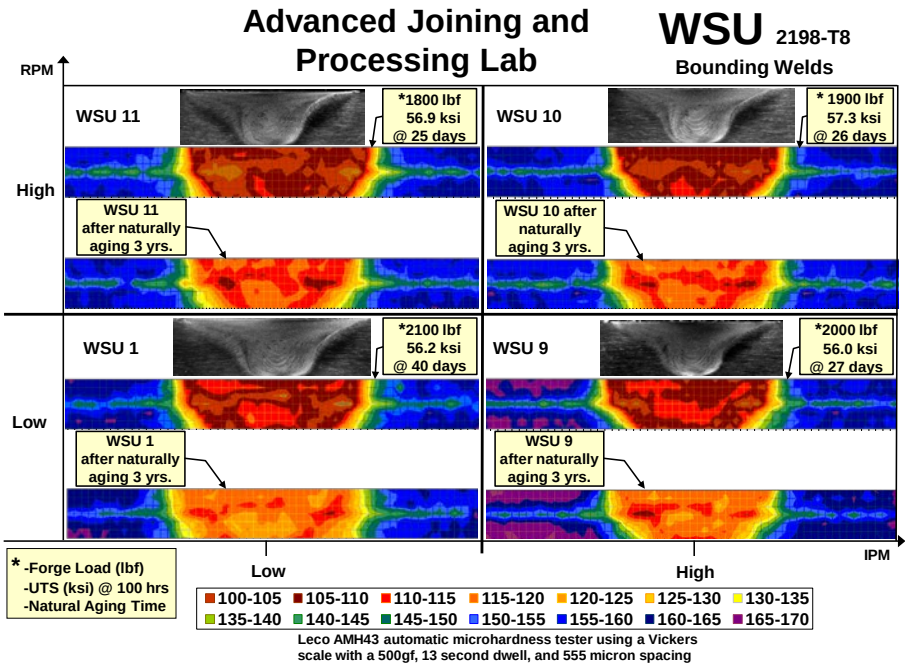

Figure 52. Comparison of original full-field microhardness contour maps of AA2198-T8 bounding weld metallographic specimens microhardness tested within 40 days of natural aging and full-field microhardness contour maps of the same metallographic specimens tested after naturally aging for 3 years

The original microhardness tests on the bounding welds were performed within 40 days of welding. A timeline showing when the bounding and study welds were tested in relation to when the welds were made is shown in figure 53. Results of the microhardness retest of the bounding welds and the repeat tensile test indicate that there was evidence the differences in the original results for testing the bounding welds was due to changes in mechanical properties with natural aging of the weld material. Previous studies have shown that the mechanical properties of Al-Lithium alloy welds improve with natural aging [83] and that some Al-Lithium alloy welds can take more than 60 days to stabilize with natural aging after welding. The stability of the alloy is dependent on the copper content; room temperature stability decreases with increasing copper content [84].

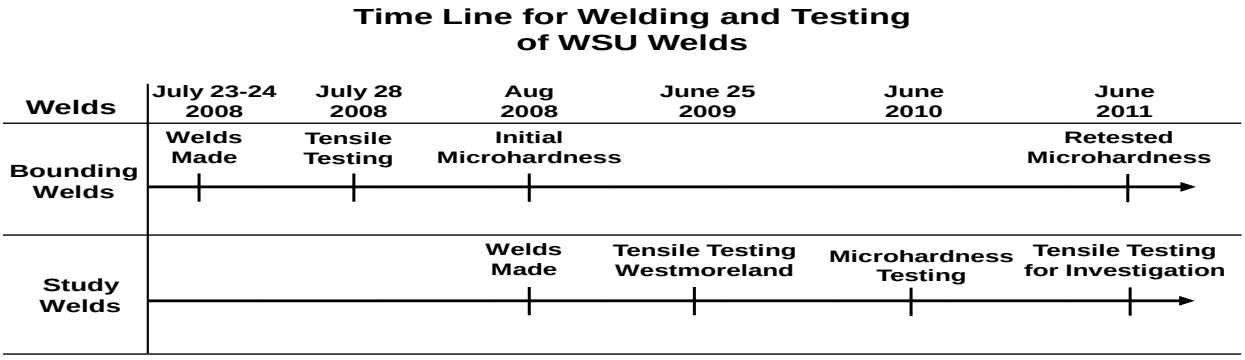

Figure 53. Timeline for welding and testing of WSU bounding and WSU study welds

Comparing results from the two sites where the material was tensile tested revealed that the WSU welds tested in the AJ&P Lab overall had lower results than Westmoreland. Retesting did not indicate any differences due to procedure, machinery, or operator between WSU and Westmoreland. This indicates that the differences could be due to different aging times for the WSU welds tested in the AJ&P Lab versus the WSU welds tested at Westmoreland. Because of possible differing natural-aging times for welds between the different sites, this issue could have contributed to more site-to-site variation in the tensile test results.

Conductivity results are shown in figure 54, with the corresponding microhardness maps. In the AA2024-T3 sample, a dramatic rise in conductivity occurred in hotter welds in the area of the HAZ/TMAZ (see figure 54(b)). This reflects the change in microstructure in the area. There is an increase in precipitates and coarse, incoherent grains in the area of the HAZ and TMAZ in precipitate-strengthened metals [64]. This results in an increase in conductivity in this area that can be confirmed by comparing the conductivity curve to the corresponding microhardness map (figure 54). In the cold weld, a peak in conductivity is observed in the area of the nugget only, which reflects an overaged microstructure in this zone of the joint (see figure 54(c)). Very little deviation from the baseline conductivity is observed for the AA2198-T8 FSW material (see figure 54(a)). The main chart figure 54(a) shows the changes on the same scale as the 2AA424-T3 weld's conductivity charts (figures 54(b) and 54(c)). The small window is shown with a finer scale to allow any potential deviations from the baseline level to be readily detected. This very small change in conductivity from baseline is typical of the welds of AA2198-T8 material.

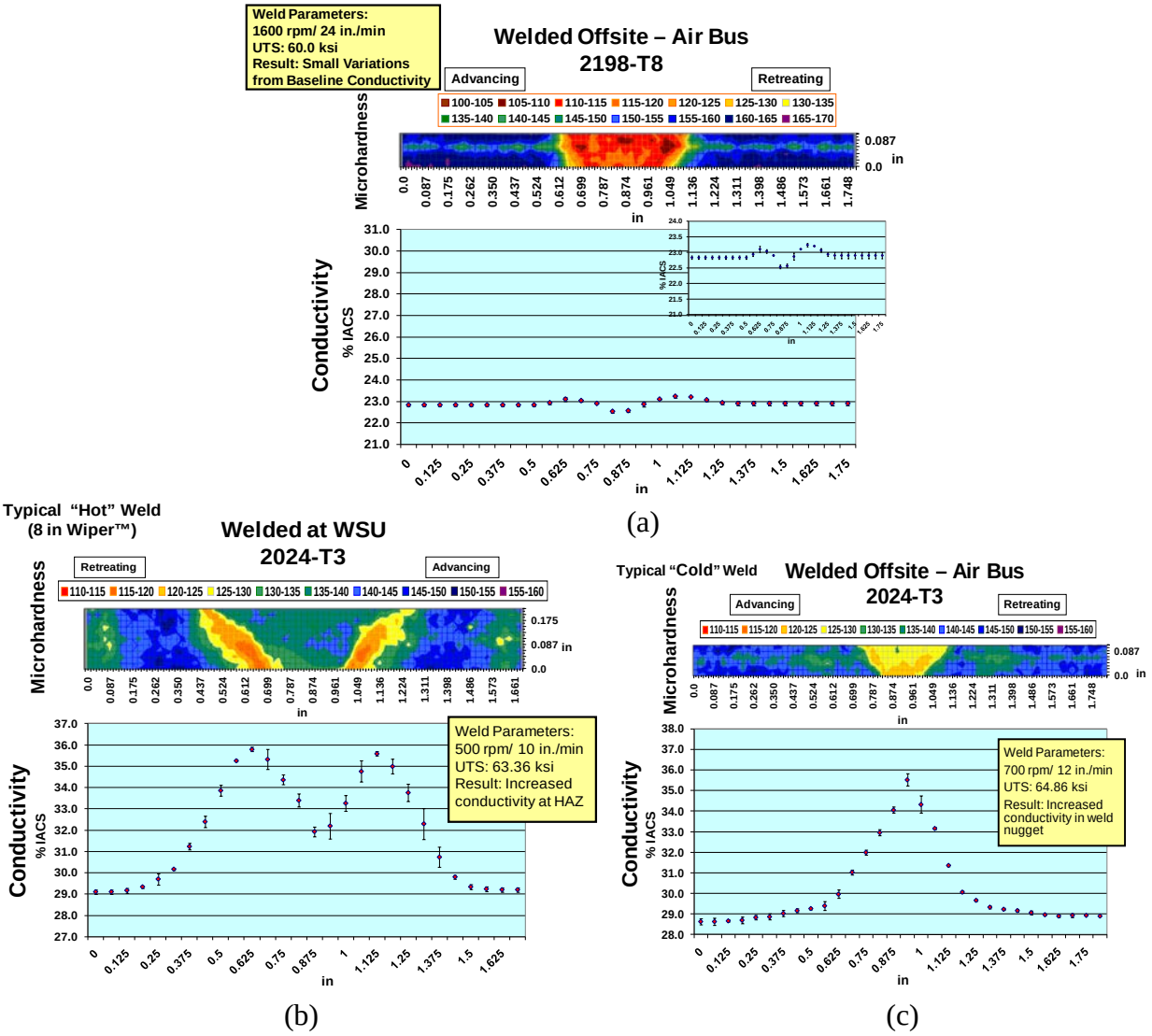

Figure 54. Microhardness maps and conductivity measurement results: a) Phase II FSW in AA2198-T8 0.150-inch sheet, b) Phase I FSW in AA2024-T3 0.0250-inch plate, and c) Phase II FSW in AA2024-T3 0.125-inch sheet

5. THE e-NDE AND POD

In FSW, the side of the weld tool presses against the workpiece in a manner similar to machining with the side of an end mill. However, unlike end mill machining, in FSW, the tool design and process parameters are selected in a way that the displaced material is captured and reconstituted into the original material—as opposed to removing it from the work zone in the form of chips, as in machining. Consequently, both similarities and dramatic differences exist in the dynamic response of the respective tools used in end milling and FSW.

In machining, it is important to clear the cut metal (chips) from the tool at a sufficient rate to prevent clogging the tool features, namely the flutes, etc. In FSW, the opposite is true. The features of a FSW tool, such as threads and grooves, are expected to become impacted with metal and thereby maintain a full frontal engagement between the tool and the material of the workpiece. On the other hand, in machining, only the tool cutting edges are expected to be in contact with the workpiece. This full engagement between the FSW tool and workpiece leads to unique dynamic behavior not typically experienced in machining.

In machining, advanced control techniques have been investigated for reducing chatter. For example, Zhang and Sims assessed the ability of "piezoelectric active vibration damping" to arrest chaotic tool behavior [85]. To reduce defect formation in FSW associated with chaotic tool motion, Boldsaikhan [86] and Jene, et al. [87], have studied machine tool-material interactions by monitoring force feedback signals. As these studies demonstrate, in both machining and FSW, process monitoring may serve as the basis for reducing chaotic tool behavior and, thereby, provide a means for improving part quality in both machining and FSW.

In FSW, the tool tends to vibrate or oscillate side to side (nominally transverse to applied loading vector) while under the local dynamic side-loading conditions imposed on the tool at the tool-workpiece interface. In machining, when the tool oscillates in a chaotic manner, a self-excited vibration phenomenon called chatter tends to form, leaving erratic markings on the newly cut surface. Similar chaotic oscillations in FSW tend to be associated with the formation of voids within the joint (resulting from the lack of consistency in the reconsolidation of material along the joint line).

The advancing, rotating FSW tool presses against the material directly ahead of it, creating a shearing action that extends around the tool front. In a generalized manner, when the material directly in front of the tool is sufficiently heated under the pressure and shearing action imposed on it by the advancing FSW tool, thin layers of material are transported from the advancing side of the tool to the retreating side of the tool.[2] This action is then repeated, with cooler material again being exposed to the leading face of the rotating, advancing tool.

This new interface or band of material is pressed on until it is sufficiently heated to be moved along the tool front from the advancing side to the retreating side. This undulation in metal movement along the leading edge of the tool promotes an oscillatory or alternating pattern in both normal and shear forces acting on the tool surface, which in turn causes the tool to move in a

[2] The advancing side of the tool is the side where the rotation direction is the same as the travel direction. The retreating side of the tool is the opposite side where the rotational direction is opposite the travel direction.

periodic motion, nominally side to side, as the tool is advanced. This process is shown in figure 55 (for simplified, idealized frontal force conditions).

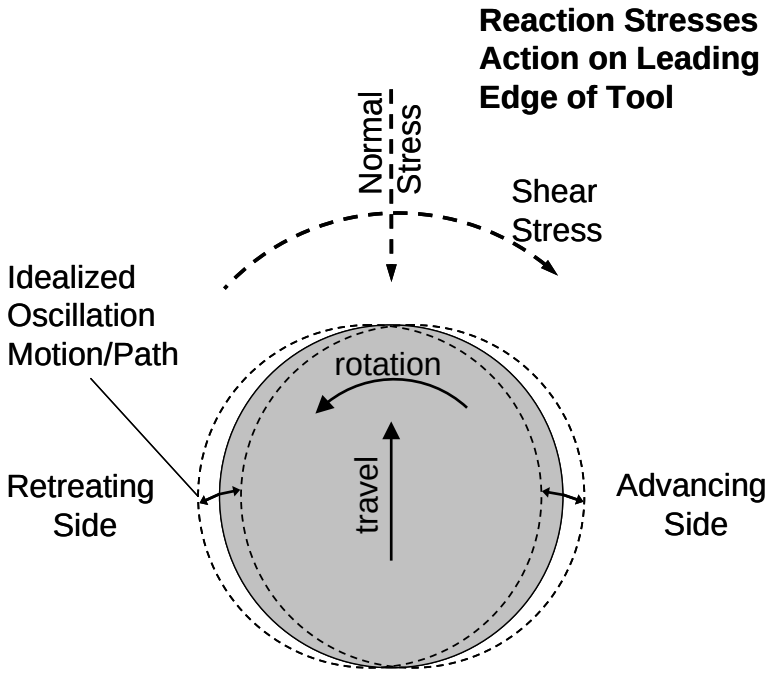

Figure 55. Swept volume cross section of a generic FSW tool probe located midway below the tool shoulder and the end of the probe [59]

Figure 55 shows the idealized oscillation of the tool as it advances. Tool rotation is counterclockwise and the travel direction is toward the top. The reaction forces act on the tool in opposition to the tool motion. A periodic shearing and movement of metal along the leading edge of the tool—from the advancing side to the retreating side—results and the tool oscillates side to side (nominally) in response to the primary reaction forces acting on the leading edge of the FSW tool probe.

Material flow and the associated resultant forces acting upon the tool in actual FSW are much more complex than idealized in the model shown in figure 55 [88]. With the tool probe completely submerged in the workpiece, forces act on the probe from all directions in response to its dynamic loading environment, the result of which may be measured experimentally [89]. The full engagement of the rotating, advancing FSW tool further aggravates its tendency to oscillate in a chaotic manner. The spinning motion of the tool shoulder face on the surface of the workpiece adds to the complexity of FSW tool oscillatory motion. This tends to cause a walking motion of the end of the tool, which even further promotes chaotic tool behavior as the tool seeks (or seeks to establish) a center of rotation on the workpiece surface.

Uniformity in FSW tool oscillations depends on the periodicity (or lack thereof) in the material flow behavior around the tool front. It is anticipated that the lower the abruptness in the material heating and shearing cycle, the less likely the tool's behavior or actions will become chaotic.

Selection of tool features and process parameters are expected to contribute to the overall stability of the tool control process.

The ability to monitor the dynamic behavior of FSW tools through force feedback signals provides an effective way to dramatically reduce or eliminate the inspection costs associated with secondary inspection techniques, such as x-ray, ultrasonic phased array (UPA), or penetrant inspections. By simply analyzing the force feedback signal of each weld, this lean and effective e-NDE technique can be used to improve production and quality, based directly on recorded weld information. It further offers the potential ability to actively and adaptively control FSW operations in production. It can also conceivably be developed to monitor tool wear, optimize design and performance of FSW tools, and compete different tooling design concepts, etc.

5.1 EXPERIMENTAL PROCEDURE

An NDE inspection round-robin was conducted on a set of 30 friction stir-welded plates [90]. The plates were selected based on the results of a "path independence" FSW study [63]. The plates were produced on a MTS ISTIR PDS welding machine located at WSU in the AJ&P Lab of NIAR. Force feedback data sets from the MTS system were analyzed with a computer software program written by Boldsaikhan [86]. Ten different combinations of process parameters and weld tools were used to prepare three sets of ten plates made from 0.25-inch (6.3-mm.)-thick aluminum alloy AA2024-T351. The tools selected for this study are shown in figure 56. They represent a wide variation in probe and shoulder features (see section 4.1.1 for further details). A schematic showing different processing parameters developed for each tool from the prior study is shown in figure 57 [63].

Figure 56. Five FSW tool designs used in NDE round-robin [88–89]

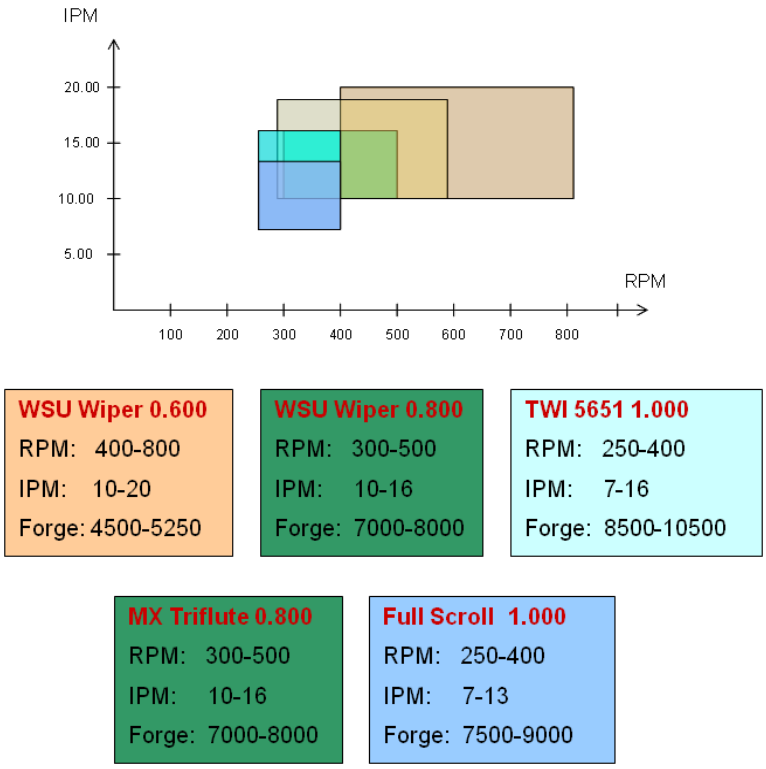

Figure 57. Welding process windows and process parameters for the five tools shown in figure 56 [90–91]

Previously, Boldsaikhan [86] demonstrated that the amplitude of the F_y signal for three welds revealed how increased low-frequency oscillations (relative to spindle frequency) are directly correlated with continuous void or wormhole defects (see figure 58). The same approach formed the basis of this study.

The F_y feedback force data were analyzed using the discrete Fourier transformation (DFT) – neural network (NN) training and a classification program prepared by Boldsaikhan. For comparison, the plates were tested using x-ray analysis by Cessna Aircraft, Spirit AeroSystems, Hawker Beechcraft, and Bombardier Aerospace (formerly Short Brothers). Each company tested the panels using their own internal specifications. One company also provided UPA results for 28 of the plates. POD curves were then constructed based on the inspection report submitted by each company. The results were compared against metallographic inspection and mechanical tensile test results performed in the AJ&P Lab.

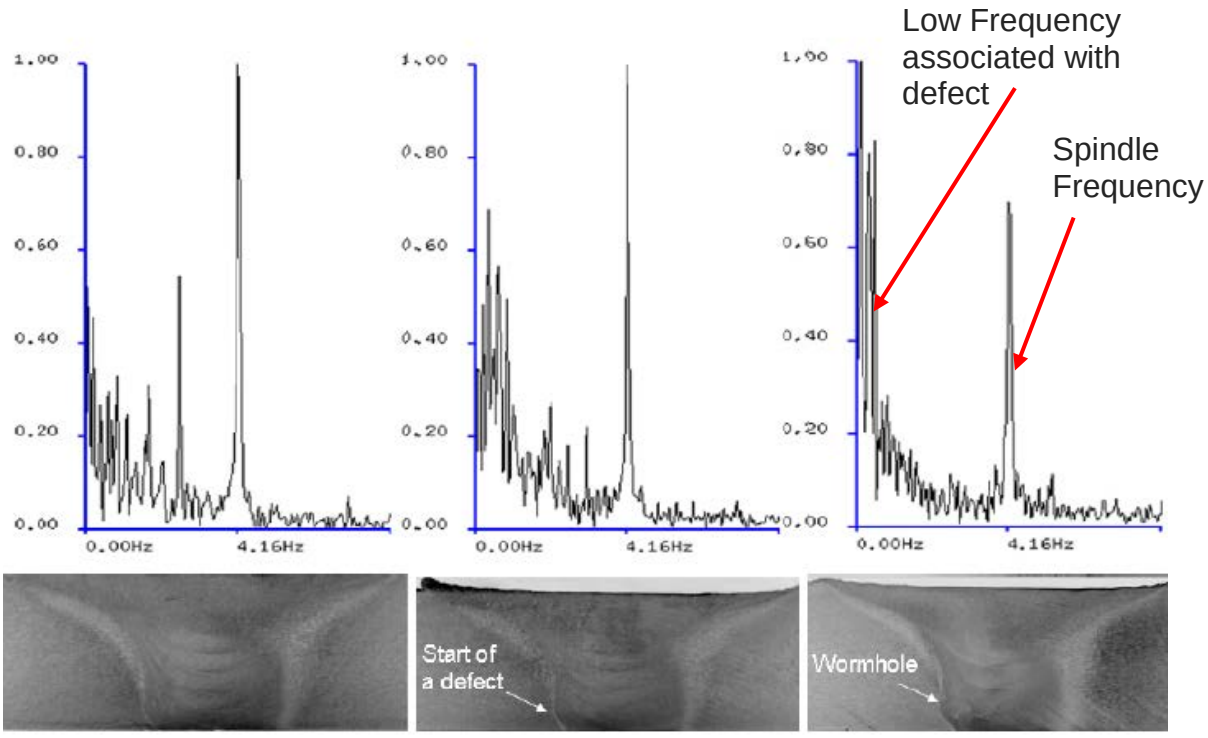

(The normalized amplitude is on vertical axis. The spindle frequency is located at 4.16 Hz (250 rpm).)

Figure 58. Frequency spectra of *Y* force feedback signal with corresponding metallographic images [86]

All indications were marked on the plates, based on the inspection reports of the round-robin participants. Metallographic inspection and mechanical test coupons were excised from each welded plate based on the collective NDE findings. A total of 83 macrosections and 82 tensile coupons were cut from the 30 welded plates. An example plate, marked and ready for excising metallographic and tensile coupons, is shown in figure 59.

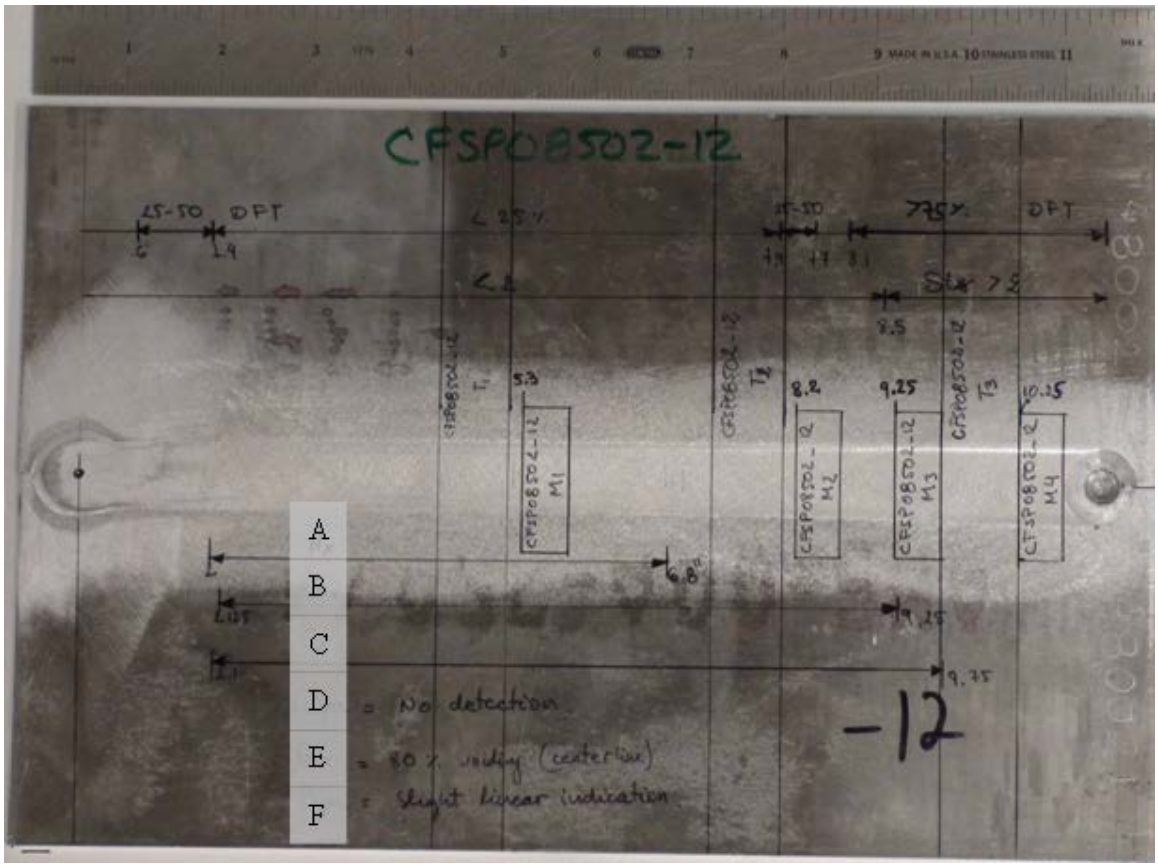

(A, B, C, and E correspond to the respective X-ray analysis reports;
D and F correspond to the respective UPA analysis reports)

Figure 59. Cut plan for weld panel CFSP08502_12 [90]

Every macrosection was inspected in the AJ&P Lab to identify and document the presence of voids. The longest dimension of each void in any direction was the recorded size of the void. In the situation of multiple voids in the same macrosection, the dimension of the largest void was used. Each void associated with a cluster of voids was recorded separately. Although a cluster of voids may affect the overall tensile properties, the primary concern in this study was the ability to detect the size of each void.

The NN algorithm, provided by Boldsaikhan and described elsewhere in references 92 and 93, was trained using three feature vectors per each point of interest obtained from the F_y feedback force signal. Two were used to train the NN and the third point was used to test the classification computed by the NN based on the other two. It was possible to train the NN with 100% of the feature vectors and the NN was able to correctly classify 92.7% of the samples. Only three of 28 samples were false classifications, and only three samples with voids were not detected.

5.2 THE POD RESULTS AND DISCUSSION

The mean POD curve computed from the three x-ray analysis reports are plotted together in figure 60. The lower 95% confidence bound is also plotted for reference.

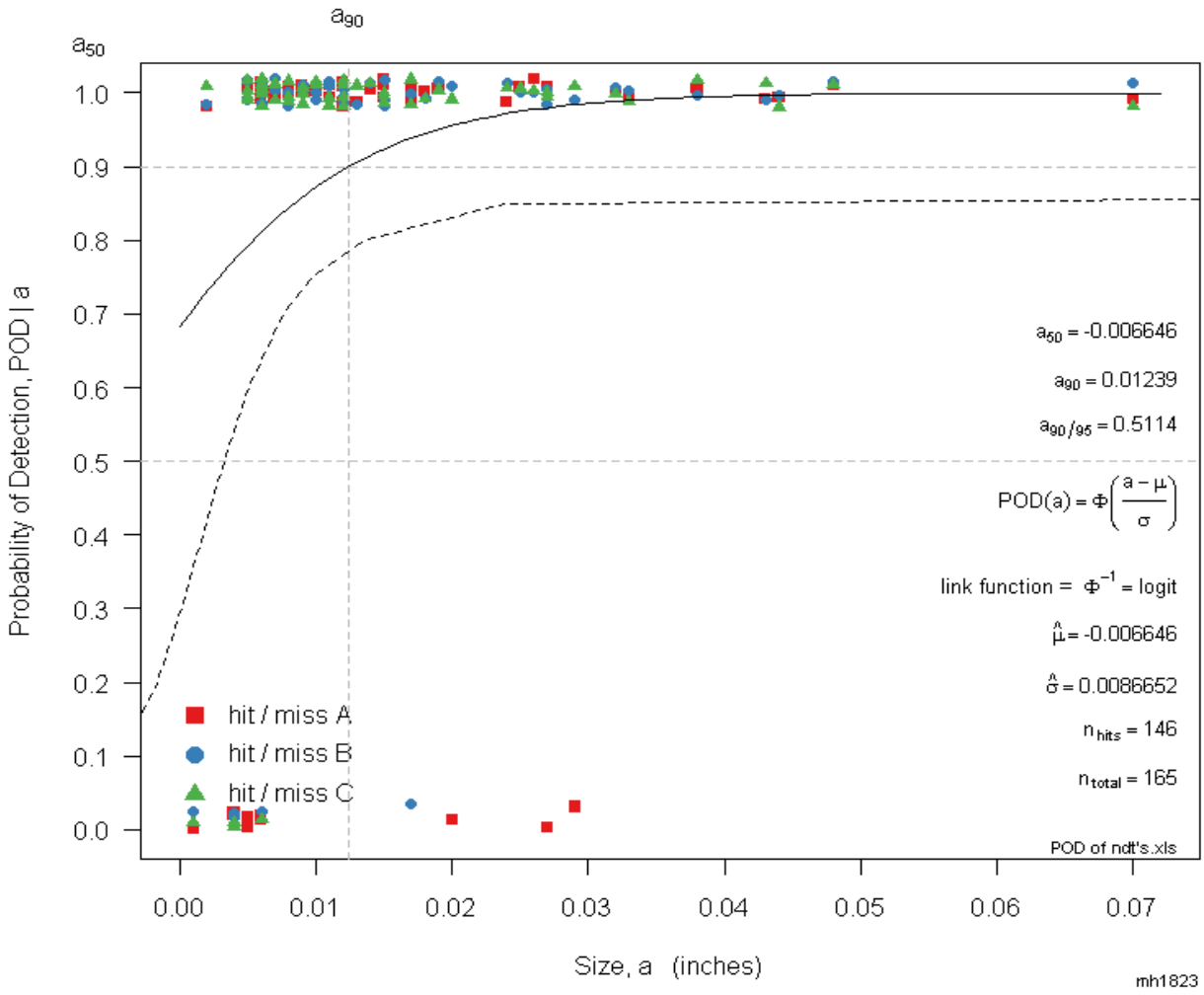

Figure 60. Mean POD curve vs. void size computed from the three reported X-Ray analyses [90]

The mean POD versus void size of the NN classification is shown in figure 61. Note that the x-ray method detected voids with a length greater than 0.012 inch (0.30 mm) with a 90% mean POD, but it could not guarantee detection at a 95% confidence level for 90% POD (see figure 60). In contrast, the NN-DFT-based method identified voids with a length greater than 0.005 inch (0.13 mm) at a 90% mean POD, and a length of 0.019 inch (0.48 mm) with a 90% POD at a 95% confidence level (figure 60).

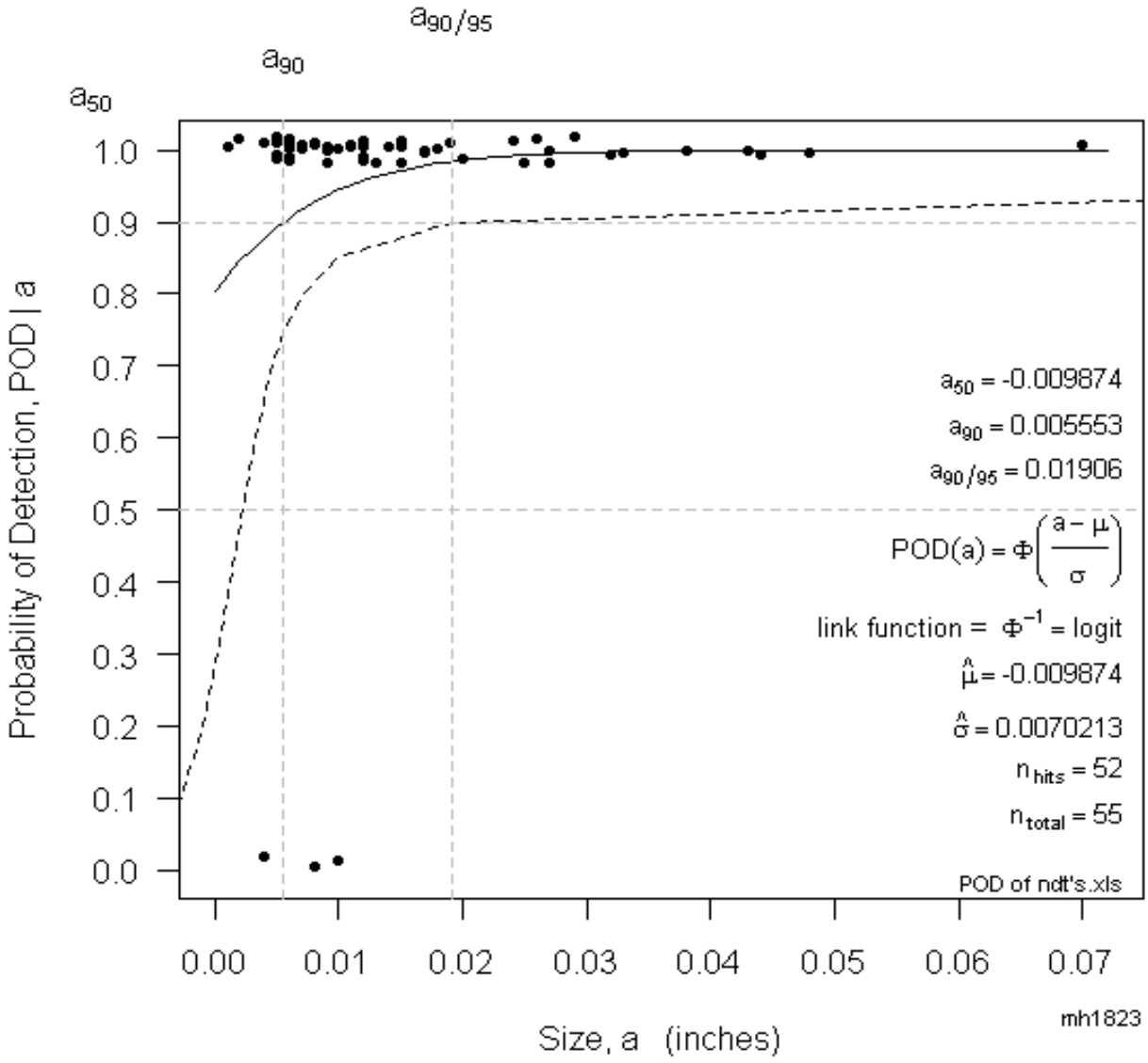

Figure 61. Mean POD vs. void size for the NN analysis results [90]

To evaluate the effects of defects, a POD curve was constructed for transverse tensile strength values as a function of wormhole or void size. The same binary regression analysis, based on a maximum-likelihood method, was applied to the tensile binary result obtained in this test program. Figure 62 shows the POD of low tensile strength due to wormhole size. As shown, a wormhole larger than 0.015 inch (0.38 mm) has 90% POD of causing low tensile strength.

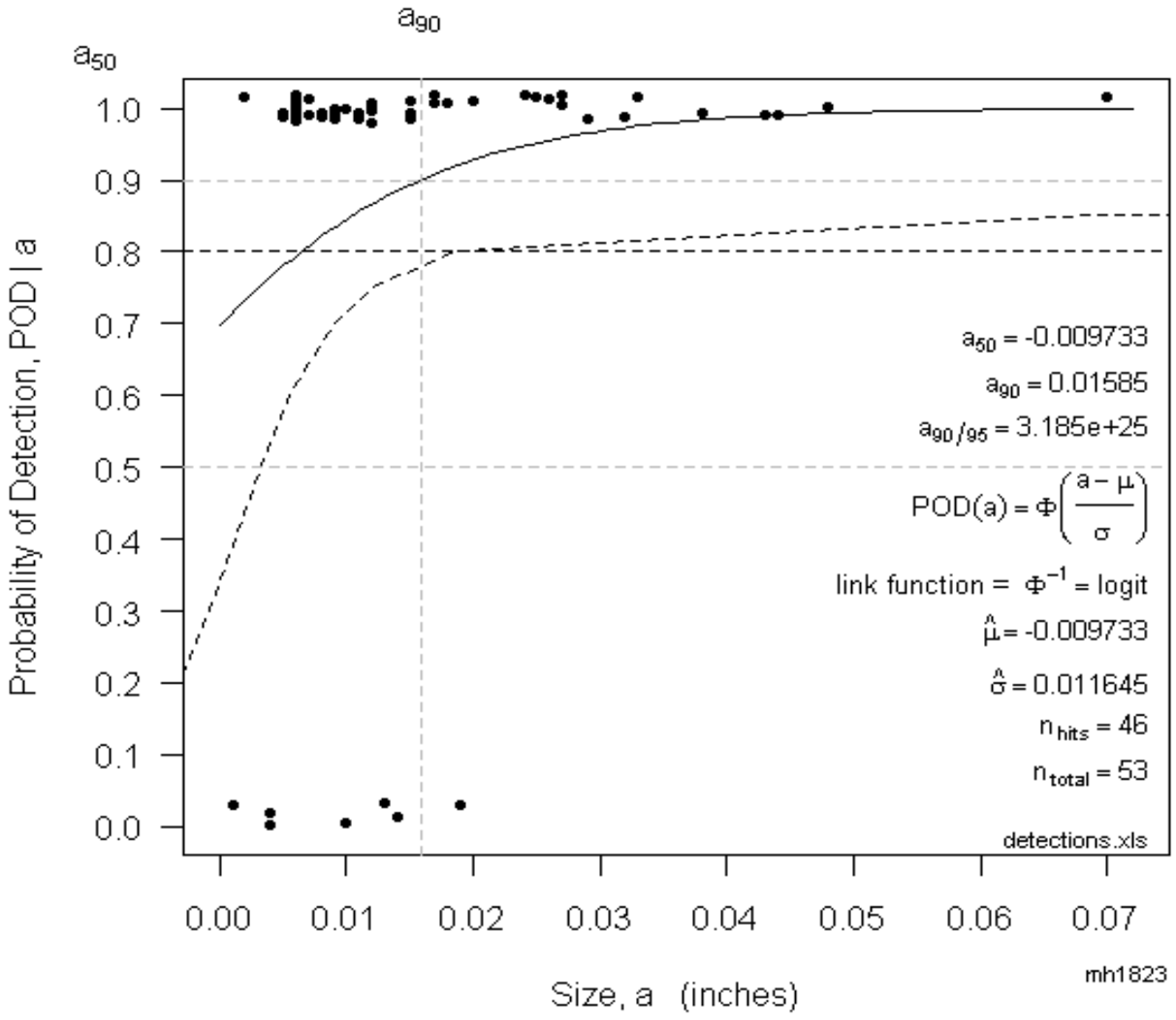

Figure 62. Effect of defect—mean POD vs. void size for the tensile test analysis results [90]

To summarize, the trained NN system was found to provide better detection capability than either x-ray (a non-destructive method) or tensile tests (a destructive test method).

5.3 DETECTION OF EMERGING VOIDS

The inspection results for one round-robin plate in particular, CFSP08502-1, provide a clear illustration of the capability of the e-NDE technique to detect the emergence of voids before they grow to sizes detectable by standard NDE and destructive test techniques. According to the findings included in the NDE inspection reports, a volumetric indication identified near the end of the weldment was found by the different participants in the round-robin test program to begin at different positions and to extend to varying lengths. The different findings for the location and extent of the indication are marked within the red box in figure 63. The mark for the e-NDE finding, which occurs sooner and extends further along the length of the weld than do the NDE location markings, is located on the plate just to the right of the red box included in figure 63.

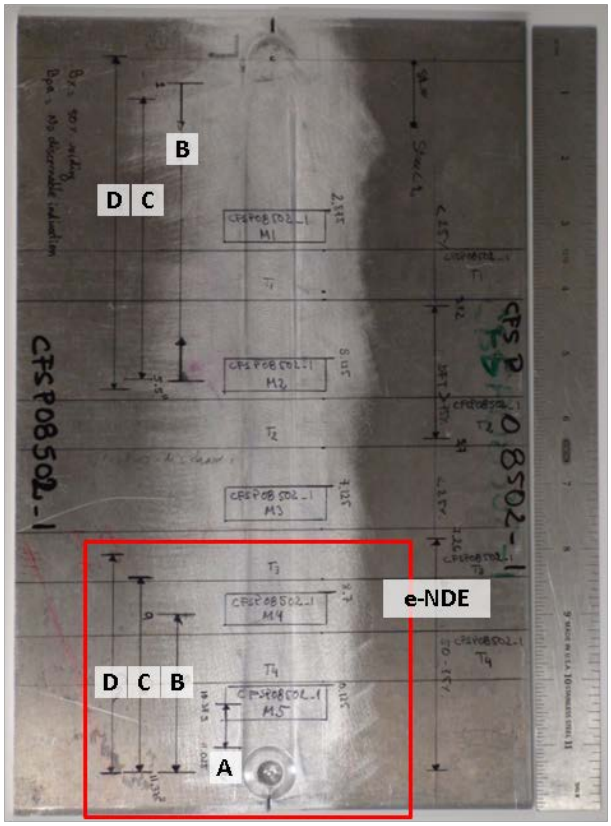

Figure 63. Plate CFSP08502-01 marked with the different NDE inspection results [92]

Figure 64 shows the area of the test plate outlined in red in figure 63. Figure 64 shows a series of macrographs taken of samples excised from the region in which the indication at the end of the weld was first detected (with respect to the direction of travel). Each section was excised transverse to the joint line and evaluated to document the presence (or absence) and size of voids in this region. Two micrographs are included in figure 64 to show the presence of the voids emerging in the last of the series of macrographs.

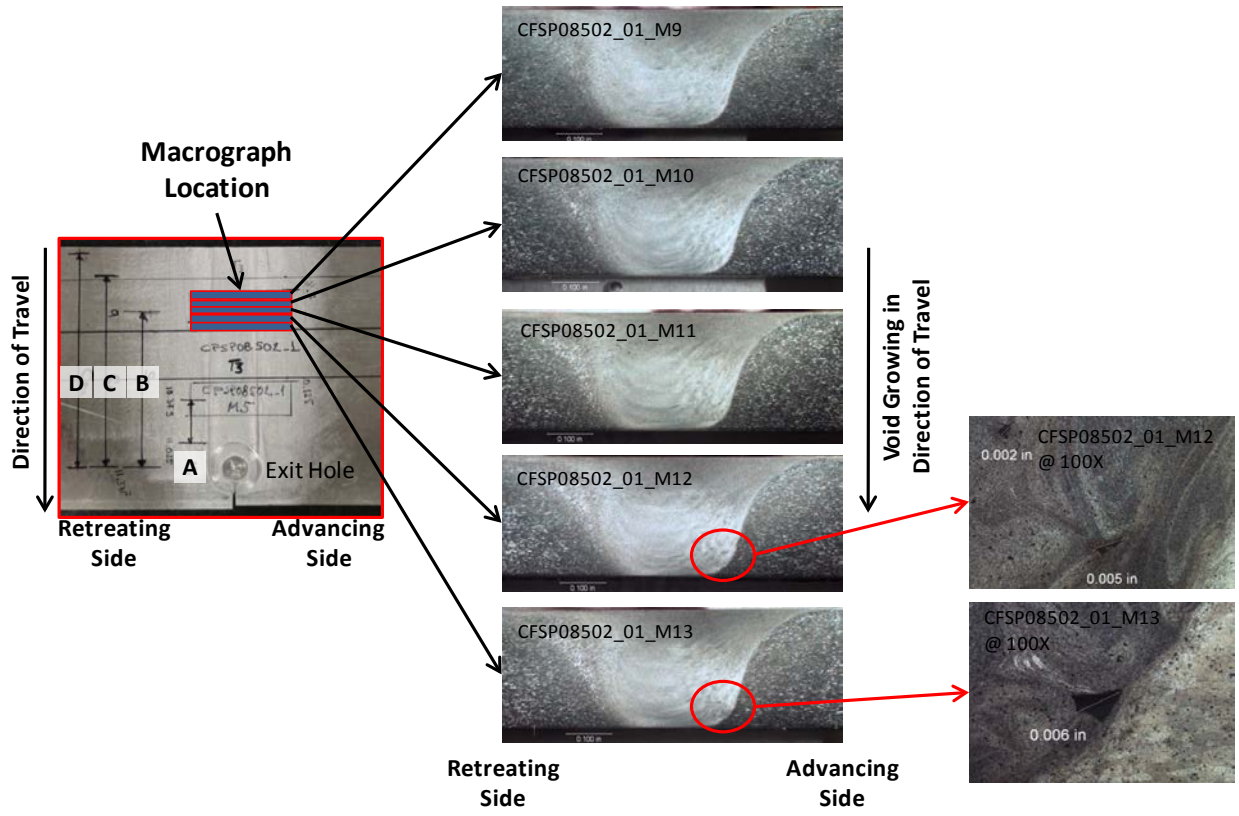

(The location of this weldment section is indicated by the red box in figure 63)

Figure 64. Macrosections taken from CFSP08502-01 that show the emergence of a void along the direction of welding [92]

A schematic showing the differences in detection of the start and extent of the indication associated with the weld in this plate is provided in figure 65. The early void formation stage was first detected by the e-NDE technique (figure 63), followed by the inspections represented by D, then C, B, and A, in that order.

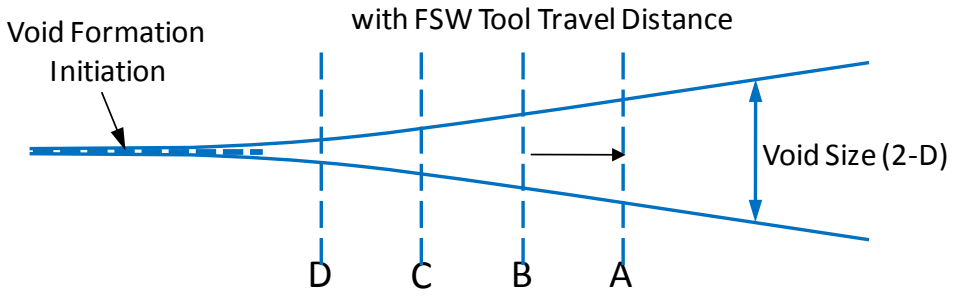

Figure 65. Evolution of void growth with FSW tool travel distance from the end of the plate [92]

As discussed in sections 5.0 and 5.1, the e-NDE technique relies on the presence of chaotic tool behavior to detect void formation. Thus, long before the volumetric defect actually emerged, as evidenced by the e-NDE results, chaotic behavior in the *Y* feedback force signal was beginning to increase as the weld progressed to the end of the plate (perhaps related to insufficient clamping coupled with end-of-the-plate effects). This growing chaotic behavior corresponded to an increasing lack of consolidation of the joint material (i.e., void formation).

In summary, this series of cross-sectional macrographs presented in figure 64 show that the e-NDE method is sufficiently sensitive to predict volumetric defects even before voids emerged during the welding process. This capability conceivably provides the time necessary to correct the FSW process through process parameter adjustments. The potential for this approach to be realized was confirmed by the correlation of the macrographic inspection of void growth along the direction of tool travel with feedback force behavior. Based on the findings of this study, it was anticipated that the e-NDE technique can be transformed into a dynamic method for controlling FSW as a self-governing, self-correcting process capable of producing void-free joints.

6. DISCUSSION OF KEY FSW PROCESS CHARTERISTICS

This section provides recommendations for implementing FSW in a production environment based on the experience of bringing the friction stir-welded 747-400F barrier beams into production [14] as well as on work completed in this and the companion NIS program.

6.1 THE FSW AS A MULTIPATH PROCESS

Situation: It is often necessary to identify multiple service providers when preparing to deploy a new technology like FSW into production (in case continued services are not provided). Given the proprietary nature of each potential supplier's process knowledge (e.g., tooling), establishing precise, common process specifications is not practical.

Approach: A viable approach (discussed in section 3) involves establishing performance specifications based on a multipath approach to FSW. Path independence is a process-development approach in which an unspecified number of weld tools and corresponding process parameters may be qualified for the production of a given joint or component. It is based on the observation (from experience and open literature) that widely varying tool designs have been used to make sound joints and processed materials with independently developed process windows in virtually all aluminum alloys. Any advantage one tool may have over another is manifest primarily in terms of productivity (i.e., in joining and processing speeds). With this approach, FSW can be effectively controlled with performance specifications as opposed to detailed process specifications. Further rationale for implementing a multipath process-development approach includes the fact that FSW may be viewed as a supplemental thermomechanical-processing operation superimposed over the parent material thermomechanical-processing history. It does not change bulk chemistry (no filler typically added), nor does it involve recasting the alloy (no bulk solid- or liquid-phase transformation). Joint properties typically increase in work-hardened, non-heat-treatable alloys (e.g., Al 5xxx) as a result of grain refinement in the stir zone (or weld nugget). In precipitation-strengthened aluminum alloys, joint properties are typically decreased as a result of overaging in the HAZ adjacent to the joint. Overall, FSW is expected to be relatively path independent of weld tool design for any given alloy system.

Individual manufacturers will still be expected to develop internal process controls. These would establish the specific control requirements for their unique equipment and their specific product. Manufacturers will need to conduct a simplified test program (see section 6.1 for information on the shared database approach) to demonstrate that their equipment provide materials with the same statistical population used to derive published industry values.

6.2 MANDREL VERSUS THREADED FSW TOOL PROBES

Situation: Conventionally, FSW tools have threaded probes in one form or another. These threads with small protruding features tend to be susceptible to breaking off (shedding) during welding, leaving small pieces of the weld tool in the joint material.

Approach: A new FSW tool probe design, known as a Mandrel™ tool (patent pending), promotes better material flow in an FSW joint without the assistance of threads, groves, channels, etc. Compared to conventional threaded probes, this new probe promotes better mixing and produces an increase in the size of the thermomechanical zone of the nugget. These stir zone characteristics were found to produce enhanced FSW and friction stir-processing properties. Unlike threaded tool probes, it is anticipated that this tool design will endure over long production runs and lengths without shedding tool material from the probe into the weld joint.

The weld zone produced by the new tool is broader and squarer than that produced by a spiral-threaded tool of the same size. Results are provided in figure 66, which shows the cross section of two welds made by different tool probes: (a) a baseline threaded tool with spiraled flats and (b) the new mandrel style probe with five flats and no threads.

It is theorized that the new tool produced a squarer, wider nugget because it produced more of a mandrel effect than the augering effect generated by a threaded tool. Threads tend to shear the stirred material in the vertical direction. In contrast, the mandrel effect of the nonthreaded style probe tends to work the material around and down the pin without the shredding or stripping effect of the threads. That is, this new pin involves the combined action of the spiraled flats and the pin taper, tending to work the material versus stripping and shredding it into chips that then must be recombined.

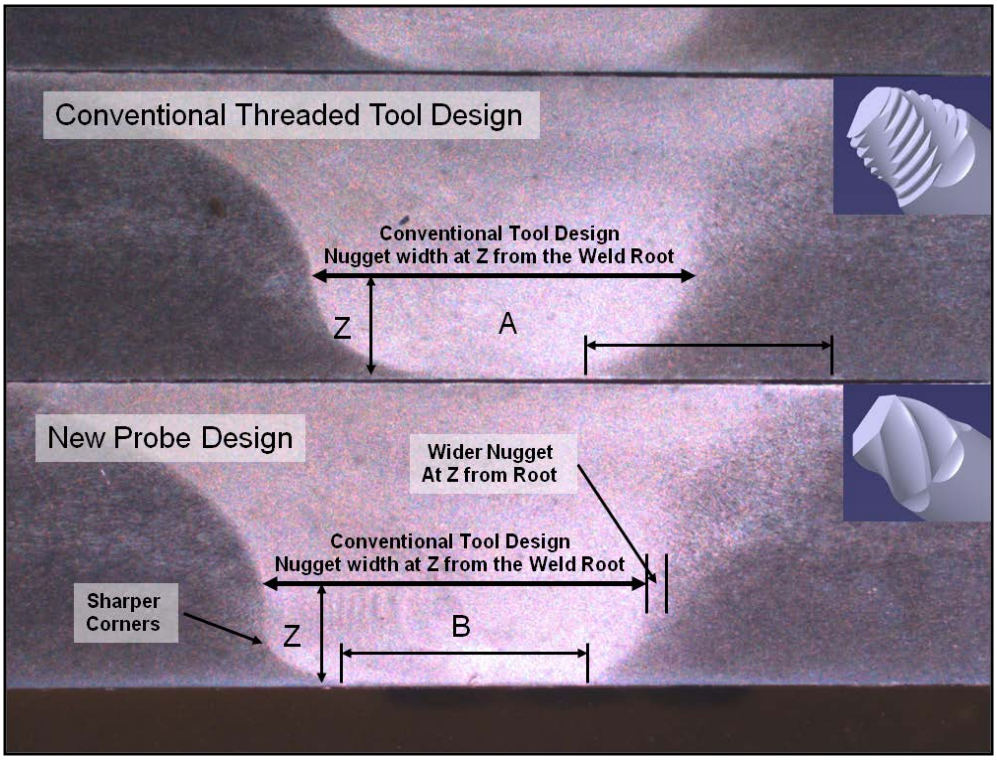

Figure 66. Cross sections of welds produced with a) a convention threaded tool (upper right) and b) the mandrel style FSW weld tool (patent pending) for scale; individual plates are 0.25-inch thick

6.3 LATERAL OFFSET OF FSW TOOL

Situation: The initial interface of a butt joint may remain discernible as a remnant oxide feature in a macrograph following FSW, sometimes referred to as a lazy *S*. Thorough mixing will potentially reduce or eliminate this artifact.

Approach: A practical solution is to process (consume) the joint line (abutting edges) across the front face of the tool probe, as shown in figure 67. This is accomplished by shifting the joint line to the advancing side of the weld tool (i.e., offsetting the weld tool laterally to the retreating side of the joint line).

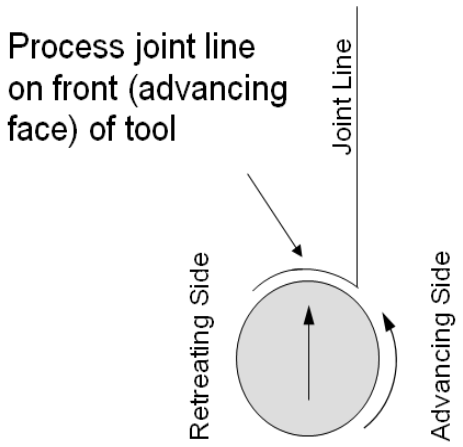

Figure 67. Cross section view of the swept volume of an FSW tool probe at nominally the mid-plane of a butt joint during FSW

The optimum lateral offset of the joint line is best determined and verified through a DOE program. This approach promotes an increase in the wrap length of the joint line around the periphery of the tool and enhances mixing the faying surface of the pre-FSW butt joint line as it is brought into the weld zone. A retreating side lateral offset also introduces the joint line into the typically hotter region of the weld zone (processed zone) as the weld tool is advanced along the joint line.

In figure 67, the weld tool is shifted to the retreating side, forcing the joint line to pass around the front of the probe (a greater distance than if the joint line is presented to the center of the advancing face, not the side, of the probe). Processing the joint line on the front (advancing) face (not side) of the tool in this manner promotes more complete mixing of the faying surface of the butt joint. Note that when offsetting the tool to the retreating side, slightly lower tensile strengths are produced (see figure 68). This effect has been effectively used as a fuse concept for establishing design data [14]. Essentially, selecting a process window that consistently produces the lowest values leads to greater consistency in minimum joint-design values (when measured by transverse tensile properties).

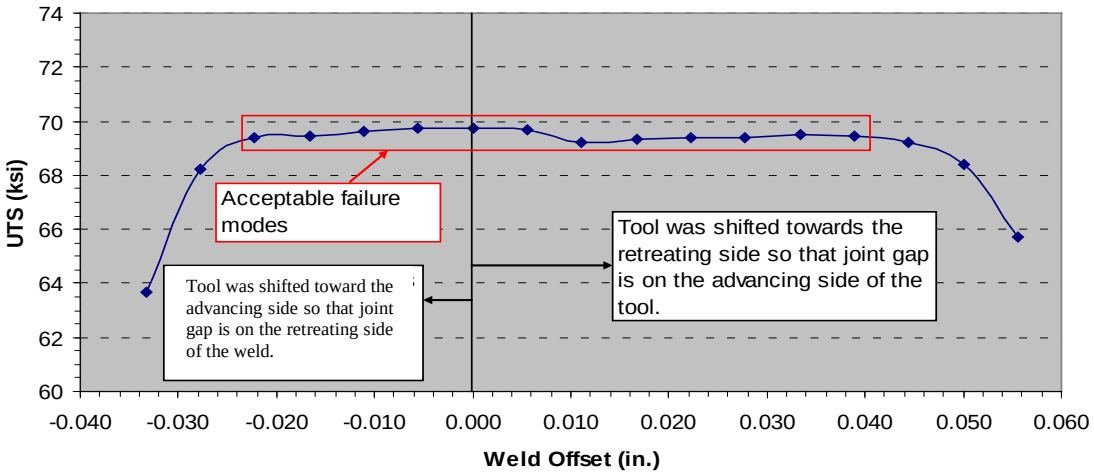

(minus denotes gap on retreating side of the weld)

Figure 68. Ultimate tensile strength as a function of weld tool lateral offset [32]

6.4 SEAM TRACKING

Situation: Proper location of the tool with respect to the joint line of the components being joined is crucial to producing consistent, sound joints. For example, allowing the weld tool to shift too far to the advancing side may still give the appearance of a sound joint, but full consolidation is not achieved (the joint passes the tool on the retreating side with minimal mixing). Tool placement relative to the joint line is particularly important for high-strength aluminum alloys. High-strength alloys have a narrower process window than lower-strength aluminum alloys and, thus, require greater care to ensure that the joint is fully mixed to complete the seam favorably with the adjoining parent material in terms of load-bearing capacity.

Approach: Providing seam tracking will promote better, more consistent, repeatable results for production environments. To facilitate visual inspection, a fiducial line (figure 69) may be placed offset from the weld track so the position of the joint may be readily checked for proper location following FSW.

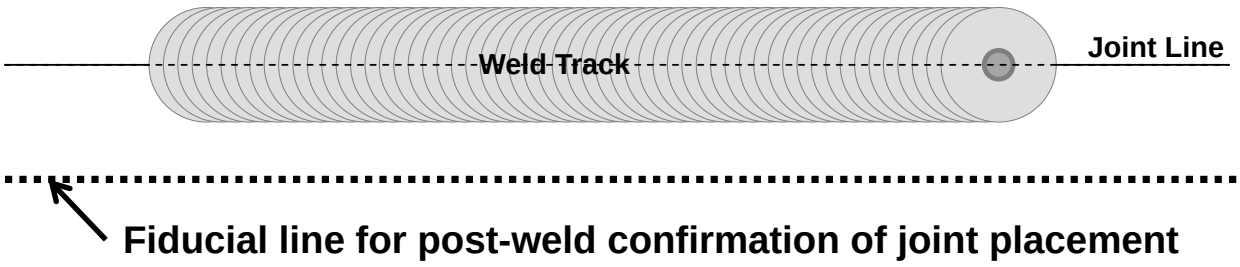

Figure 69. Placement of an offset fiducial line along the joint line prior to FSW to positively locate the weld track relative to the joint line during (e.g., via an optical system) and after FSW

6.5 THE E-NDE FORCE FEEDBACK SIGNAL MONITORING

Situation: Incomplete consolidation of the joint material may result from improper process parameters (e.g., using too-cold conditions). Because these voids are often subsurface, they may go undetected during welding. If they could be detected during welding, an adjustment could be made to the process window to eliminate the occurrence of subsurface voids.

Approach: As described in section 5 of this report, the results of a round-robin test program demonstrated the power of using an e-NDE technique for evaluating post-weld quality [90]. This technique is based on monitoring and analyzing force feedback signals to identify the presence of significant frequencies that indicate the formation of internal voids. The research published in this report demonstrates that the technique evaluated provided better POD in the cases studied than did conventional NDE techniques and destructive tests (transverse tensile tests). Using a signal analysis-based inspection technique makes FSW even greener by potentially reducing the need for post-NDE operation [61]. Eventually, applying concepts found in adaptive machining to FSW force feedback analysis in real time is expected to lead to self-correcting, adaptive FSW for improved quality and productivity. It may also be useful to monitor tool wear.

6.6 A COUNTERFLOW PROBE DESIGN TO REDUCE STRAIN IN THE TMAZ

Situation: When examining micrographic sections of a set of FSW joints produced in a prior research program, fine microcracks were observed in the TMAZ of high-strength, 7000 series alloys between the upturned, plate-shaped grains adjacent to the stir (fully recrystallized) zone, or weld nugget. Figure 70 shows a schematic depicting the location of the microcracking. At the time, the solution was to adjust the process parameters to lessen the severity of the upturned distortion of grains, the effectiveness of which was confirmed with microstructural examination and mechanical tests. It was conjectured that the presence of these fine microcracks may have been responsible for a greater amount of scatter observed in failure loads in this set of welds (which also exhibited TMAZ failures) compared to what other sets of test coupons demonstrated.

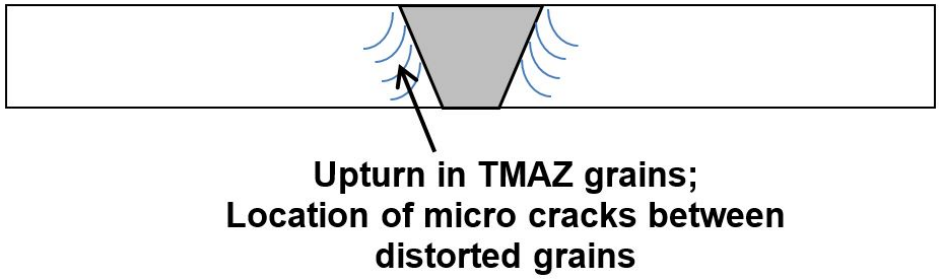

Figure 70. Schematic cross section of a macrosection with upturned grains in the TMAZ

Approach: As an alternative to reducing (restricting) the process window, it was envisioned that a flow path could be machined into the probe to allow reverse material flow inside the dynamic profile (swept volume) of the rotating tool probe (see figure 71). The objective would be to reduce the amount of recirculating material flow responsible for the TMAZ upturn and thus effectively reduce the propensity for microcracking in the TMAZ. Achieving this goal would open up a potentially larger process window. This approach was tested when developing FSW lap joints. Lap

joints provided an effective marker to simulate the upturn in the TMAZ of a butt joint for evaluating the degree of upturn (hooking) as a result of the presence or absence of a Counterflow channel [55]. The results proved the approach to be effective, with minimal upturn in the faying surface produced and more than 90% of the lap joint cross section fully consolidated.

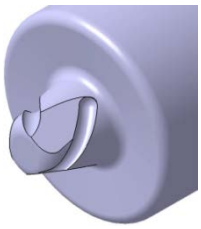

Figure 71. The FSW tool with counterflow grooves or channels [55]

Further experience suggested that if the Counterflow feature was too aggressive, it could produce a continuous internal void on the advancing side. Followup work was conducted to determine if an optimum depth of the Counterflow (secondary) features could be identified for a given application and primary probe feature. The results demonstrated that an optimum depth may be expected, as shown in figure 72 [75]. Thus, when using a Counterflow feature, it should be sized for the application (alloy and gage). The data in figure 72 are from coupons produced with a weld tool probe similar to the design shown in figure 71. It had a 0.056" long probe with a set of three inclined, tapered flats and a set of three Counterflow grooves linking the bottoms of each flat to the top of the adjoining flat. The strength of the coupon tested in tension was shown to be a function of the depth of the grooves. Note that as the groove depth increased, the scatter in the data was observed to increase from 11 lb for a 0.004-inch-deep Counterflow groove to 57 lb for a 0.016-inch-deep Counterflow groove.

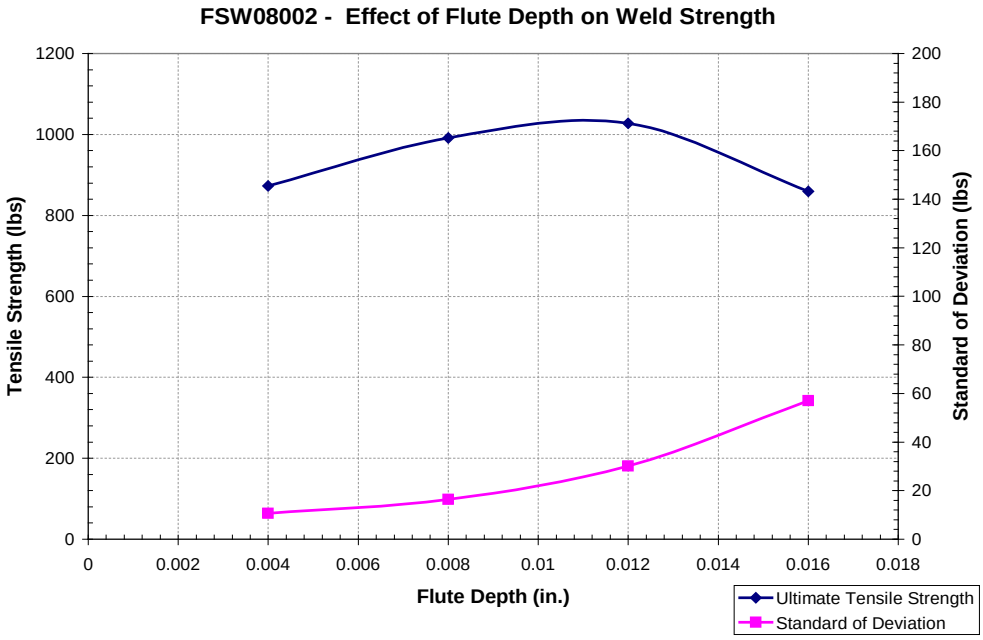

Figure 72. Unguided lap shear strength of a single octaspot joining two 0.040-inch-thick, bare AA 5182 strips in a lap joint configuration [75]

6.7 A WIPER SHOULDER DESIGN TO REDUCE SURFACE ROUGHNESS OF THE WELD TRACK

Situation: In a production environment, debris from tooling, fixturing, various other sources in the factory, etc., can potentially become entrapped in the joint material by being drawn under a concave tool shoulder or by a full scroll shoulder.

Approach: By introducing a Wiper shoulder design feature [42], shown in figure 73, with a zero degree tilt, it was expected that debris could be readily pushed aside by an advancing tool. Tests were conducted to evaluate tools with both a full scroll and a Wiper scroll, (figure 73). The results showed that the Wiper shoulder produced a smoother surface finish and improved fatigue properties compared to welds produced by a tool having a full scroll on the shoulder [41].

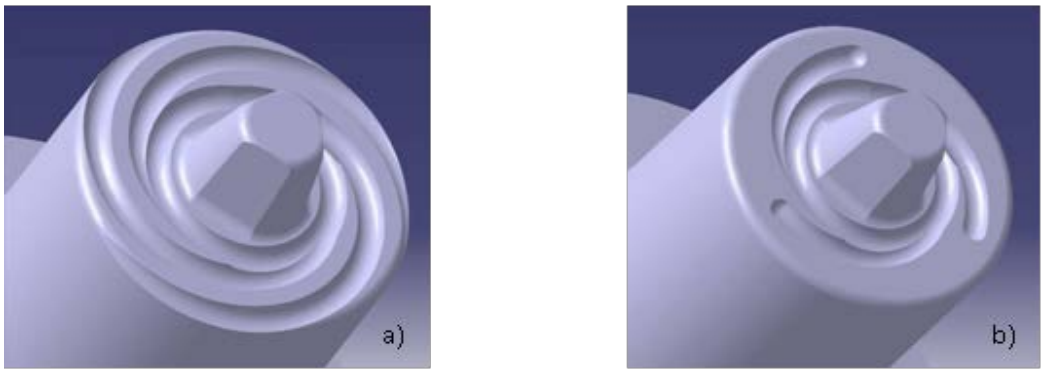

(a) (b)

Figure 73. Typical FSW tool scrolled shoulder configuration with a) the scrolls extending out to the edge of the shoulder face and b) with wiper features [42] added [41]

Scroll features, such as the Wiper, are designed to provide a surface traction force that directs material toward the probe. However, such shoulder features (i.e., scrolls) must also be tuned properly to ensure full consolidation of the joint material. For example, the shoulder features should be sized, spaced, and oriented (tuned) to supply ample material so the probe is not starved of material at the selected processing rates. Properly sizing tool features will ensure that a minimum tool axial force will be needed to provide full compaction of the joint material (suppress the formation of internal voids).

6.8 TOOL WEAR MANAGEMENT

Situation: Although FSW tools are intended to be nonconsumable, they experience wear during use and, therefore, must be managed as perishable tools. General and preferential wear of tool features (e.g., threads on the probe and grooves on the face of the shoulder) will change the geometry of the tool and may lead to changes in weld tool performance and corresponding changes in joint properties. Furthermore, monitoring tool wear is complex because of the difficulty in measuring changes in the three-dimensional features of FSW tools. It requires time, specialized equipment, and skilled inspectors.

Approach: One method for managing the wear of tools used for FSW aluminum alloys involves applying a hard, wear-resistant coating to the surfaces of the tools. The coating not only serves to extend the life of the tool, but serves as a wear indicator as well. On inspection, when the coating is observed to wear through at any given location on the tool surface, it may be concluded that further use of that tool will lead to a significant departure from the prescribed tool geometry (since the base metal is expected to wear at a greater rate than the coating). The tool is retired at that point, or it may be recoated if it is determined that the tool geometry has not been compromised. Tool coatings developed for the machining industry may be considered for use on FSW tools; for example, titanium nitride (TiN), titanium carbonitride (TiCN), titanium aluminum nitride (TiAlN), and multilayered coatings.

6.9 APPROPRIATE FSW AND FSSW EQUIPMENT

Situation: As evidenced by the open literature, many different machine platforms have been used to develop and deploy FSW and FSSW, ranging from the large, purpose-built FSW machines (for constructing rocket sections) to articulated arm robotics with special C-frame end effectors (for FSSW automotive sheet metal components).

Approach: While there is no single solution for any given application, care must be taken when selecting equipment to ensure consistency (repeatability and accuracy) in the essential process parameters (e.g., rotational speed, travel speed, axial force). One of the innovations considered in this program (and the companion NIS program) was to use robotics to automate FSSW for sheet metal applications [16, 45]. In support of this initiative, a new end effector that produces discrete joints via Swept FSSW has been devised [96] and is currently under development [97–98]. This new end effector is being designed for use on robots and machining centers, as well as purpose-built FSW and FSSW systems. Another innovation initiative expected to support the initiatives of this program has been to develop mechanical-assisted robotic FSW and FSSW. At least one robot-based welding system is commercially available for performing FSW directly (e.g., without a C-frame). It features a controller-based solution to implementing FSW on robots [99]. As an alternative to this approach (or to supplement it), a straightforward approach has been formalized in association with this research. It involves mechanically assisting robots at the end-of-arm tooling through specially designed fixtures to guide the robot at the point of application, thus improving repeatability (accuracy and precision) and increasing the robustness of the overall process. Under the title "Guided Robotic Friction Stir Welding (FSW) and Friction Stir Spot Welding (FSSW)," several variants involving different levels of complexity have been targeted [100]:

- Variant 1. Clamping shoes that can both hold the parts being welded together and guide the robot arm along the joint line of the weld by providing a mechanical guide that constrains the weld tool shoulder to follow a prescribed path, thus assisting the robot motion control system. These clamping shoes are attached to the end of end effectors and may be specialized or generic. The spindle mounted on the robot arm provides the torque through an end effector.
- Variant 2. Physical guides incorporated in weld fixtures to assist in directing the friction tool (or spindle) mounted in the end of a robot along the joint line for producing accurate and precise FSW joints welds and increasing repeatability in production. The spindle mounted on the robot arm provides the torque.
- Variant 3. Nested end effectors built into fixtures to produce FSW and swept FSSW joints. The robot primarily provides the positioning along or at the joint line location as well as the force required to make the joint. The built-in or nested end effector provides the torque.

These and other innovations, such as those outlined above and those reported in the various sections of this report, increase the viability of friction stir-related technologies as a production process for many structures, including those for aerospace applications.

6.10 THERMAL MANAGEMENT PLAN DEVELOPED FOR THE SPECIFIC CONDITIONS

Thermal management is the topic of discussion in section 3.2. In all cases, it is important to note and plan for any changes in the proportion of heat transfer in the various thermal paths along the weld joint line because these are expected to affect mechanical properties. The e-NDE may be useful in detecting thermal changes during processing, allowing for corrective programming to incorporate sufficient changes during processing for ensuring that design joint properties are achieved.

7. RECOMMENDATIONS

In the first 20 years of the invention of FSW, great advancement have been made in understanding and applying this unique joining and processing technology to aircraft and aerospace structures. Research, development, and implementation program have been carried out in many different industries throughout the world. A substantial body of knowledge now exists in open literature [3-4]; however, an even greater proportion of work remains within companies that develop on a site-specific or part specific proprietary basis, including the aerospace industry [9]. In this section, two areas of recommendations are presented with the intent of promoting a path forward to mature the technology for general industry use as well as bring about a safe, consistent, and effective (responsible) use of FSW technology for building airframe and wing structures.

To safely allow the expansion of FSW technology to a broader portion of the aerospace industry several actions are needed; industry available of specifications, the available of design values published in industry handbooks which are acceptable to regulatory agencies, and an acceptable procedures which would allow individual manufacturers to demonstrate that FSW method being employed in their manufacturing facilities yield similar results as the FSW method used to derive the published design values. To achieve these will require a concretive effort of industry, standard organizations, academia and regulatory agencies.

7.1 DEVELOPMENT OF FSW SPECIFICATIONS

As demonstrated by the data collected during this research, it is possible to achieve similar using different FSW setting. Based on observation (from experience and open literature) that widely varying tool design has been used to make sound joints and processed material with independently developed process windows in virtually all aluminum alloys. Any advantage one tool may have over another is manifest primarily in terms of productivity (i.e., in joining and processing speeds). As such it may be possible that industry performance specifications could be developed which adequately defines the results of various FSW methods. Further rationale for using performance specifications is that FSW may be viewed as a supplemental thermo mechanical-processing operation superimposed over the parent material thermo mechanical-processing history. It does not change bulk chemistry (no filler transformation). Nor does it does it involve recasting the alloy (no bulk solid- or liquid-phase transformation). Joint properties typically increase in work-hardened, non-heat-treatable alloys (e.g., Al 5XXX) as a result of grain refinement in the stir zone (or weld nugget). In precipitation-strengthened aluminum alloys, joint properties are typically decreased as a result of overaging in the HAZ adjacent to the joint.

While the development of industry performance specifications would possibly allow the publication in industry handbooks, individual manufacturers will still be required to develop their internal process specifications controlling the FSW methods being employed in their facilities. These specifications would reflect the unique equipment being used to fabricate their specific product. To allow individual manufacturers to use any industry published design values they need to conduct a simplified test program. (See section 7.2 below.)

7.2 SHARED DATABASES

Industry specifications and standards for FSW and related technologies are beginning to be released [94–95]. However, design data minimums for use by the aviation industry have not yet been developed and published. Consequently, the development and implementation of commercial aviation applications incorporating these new technologies have required more effort, in terms of testing and verification, than developing the applications based on conventional joining technologies (namely, installed fasteners) for which industry specifications and standards have been established for many years.

In general the shared database approach has been adopted by the Composite Materials Handbook 17 (CMH-17), which is the equivalent handbook to MMPDS for composite materials. Like FSW, composite materials are process dependent materials for which global design values are published based on industry specifications and with a process where individual manufactures verify their internal processes meet the global requirements via a simplified test program. In the case of FSW, there is a need for both industry-wide specifications that outline the general requirements and specific company specifications that detail how the requirements from the industry specifications are being met by that company's equipment.

8. SUMMARY

The NIAR Advanced Joining & Processing Lab conducted a program entitled "Evaluation of Friction Stir Weld Process and Properties for Aircraft Applications" over a 7-year period, funded by FAA grants with cost-match funds provided through the Kansas NIS grant program. The most important results produced during this period of performance were chronicled in annual reports submitted to the NIS executive board in partial fulfillment of the NIS program requirements. A final report was prepared for the FAA in partial fulfillment of the FAA grant-reporting requirements. This final report features several key findings of the program and references the more comprehensive annual reports prepared for the NIS board.

The four main areas of research findings featured in this final report submitted to the FAA were (1) a summary of the annual reports (prepared for the parallel NIS program), (2) a brief discussion of a roadmap for developing design data for FSW and FSSW, (3) an analysis of data measured from welds prepared for the MMPDS round-robin study (see section 8 and appendix A), and (4) an introduction to e-NDE and its capability in terms of POD.

From the MMPDS evaluation program, it was determined that with a proper combination of industry and company specification data from FSW joints can be combined (pooled) to provide a minimum design value. Regarding the properties of the alloys studied, AA2198-T8 welds had

good uniform tensile strength of at least 68% of the parent tensile strength; 75% of the data were greater than 58 ksi, or 72.7% of the parent tensile strength. The weld nugget was found to be softer than the parent material and had a very small HAZ and TMAZ.

The AA2024-T3 material demonstrated a dramatic increase in conductivity in the HAZ of a hot weld and in the nugget of the cold weld, which corresponds to areas with an increased concentration of precipitate microstructure. The AA2198-T8 welds had very little change in conductivity in the weld area. Overall, the welds of AA2024-T3 material were strong, with at least 88% parent strength and uniform tensile strength within the weld. The welds did not have a statistically significant variation in tensile specimen properties when compared according to weld parameters or location. The variation in the tensile data between sites was statistically significant.

All Phase II AA2024-T3 weld data, except for three data points, were above the T_{90} allowable of 62.5 ksi calculated in Phase I, and only one was significantly lower than the calculated allowable value of 62.5 ksi. Two of the three welds with the lower UTS values offer the possibility of improvement since they are not significantly below the T_{90} allowable value. The other UTS values for welds made with the same tool are above the T_{90} allowable value.

Because all LM data were below the results from the other sites, weld UTS values could be improved by refining their process window. At least one UTS value was significantly below the T_{90} allowable value. Thus, it was possible that more than process-window refinement may be needed to improve the UTS on this weld. The welds were produced using different machinery, various weld-tool designs, and a wide variety of weld parameters at four production sites with their own process controls and procedures.

Therefore, it was shown that an unspecified number of tool designs could be used to make equally sound joints with independently developed process windows. In addition, there is significant evidence that the process can be effectively controlled via performance specifications in combination with specific local company specifications because of the significant evidence that FSW can be controlled independently at different sites to achieve a commonly defined engineering requirement. It was also shown that there is support for the statement that any advantage one tool may have over another is primarily in terms of productivity (i.e., welding and processing speeds) according to the findings. The AA2198-T8 material will require further research to improve the weld joint efficiency of 68% to 72.7% of the parent UTS. Since the material used in this study was not in the ideal, optimum starting temper for FSW, low joint efficiency resulted. Therefore, further work with material in an optimized temper for FSW is expected to demonstrate much greater joint efficiencies. More data are needed to generate sufficient data to support standards and specifications for FSW.

A new e-NDE technique was evaluated in this program. It was a significant innovation that provided greater POD than conventional NDE techniques. Combining advanced force feedback signal analysis with FSW, results in a layering of a green inspection technology over a green manufacturing technology, thus creating a green-squared (Green^2 or G^2) synergistic, robust production system. The greenness of e-NDE as an electronic-inspection technique is realized in reducing and potentially eliminating the need for secondary inspection operations like penetrant, x-ray, and ultrasonic inspections. It can also conceivably be developed to monitor tool wear,

optimize the design and performance of FSW tools, and compete different tooling design concepts, etc. In terms of establishing standards and specifications for friction stir technologies, the e-NDE technique featured in this report will greatly facilitate the establishment of performance-based specifications for FSW that will ultimately become the basis for developing design data for FSW joints in multiple structures made from multiple alloys and product forms. The ability to both monitor and correlate F_y force feedback signals to the occurrence of defect formation also provides a major opportunity to actively and adaptively control FSW operations in production operations. This unique process-monitoring tool will form the basis of a powerful e-NDE technique that will greatly reduce inspection costs, both in terms of time and resources, as well as increase accuracy and the quality of an inspection that adapts to the production system to which it is applied. Because of its evaluation capability, process monitoring of F_y (transverse) feedback forces holds the potential of being a strong complement to conventional NDE techniques for producing safe airframe structures and assemblies.

9. REFERENCES

1. Thomas, W.M., Nicholas, E.D., Needham, J.C., Murch, M.G., Templesmith, P., and Dawes, C.J., "Improvements to Friction Welding," Application (Priority) EP 0615480, December 6, 1991.

2. "Friction Stir Welding at TWI," available at http://www.twi.co.uk/content/fswintro.html (accessed 07/09).

3. Threadgill, P.L., Leonard, A.J., Shercliff, H.R., and Withers, P.J., "Friction Stir Welding of Aluminium Alloys," *International Materials Reviews*, Vol. 54, No. 2, 2009, pp. 49-93.

4. Mishra, R.S. and Ma, Z.Y., "Friction Stir Welding and Processing," *Materials Science and Engineering R*, Vol. 50, 2005, pp. 1-78.

5. "Space Shuttle Technology Summary: Friction Stir Welding," available at http://www.nasa.gov/centers/marshall/pdf/104835main_friction.pdf (accessed on 05/10/11).

6. "Lockheed Martin Capabilities," available at http://www.lockheedmartin.com/products/FrictionStirWelding/Experience.html (accessed on 05/10/11).

7. Kumar, B., Widener, C., Jahn, A., Tweedy, B., Cope, D., and Lee, R., "Review of the Applicability of FSW Processing for Aircraft Applications," *46th AIAA SDM*, Austin, Texas, April, 2005.

8. "Delta Rocket Gallery," available at http://www.boeing.com/companyoffices/gallery/images/space/delta_iv/d4_mfg_06.html (accessed on 05/10/11).

9. "Known Friction Stir Welding Patents and Patent Applications," available at http://www.twi.co.uk/content/fswpatents.html (accessed on 05/10/11).

10. Burford, D.A., Widener, C.A., and Tweedy, B.M., "Advances in Friction Stir Welding for Aerospace Applications," *6th AIAA Aviation Technology Integration and Operations Conference (ATIO)*, Vol. ATIO-12 Materials for Aerospace Vehicles, Wichita, Kansas, 2006.

11. Arbegast, W.J., "Application of Friction Stir Welding and Related Technologies," *Friction Stir Welding and Processing*, ASM International, Mishra, R.S. and Mahoney, M.W., Eds., 2007, chapter 13, pp. 273-308.

12. "Eclipse Aerospace," available at http://eclipseaerospace.net/files/pdf/FSW.pdf. (accessed on 05/10/11).

13. "Fuji Heavy Industries Delivers the First Eclipse 500 Production Wing to Eclipse Aviation," available at http://www.fhi.co.jp/english/news/press/2006/06_06_02e.pdf.

14. Burford, D.A., "Friction Stir Welding of Airframe Structure: From One Delivery System to Another," *SAE 2003 Transactions, Journal of Aerospace*, Section 1, Vol. 112, pp. 295-300.

15. Polt, W., "A Little Friction at Boeing," *Boeing Frontiers Onlines*, Vol. 03, No. 5, September 2004.

16. Burford, D.A., "Friction Stir Welding and Related Topics," N*IS End-of-Year Progress Report NIS Project No. 09-006*, NIAR, WSU, Wichita, Kansas, August 2009.

17. Lohwasser, D., "Friction Stir Welding of Longitudinal Fuselage Splices," *Proceedings of the 6th International Friction Stir Welding Symposium*, Session 4A, Saint-Sauveur, Northern Montreal, October 10, 2006.

18. "Webinar Highlights EADS Technology Licensing," available at http://www.eads.com/eads/int/en/our-company/innovation-at-eads/ip-tech-licensing/Technology-Licensing-News/EADS-Webinar-highlights.html. (accessed on 05/10/11).

19. Silvanus, J., "EADS Technology Licensing Initiative Webinar," available at C:\\Temp\\PKA.tmp\\www.eads.com\\dms\\eads\\int\\..\\EADS-Technology-Licensing-Webinar.ppt (accessed on 05/10/11).

20. Baumann, J.A., Burton, K., Bommer, H., and Matlack, M., "Friction Stir Process Capabilities for Highly Contoured Applications: System Design Details for 3D Welding," *6th International Symposium on Friction Stir Welding*, Vol. 6ISFSW, Saint-Sauveur, Quebec, Canada, 2006.

21. Fortes, L., "Friction Stir Welding Applied on Mid Size Aircraft," *AeroMat 2009 Conference & Exibition*, Welding & Joining, Session 2: Friction Stir Welding Processing, Dayton, Ohio, 2009.

22. Fernandez, F., "Friction Stir Welding Applied on Mid Size Aircraft," *8th International Friction Stir Welding Symposium*, Session 5A, Timmendorfer Strand, Germany, 2010.

23. "An Embraer Web site," available at http://www.paper4web.com/banca/embraer/reader2/?pid=1&eid=174 (accessed on May 10, 2011).

24. Kok, L.J.J., Poston, K., and Moore, G., "Bombardier Aerospace FSW Demonstrator," *26th ICAF Symposium*, ICAF, Montreal, Canada, 2011.

25. Cope, D., "Friction Stir Welding Study and Laser Welding Feasibility Study," NIAR, WSU, Wichita, Kansas, NIS Annual Progress Report NIS Document Nos: 04-009, 04-010, and 04-012, June 2004.

26. Cope, D., "Friction Stir Welding and Related Topics," NIAR, WSU, Wichita, Kansas, NIAR End-of-Year Progress Report NIS Document No. 05-009, July 2005.

27. Widener, C.A., Burford, D.A., Kumar, B., Talia, J.E., and Tweedy, B., "Evaluation of Post-Weld Heat Treatments to Restore the Corrosion Resistance of Friction Stir Welded Aluminum Alloy 7075-T73 vs. 7075-T6," *Materials Science Forum*, Vol. 539-543, 2007, pp. 3781-3788.

28. Widener, C.A., Talia, J.E., Tweedy, B.M., and Burford, D.A., "Investigation to Restore the Exfoliation Resistance of Friction Stir Welded Aluminum Alloy 2024," *Friction Stir Welding and Processing IV*, Orlando, Florida, 2007, pp. 459-468.

29. Widener, C.A., Talia, J.E., Tweedy, B.M., and Burford, D.A., "High-Rotational Speed Friction Stir Welding With a Fixed Shoulder," *6th International Symposium on Friction Stir Welding*, Saint-Sauveur, Nr Montréal, Canada, 2006.

30. Tweedy, B.M., Sellmeyer, S., Jahn, A., and Burford, D.A., "Static Strength Comparison of Riveted Versus Friction Stir Welded Stiffened Panels," *47th AIAA-ASME-ASCE-AHS-ASC Structures, Structural Dynamics, and Materials Conference*, Newport, Rhode Island, 2006.

31. Burford, D.A., Widener, C.A., and Tweedy, B.M., "Friction Stir Welding and Related Topics," NIAR, WSU, Wichita, Kansas, NIS End-of-Year Progress Report NIS Project No. 06-006, July 2006.

32. Widerner, C.A., Tweedy, B.M., and Burford, D.A., "Effect of Fit-Up Tolerances on the Strength of Friction Stir Welds," *47th AIAA/ASME/ASCE/AHS/ASC Structures, Structural Dynamics, and Materials Conference*, Newport, Rhode Island, 2006.

33. Widener, C.A., Talia, J.E., Tweedy, B.M., and Burford, D.A., "Corrosion in Friction Stir Welded Dissimilar Aluminum Alloy Joints of 2024 and 7075," *Friction Stir Welding and Processing IV*, Orlando, Florida, 2007, pp. 449-458.

34. Cook, R. Handboy, T., Long Fox, S., and Arbegast, W.J., "Friction Stir Welding of Dissimilar Aluminum Alloys," *Friction Stir Welding and Processing III*, TMS Annual Meeting, San Diego, California, 2005, pp. 35-42.

35. Burford, D.A., Tweedy, B.M., and Widener, C.A., "Friction Stir Welding and Related Topics," NIAR, WSU, Wichita, Kansas, NIAR End-of-Year Progress Report NIS Project No. 07-006, July 2007.

36. "12th MMPDS Coordination Meeting Minutes," available at http://projects.battelle.org/mmpds/PUBLICMinutesandAgendas/12thMINUTESpublic.pdf.

37. Burford, D.A. and Widener, C.A., "FSW Path Independence Study," 2007, 12th MMPDS Coordination Meeting.

38. Widener, C.A., Tweedy, B.M., and Burford, D.A., "Path Independence of Allowables Based Friction Stir Butt Welds," *7th AIAA Aviation Technology, Integration, and Operations Conference*, Belfast, Northern Ireland, Ireland, 2007, pp. 1702-1711.

39. Tweedy, B.M., Widener, C.A., and Burford, D.A., "The Effect of Surface Treatments on the Faying Surface of Friction Stir Spot Welds," *Friction Stir Welding and Processing IV*, Orlando, Florida, 2007, pp. 333-340.

40. Tweedy, B.M., Widener, C.A., and Burford, D.A., "Fundamental Properties of Friction Stir Welded Al 7136 Including Effects of Post-Weld Artificial Aging," *6th International Symposium on Friction Stir Welding*, Saint-Sauveur, Northern Montréal, Canada, 2006.

41. Burford, D.A., Tweedy, B.M., and Widener, C.A., "Influence of Shoulder Configuration and Geometric Features on FSW Track Properties (Paper 36)," *Proceedings of the 6th International Friction Stir Welding Symposium*, Saint-Sauveur, Northern Montreal, Canada, October 10–13, 2006.

42. Burford, D.A., "Friction Stir Welding Tool Having a Scroll-Free Concentric Region," Patent No. 8,016,179, September 13, 2011.

43. Burford, D.A., Widener, C.A., Tweedy, B.M., and Brown, J., "Friction Stir Welding and Related Topics," NIAR, WSU, Wichita, Kansas, NIS End-of-Year Progress Report NIS Project No. 08-006, July 2008.

44. Merry, J.D., Tweedy, B.M., Widener, C.A., and Burford, D.A., "Static Strength Comparison of Discontinuous Friction Stir Welded Stiffened Panels," *Friction Stir Welding and Processing IV*, Orlando, Florida, 2007.

45. Burford, D.A., Tweedy, B.M., and Widener, C.A., "Fatigue Crack Growth in Integrally Stiffened Panels Joined Using Friction Stir Welding and Swept Friction Stir Spot Welding," *Journal of ASTM International*, Vol. 5, No. 4.

46. Tweedy, B.M., Widener, C.A., Merry, J., Brown, J., and Burford, D.A., "Factors Affecting the Properties of Swept Friction Stir Spot Welds," *SAE 2008 World Congress*, Detroit, Michigan, 2008.

47. Cederqvist, L. and Reynolds, A., "Factors Affecting the Properties of Friction Stir Welded Aluminum Lap Joints," *Welding Journal*, Vol. 80-12, December 2001, pp. 281-287.

48. Widener, C.A., Tweedy, B.M., and Burford, D.A., "An Investigation of the Effects of Tool Design and Welding Parameters on Fatigue Life In Friction Stir Welded 2024-T3," *7th International Friction Stir Welding Symposium*, Awaji Island, Japan, May 20-22, 2008.

49. Tweedy, B.M., Widener, C.A., Jurak, S.F., and Burford, D.A., "Effects of Weld Tool Design and Welding Parameters on Swept Friction Stir Spot Welding in Thin Gage Aluminum," *7th International Friction Stir Welding Symposium*, Awaji Island, Japan, 2008.

50. Widener, C.A., Lam, T.L., and Burford, D.A., "Corrosion in 2XXX-T8 Aluminum Alloys," *Friction Stir Welding and Processing V*, San Francisco, California, 2009, pp. 257-264.

51. Gimenez, P., Widener, C.A., Brown, J., and Burford, D.A., "Correlation Between Ultrasonic Phased Array and Feedback Force Analysis of Friction Stir Welds," *Friction Stir Welding & Processing V*, San Francisco, California, 2009, pp. 265-272.

52. Misak, H., Widener, C.A., Burford, D.A., and Asmatulu, R., "The Distribution and Flow of Nickel Powder and Carbon Nanotubes Mixed in an Aluminum Matrix via Friction Stir Welding," *SAMPE Fall Technical Conference*, Wichita, Kansas, 2009.

53. Gross, J., Akhtar, F., Tweedy, B.M., Widener, C.A., and Burford, D.A., "Development of an End-Effector for Friction Stir Spot Welding," *Aerospace Manufacturing and Automated Fastening Conference*, Charleston, South Carolina, 2008.

54. Tweedy, B.M., Widener, C.A., Lam, T., Burford, D.A., and Brown, J., "Fatigue of Swept Friction Stir Spot Welds In Thin Sheet 2024-T3 Aluminum," *Aerospace Manufacturing and Automated Fastening Conference & Exhibition*, Charleston, South Carolina, 2008.

55. NASM 1312.21 "Fastener Test Methods, Method 21, Sheer Joint Fatigue Constant Amplitude," National Aerospace Standard, 1997.

56. Burford, D.A., "Friction Stir Welding Tool Having a Counterflow Pin Configuration," Patent No. 7,942,306, May 17, 2011.

57. Brown, J., Widener, C.A., Moore, G., Poston, K., and Burford, D.A., "Evaluation of Swept Friction Stir Spot Welding in Al 2219-T6," *Friction Stir Welding & Processing V*, San Francisco, California, 2009, pp. 215-224.

58. Brown, J., Burford, D.A., Widener, C.A., Horn, W., Talia, J., and Tweedy, B.M., "Corrosion and Fatigue Evaluation of Swept Friction Stir Spot Welding Through Sealants and Surface Treatments," *Friction Stir Welding & Processing V*, San Francisco, California, 2009, pp. 273-285.

59. Lam, T.J., Widener, C.A., Brown, J., and Burford, D.A., "Low Z-Force Friction Stir Spot Welds Conventional Tool & Process Development Approach," *Friction Stir Welding & Processing V*, San Francisco, California, 2009, pp. 181-190.

60. Burford, D.A., "Friction Stir Welding and Related Topics," NIAR, WSU, Wichita, Kansas, NIAR End-of-Year Progress Report NIS Project No. 10-006, August 2010.

61. Burford, D.A., Gimenez Britos, P., Boldsaikhan, E., and Brown, J., "Evaluation of Friction Stir Weld Process and Properties for Aerospace Application: e-NDE for Friction Stir Processes," *6th Annual Technical Review Meeting*, May 2010.

62. Brown, J., Gross, J., Buller, J., and Burford, D., "Retractable vs. Fixed Probe Tools in Swept Friction Stir Spot Welding," *Friction Stir Welding & Processing IV*, San Diego, California, 2011.

63. Burford, D.A. and Widener, C.A., "Evaluation of Friction Stir Welding Process and Properties for Aerospace Application: Standards and Specifications Development," Wichita State University, Wichita, Kansas, July 21-22, 2009.

64. Widener, C.A., Burford, D.A., and Jurak, S.F., "Effects of Tool Design and Friction Stir Welding Parameters on Weld Morphology in Aluminum Alloys," *Materials Science Forum*, Vol. 638-642, 2010, pp. 1261-1266.

65. Kumar, K. and Kailas, Satish V., "The Role of Friction Stir Welding Tool on Material Flow and Weld Formation," *Materials Science and Engineering A*, Vol. 485, No. 1-2, June 2008, pp. 367-374.

66. Colligan, K.J., "Relationships Between Process Variables Related to Heat Generation in Friction Stir Welding of Aluminum," *4th Symposium on Friction Stir Welding and Processing-TMS 2007 Annual Meeting and Exhibition*, Orlando, Florida, February 25, 2007- March 1, 2007, pp. 39-54.

67. Burford, D.A., Tweedy, B.M., and Widener, C.A., "Development of Design Data for FSW and FSSW," *7th International Friction Stir Welding Symposium*, Awaji Island, Japan, May 20-22, 2008.

68. Iwashita, T., "Method and Apparatus for Joining," U.S. Patent 6601751, 2003.

69. Shilling, C. and Dos Santos, J., "Method and Device for Joining at Least Two Adjoining Work Pieces by Friction Welding," U.S. Patent Application 2002/0179682, 2002.

70. Okamoto, K., Hunt, F., and Hirano, S., "Development of Friction Stir Welding Technique and Machine for Aluminum Sheet Metal Assembly—Friction Stir Welding of Aluminum for Automotive Applications," *2005 SAE World Congress*, Detroit, Michigan, April 2005.

71. Addison, A.C. and Robelou, A.J., "Friction Stir Spot Welding: Principle Parameters and Their Effects," *Proceedings of the 5th International FSW Symposium*, Metz, France, September 14-16, 2004.

72. Reynolds, A.P., Tang, W., Khan, J.A., and Lindner, K., "Relationships Between Weld Parameters, Hardness Distribution and Temperature History in Alloy 7050 Friction Stir Welds," *Science and Technology of Welding and Joining*, Vol. 2, No. 9, 2005, pp. 190-199.

73. Rao, J.C., Payton, E.J., Somsen, C., et al., "Where Does the Lithium Go—a Study of the Precipitates in the Stir Zone of a Friction Stir Weld in a Li-containing 2xxx Series Al Alloy," *Advanced Engineering Materials*, Vol. 12, Issue 4, 2010, pp. 298-303.

74. Widener, C.A., Tweedy, B.M., and Burford, D.A., "FSW Path Independence Study," *13th Annual MMPDS Coordination Meeting*, March 31-April 3, 2008.

75. Burford, D.A., Widener, C.A., Tweedy, B.M., and Brown, J., "Industry Review Meeting, Evaluation of Friction Stir Weld," WSU, Wichita, Kansas, Project Review, January 31, 2008.

76. Ehrström, J.C., Bigot, A., and Gérard, H., "Microstructure and Properties of Aluminum Alloys Friction Stir Welds for Aircraft Application," *Materials Science Forum*, Vol. 426-432, No. 4, 2003, pp. 2941-2946.

77. Rice, R., "Statistical Analysis of Friction Stir Weld Round-Robin Test Data," Emerging Materials Working Group, *17th MMPDS Coordination Meeting*, Atlanta, Georgia, April 29, 2010.

78. American Welding Society, "Specification for Friction Stir Welding of Aluminum Alloys for Aerospace Hardware," Report No. AWS D17.3/D17.3M: 200X.Draft.

79. ASM International, "Vol. 2—Properties and Selection: Nonferrous Alloys and Special-Purpose Materials," *Metals Handbook*, ASM International, 10th Ed., 1990.

80. Jurak, S.F., "Statistical Analysis of the Mechanical Properties of Friction Stir Welded AA2024 and AA2198 Aluminum Alloys," Master's Thesis, Mechanical Engineering, Wichita State University, December 2011.

81. Jones, M.J., Heurtier, P., Desrayaud, C., Montheillet, F., Allehaux, D., and Driver, J.H., "Correlation Between Microstructure and Microhardness in a Friction Stir Welded 2024 Aluminium Alloy," *Scripta Materialia*, Vol. 52, No. 8, April 2005, pp. 693-697.

82. Le Jolu, T., Morgeneyer, T.F., and Gourgues-L, A.F., "Effect of Joint Line Remnant on Fatigue Lifetime of Friction Stir Welded Al-Cu-Li Alloy," *Science and Technology of Welding and Joining*, Vol. 15, No. 8, 2010, pp. 694-698.

83. Lertora, E. and Gambaro, C., "AA8090 Al-Li Alloy FSW Parameters to Minimize Defects and Increase Fatigue Life," *International Journal of Material Forming*, Vol. 3, Supplement 1, 2010, pp. 1003–1006.

84. McDarmaid, D.S., "Effect of Natural Aging on the Tensile Properties of the Al-Li Alloys 8090, 8091 and 2091," *Materials Science and Engineering*, Vol. 101, Supplement 1, May 1988, pp. 193-200.

85. Zhang, Y. and Sims, N., "Milling Workpiece Chatter Avoidance Using Piezoelectric Active Damping: A Feasibility Study," *Smart Material Structure*, Vol. 14, 2005, pp. N65–N70.

86. Boldsaikhan, E., "The Use of Feedback Forces for Nondestructive Evaluation of Friction Stir Welding," South Dakota School of Mines and Technology, Doctoral Dissertation, Materials Science, 2008.

87. Jene, T., Dobmann, G., Wagner, G., and Eifler, D., *MonStir—Monitoring of the Friction Stir Welding Process*, 7th ed., Awaji Island, Japan, May 20-22, 2008.

88. Arbegast, W., "Modeling Friction Stir Joining as a Metalworking Process," *Hot Deformation of Aluminum Alloys III*, 2003.

89. Balasubramanian, N., Gattu, B., and Mishra, R., "Process Forces During Friction Stir Welding of Aluminium Alloys," *Science and Technology of Welding and Joining*, Vol. 14, No. 2, pp. 141-145.

90. Gimenez Britos, P., "Probability of Detection in Friction Stir Welding Using Nondestructive Evaluation Techniques," Master's Thesis, Industrial Engineering, Wichita State University, May 2010.

91. Burford, D.A., Widener, C.A., and Tweedy, B.M., "Path Independence of Friction Stir Welding and Friction Stir Spot Welding Developed as an "In Situ" Integral Fastener System," *8th International Conference on Trends in Welding Research Conference*, Callaway Gardens Resort, Pine Mountain, Georgia, June 1-6, 2008.

92. Gimenez-Britos, P., Widener, C., Boldsaikhan, E., and Burford, D., "Probability of Detection Analysis of NDT Methods for Friction Stir Welded Panels," *8th International Friction Stir Welding Symposium*, Timmendorfen Strand, Germany, May 18-20, 2010.

93. Boldsaikhan, E., Logar, A., and Corwin, E., "Real-Time Monitoring in Friction Stir Welding: The Use of Feedback Forces for Nondestructive Evaluation of Friction Stir Welding," Lambert Academic Publishing, 2010.

94. American Welding Society, “Specification for Friction Stir Welding of Aluminum Alloys for Aerospace Applications,” Report No. AWS D173/D17.3M:2010 available at http://files.aws.org/pr/122109.pdf (accessed on 05/12/11)

95. “International Standards for Business, Government and Society,” available at http://www.iso.org/iso/iso_catalogue/catalogue_tc/catalogue_detail.htm?csnumber=44056. (accessed on 05/10/11).

96. Burford, D.A., “End Effector for Forming Swept Friction Stir Spot Welds,” Application number: 12/703,648, February 10, 2010.

97. Price, A., Diouf, D., Chong, H., Stahl, P., Wereagoda, T., and Kok, W., “Motion Enhancement to Friction Stir Welding End Effector,” WSU Mechanical Engineering, Wichita State University, Wichita, Kansas, Senior Design Project Final Report ME 662, May 4, 2011.

98. Manufacturing Technology, Inc., http://www.mtiwelding.com/equipment/1/Friction-Stir-Welding (accessed on 2011).

99. “ESAB Welding & Cutting,” http://products.esab.com/Templates/T041.asp?id=177852.

100. Burford, D.A., “Guided Robotic Friction Stir Welding (FSW) and Friction Stir Spot Welding (FSSW),” April 28, 2010.

APPENDIX A—MMPDS FSW ROUND-ROBIN TEST PLAN

This Appendix contains a test plan for a round-robin test program conducted by the Emerging Technologies Working Group (ETWG) (formerly the Process Intensive Materials Working Group) of the Metallic Material Properties Development and Standardization (MMPDS) coordinating committee [A-1 through A-9]. The test plan, prepared by a subcommittee of the ETWG, is included in this Appendix. Roger Reinmuller of Lockheed Martin chaired the committee and drafted and compiled the information from the subcommittee for the plan.

Mechanical Testing of Friction Stir Weld Butt Welds
Dec. 5, 2007

A.1 SCOPE

This document establishes a standard practice to determine the mechanical properties of full penetration butt welds produced via friction stir welding (FSW). This standard practice focuses on FSW of 2XXX aluminum (Al) alloys and is based on draft American Welding Society (AWS) D17.3 Class A welds. A comparable draft specification is ISO/CD draft "Friction Stir Welding of Aluminum-General Requirements." Ref: ISO/CD draft 25239 parts 1 through 5.

Test data will be used to estimate mechanical property design strengths for FSW. Specifications equivalent to those cited by AWS or ISO may be used (e.g., ASTM specifications).

This program is not intended to produce production weld schedules for any participant and should not be construed as such. This is a demonstration program solely for the purpose of producing data for MMPDS use. If these weld schedules were to be used for a specific design, then further development (e.g., repair procedures) would need to be developed.

A.2 GENERAL DESCRIPTION

Multiple contributors will submit FSW test panels for mechanical properties tests of ultimate tensile and yield strengths and percent elongation as well as nondestructive testing. The test weldment configuration to be studied is full penetration FS butts weld in 2XXX Al plate and sheet thickness. Each contributor shall submit a minimum of 16 test panels total consisting of four each Al 2024 T3 (T351) welds in 0.25-inch and 0.125-inch thickness, and four each Al 2098 T8 welds in 0.25-inch and 0.125-inch thickness (reference table A-1 and figure A-1). The following material will be provided:

- 30 ft. of 2024-T351 0.25 inch thick by 4 inch wide in 24 inch lengths
- 30 ft. of 2024-T3 0.125 inch thick by 4 inch wide in 24 inch lengths
- 30 ft. of 2098-T851 0.25 inch thick by 4 inch wide in 24 inch lengths
- 30 ft. of 2098-T8 0.125 inch thick by 4 inch wide in 24 inch lengths

Table A-1. Test panel general submission requirement

Alloy	Temper	Thickness (inches)	Length of material provided (4-inch wide)	Panels (min. to be submitted)
Al 2024	-T3	0.125	30 ft.	4
Al 2024	-T351	0.250	30 ft.	4
Al 2098	-T8	0.125	30 ft.	4
Al 2098	-T851	0.250	30 ft.	4

Process development is to be based on a statistically based design of experiments or equivalent. The process window is to be in terms of travel speed, spindle rotation speed, and forging force.

The four supplied panels are to be produced at different combinations of process parameters within the developed process window, preferably the four extremities of the process window.

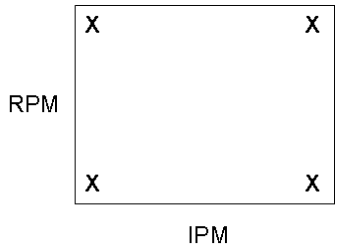

Figure A-1. Production of panels from four extremities of process window

All test panels for this study shall be welded by certified welders in accordance with a certified Weld Procedure Specification (WPS) and documented per draft AWS D17.3, Annex C or equivalent (where available). The following sections contain the minimum requirements for welding, inspection and testing for this study. The requirements are in accordance with draft AWS D17.3 or CD/ISO draft 25239 requirements pertinent to this test. General requirements for welder certification, quality inspector qualification, mechanical test requirements, shall be in accordance with the contributor's industry requirements and equivalent to those of draft AWS D17.3 or ISO draft 25239.

As a minimum the following information shall be documented and reported for all test panels submitted to this requirement.

- Contributor:

  - Name and site location
  - Parent material specifications
  - Alloys and Tempers
  - Parent material specification
  - Material thickness
  - Surface condition prior to welding, including any coatings

- Weld detail specifications are as follows:

  - Welding shall be performed in the direction parallel to the grain direction of the parent metal (refer to figure 2).
  - Welds shall be a full penetration (i.e. full thickness) friction stir butt weld. This is also expressed as "there shall be no lack of penetration (LOP)" or "The ligament penetration shall be 0.020-inch maximum and 0.005 inch minimum."
  - As a minimum, the following weld details shall be reported:

    - Primary weld control method: load control. (If position control is used, the load is to be monitored and shown not to vary more than ±10%.)
    - Pre-weld preparation. (It is assumed that machined surfaces with isopropyl alcohol wipe is the minimum weld prep procedure.)
    - Weld pin tool type used, fixed or adjustable pin. Bobbin or self-reacting tools shall not be used. Shoulder diameters in the 0.6 inch to 0.8 inch (15 to 20 mm) range are recommended. Note: It is recognized that standard pin tools are not available and vendors shall provide their own. Typical production style pin tool designs shall be used with features documented. Configurations similar to the Classic TWI 5651 Wiper™ or Tri-Flute™ have been demonstrated and are acceptable.
    - Pre-weld joint gaps shall be less than 0.030 inch (0.75 mm)
    - Pre-weld joint offset (mismatch) shall be less than 5% of thickness
    - Pre-weld joint peaking shall be less than 3°
    - Pin tool to weld center line offset shall be less than 0.060 inch (1.5 mm)
    - Tack welds or run-on/run-off tabs, if used, shall be reported

  - Tool rotation relative to travel (e.g., clockwise or counter clockwise)
  - Weld travel speed (in./min. or mm/min.).
  - Tool rotational speed (revolutions per minute, rpm).
  - Plunge force or down force (pounds or kN)
  - Heel plunge depth (in. or mm.).
  - Tilt angle and side tilt angle (degrees).
  - Final weld contour shall be post weld sanded to remove flash.
  - Final joint thickness shall not varying beyond acceptable material tolerances (e.g., Aluminum Association, Aluminum Standards & Data, Table 7.7b, 2003 edition).
  - Surface roughness along the direction of the joint shall be less than 125 micro inches
  - No post weld heat treatment shall be performed.

Test panel shape and minimum dimensions (figure A-2):

- Minimum width (a): 4-inch (~100-mm)
- Minimum length (b): 20-inch (~500-mm)
- Thickness (t): 0.25-inch to 0.35-inch sheet and 0.125-inch to 0.175-inch plate (6.35-mm to 8.9-mm and 3.175-mm to 4.45-mm, respectively)

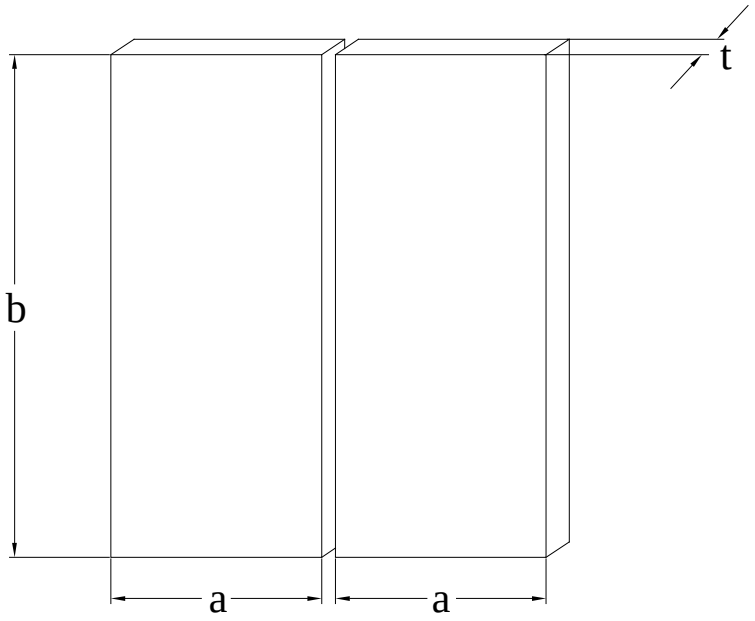

Figure A-2. Butt Weld test panel

A.3 TEST PROCEDURE

Testing of the welded panels shall encompass destructive and nondestructive evaluation (NDE). All NDE shall be performed prior to sectioning test pieces from the welded test panels. As a minimum, testing shall be performed in accordance with the requirements listed in table A-2.

Table A-2. Examination and tests of the test pieces for butt joints (draft AWS D17.3 or ISO/CD 25239-4, 2006)

Type Of Examination And Test	Extent of Examination and Test	Specification	Equivalent Specification
Transverse tensile test	Refer to Section 5	ISO 4136	ASTM E8
Macroscopic examination	1 test specimen (Optional)	ISO 17639	N/A
Shear test	2 test specimen	None identified	ASTM B831

A.4 NON-DESTRUCTIVE EVALUATION (100%)

- Visual inspection
- Volumetric inspection
    - Radiography as per ISO 17636 (equivalent specification ASTM E94) or
    - Ultrasonic inspection in accordance with ISO/DIS 17640 (equivalent specification ASTM E164)
    - Phased array
- Optional Penetrant Inspection per ISO 3452 (Equivalent specification ASTM E1417)
    - Root side weld to inspect for LOP
    - End of cut of weld to look for worm hole defect

A.5 DESTRUCTIVE TESTS

As shown in figure A-3, at least 2-inches (~50-mm) shall be discarded from each end of the test panel. Five tensile test specimens shall then be extracted and machined from the remainder of the test panel material as per ISO 4136 (equivalent specification ASTM E8) with tolerances specified in ISO 6892. (The ultimate strength, 0.2% offset yield strength, and elongation shall be recorded. Two inches, or equivalent, gage length extensometers shall be used.) Two shear test specimens per ASTM B831.

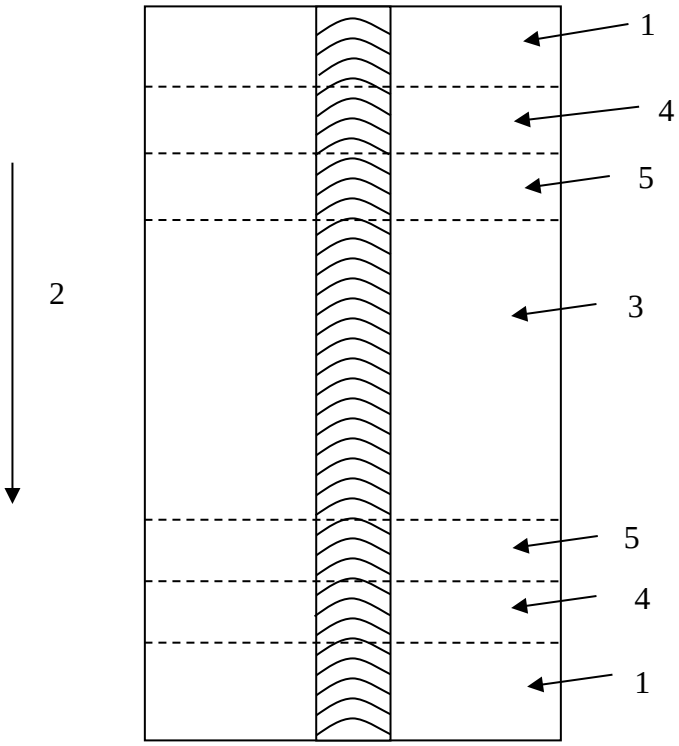

1) discard at least ~2-in (50-mm) from each end of the test panel or the start and stop of the weld, 2) direction of welding/grain direction, 3) area for tensile test specimens, 4) area for macro test specimen, and 5) area for shear test specimen

Figure A-3. Test specimen locations for Butt Weld joints

Dimensions of tensile test specimens: thickness of the specimens shall be equal to the minimum thickness of the parent metal near the welded joint. Refer to table A-3 and figure A-4 for additional specimen dimensions.

Record failure mode or location: The failure location such as parent metal, Thermo-Mechanical Affected Zone (TMAZ), Heat Affected Zone, or weld bead shall be recorded. The failure shall be characterized as advancing or retreating side. Multiple mode failures (for example TMAZ/weld) may be noted.

Table A-3. Dimensions for transverse tensile test specimens obtained from plates (ISO 4136, 2001)

Denomination	Symbol	Dimensions	
		in.	mm
Total length of the test specimen	L_t (max)	8	203
Width of shoulder	b_1	1.45	37
Width of the parallel length (plates)	b	1	25
Parallel length	L_c	≥ 2.4	≥ 60
Radius at shoulder	r	≥ 1	≥ 25
Gage length	L_O	≥ 2	≥ 50

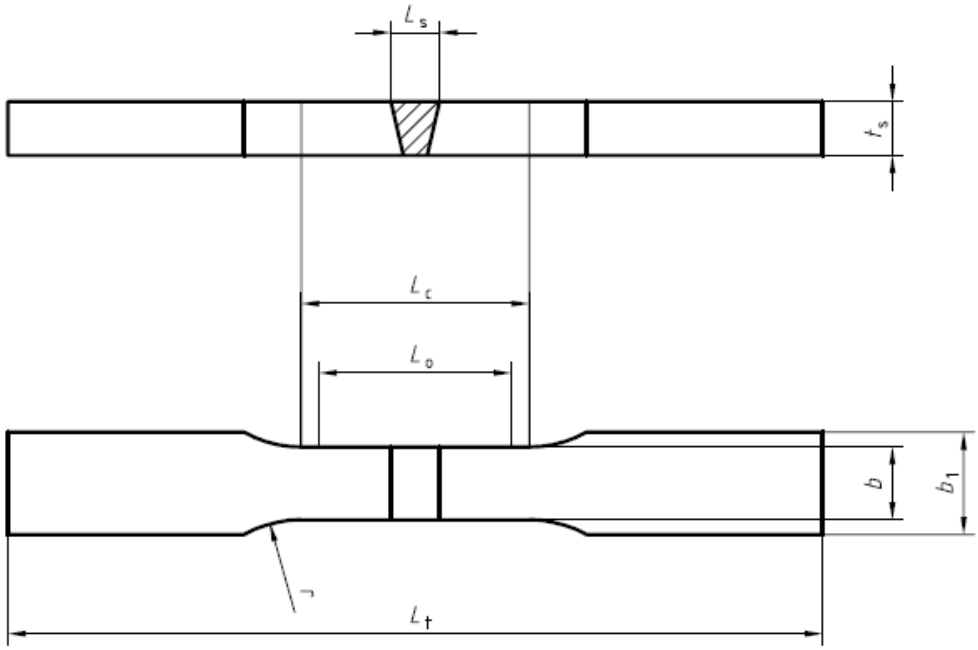

Figure A-4. Test specimens for plates (ISO 4136, 2001)

Dimensions of shear test specimens: thickness of the specimens shall be equal to the minimum thickness of the parent metal near the welded joint. Refer to table A-4 and figure A-5 for additional specimen dimensions.

- This test method is not interchangeable with that described in ASTM B565 or ASTM B769.
- The specimen orientation is considered to be the L-T orientation because the grain direction and the welding direction are parallel while the loading is in the transverse direction.

Table A-4. Dimensions for shear test specimens obtained from plates (ASTM B831)

Denomination	Symbol	Thick Weld		Thin Weld	
		in.	mm	in.	mm.
Thickness	t_s	0.25 - 0.35	6.35 - 8.9	0.125 - 0.175	3.18 - 4.45
Width	b	1.5	38.1	1.5	38.1
Length	L_t	4.5	114	4.5	114
Slot Width		0.064	1.63	0.064	1.63
Distance between slots		0.250	6.35	0.250	6.35

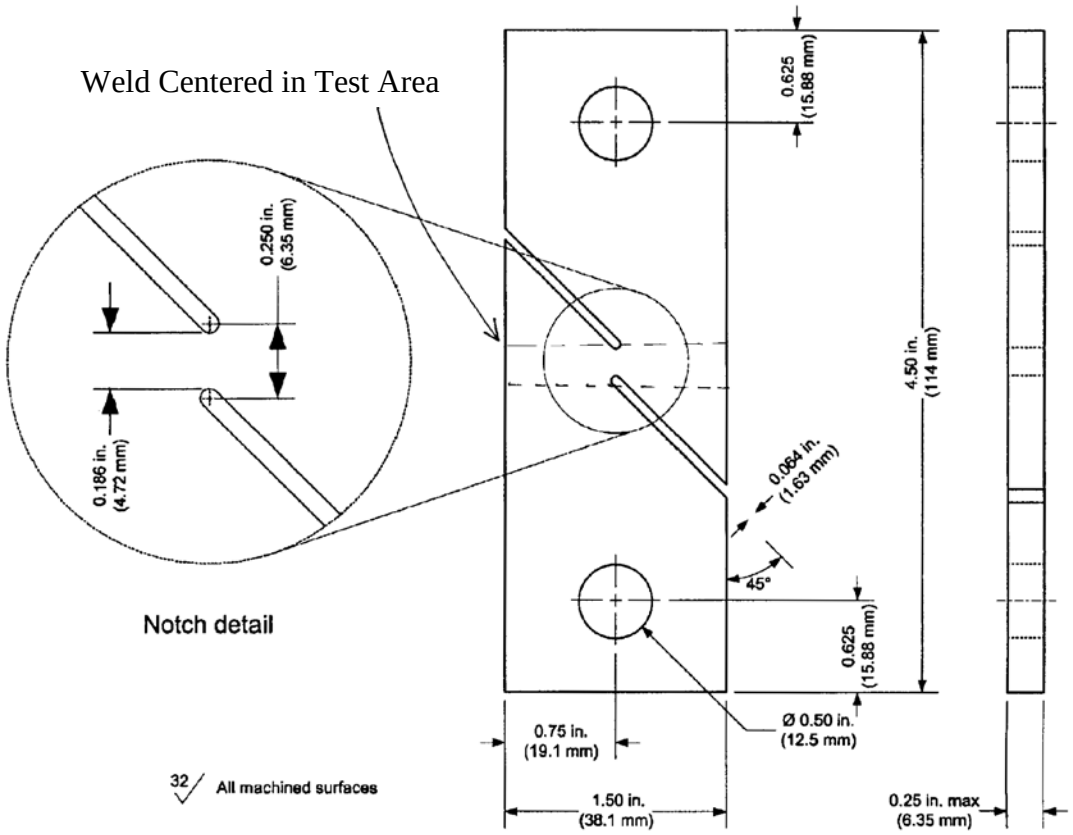

Figure A-5. Test specimen for shear test (ASTM B831)

A.6 REFERENCES

A-1. "9th MMPDS Coordination Meeting Minutes," available at http://projects.battelle.org/mmpds/PUBLICMinutesandAgendas/9thMMPDSMINUTESPublic.pdf.

A-2. "10th MMPDS Coordination Meeting Minutes," available at http://projects.battelle.org/mmpds/PUBLICMinutesandAgendas/10thMMPDSMinutesPublic.pdf.

A-3. "11th MMPDS Coordination Meeting Minutes," available at http://projects.battelle.org/mmpds/PUBLICMinutesandAgendas/11th%20MMPDS%20Minutes-Public.pdf.

A-4. "12th MMPDS Coordination Meeting Minutes," available at http://projects.batelle.org/mmpds/PUBLICMinutesAgendas/12thMINUTESpublic.pdf.

A-5. "13th MMPDS Coordination Meeting Minutes," available at http://projects.battelle.org/mmpds/13thMeetingMinutes-PUBLIC.pdf.

A-6. "14th MMPDS Coordination Meeting Minutes," available at http://projects.battelle.org/mmpds/14MinFinal-public.pdf.

A-7. "15th MMPDS Coordination Meeting Minutes," available at http://projects.battelle.org/mmpds/15thmtg/15MtgMinutes-Public.pdf.

A-8. "16th MMPDS Coordination Meeting Minutes," available at http://projects.battelle.org/mmpds/16thMtgAnnouncement/16th%20MMPDS%20Minutes-public.pdf.

A-9. "17th MMPDS Coordination Meeting Minutes," available at http://projects.battelle.org/mmpds/17thMMPDSMtg/17thMMPDSMinutes-PUBLIC.pdf.

APPENDIX B—PROPOSED GENERAL AMS MINIMUM REQUIREMENTS FOR FRICTION STIR WELDING

This appendix contains a proposed early draft Aerospace Material Specification (AMS) titled: *Friction Stir Welding and Processing of Aluminum Products and Parts General Minimum Requirements*. This proposed draft was prepared and presented to the SAE AMEC committee in meeting No. 214 on January 21, 2011, by Dr. D.A. Burford.

RATIONALE

AMSxxxx is a proposed new specification that covers mechanical properties of friction stir joined and processed aluminum material.

B.1 SCOPE

This specification establishes general mechanical property minimum requirements listed in B-3.1 for aluminum materials friction stir welded and processed product forms or parts fabricated by users or their vendors or subcontractors.

Reference to AMSxxxx on a drawing, fabrication order, purchase order, etc., constitutes a requirement to conform to the applicable provisions of the specifications listed in B-3.1 for the friction stir welding (FSW) and processing of products and parts of the particular alloy or alloys (e.g., bi-alloy joints) described. Parts made from other materials than those specified in the detail specifications may be friction stir welded or processed in accordance with the applicable requirements using processing parameters and other applicable parameters (e.g., heat treating) recommended or called out by the material producer or engineering authority unless otherwise specified by the purchaser.

The thermal-mechanical processing (processing rates, etc.) used by FSW and/or the processing service provider or fabricator for qualification of response to mechanical properties of their products shall conform to the requirements of the specifications listed in B-3.1.

Safety - Hazardous Materials and Processes

While the materials, methods, applications, and processes described or referenced in this specification may involve the use of hazardous materials or processes, this specification does not address the hazards that may be involved in such use. It is the sole responsibility of the user to ensure familiarity with the safe and proper use of any hazardous materials and processes and to take necessary precautionary measures to ensure the health and safety of all personnel involved.

B.2 APPLICABLE DOCUMENTS

The issue of the following documents in effect on the date of the purchase order forms a part of this specification to the extent specified herein. The supplier may work to a subsequent revision of a document unless a specific document issue is specified. When the referenced document has been cancelled and no superseding document has been specified, the last published issue of that document shall apply.

B.2.1 SAE PUBLICATIONS

Available from SAE International, 400 Commonwealth Drive, Warrendale, PA 15096-0001, Tel: 877-606-7323 (inside USA and Canada) or 724-776-4970 (outside USA and Canada), www.sae.org.

AMS2355	Quality Assurance Sampling and Testing of Aluminum Alloys and Magnesium Alloys, Wrought Products, Except Forging Stock, and Rolled, Forged, or Flash Welded Rings
AMS2772	Heat Treatment of Aluminum Alloy Raw Materials
AS1990	Aluminum Alloy Tempers
AMS2750	Pyrometry
ARP1962	Training and Approval of Heat Treating Personnel
ARP1917	Clarification of Terms Used in Aerospace Metals Specification
ARP823	Minimizing Stress Corrosion Cracking in Wrought Heat Treatable Aluminum Alloy Products
AMS2808	Identification, Forgings
AMS 2360	Room Temperature Tensile Properties of Castings
AMS 2694	Repair Welding of Aerospace Castings
AMS 2771	Heat Treatment of Aluminum Alloy Castings
AMS 2804	Identification, Castings
AMS-STD-2175	Classification and Inspection of Castings

B.2.2 ASTM PUBLICATIONS

Available from ASTM International, 100 Barr Harbor Drive, P.O. Box C700, West Conshohocken, PA 19428-2959, Tel: 610-832-9598, www.astm.org.

ASTM E 8 / 8M	Tension Testing of Metallic Materials
ASTM E 10	Brinell Hardness of Metallic Materials
ASTM E 18	Rockwell Hardness and Rockwell Superficial Hardness of Metallic Materials
ASTM E 384	Microindentation Hardness of Materials
ASTM B881	Standard Terminology Relating to Aluminum- and Magnesium- Alloy Products
ASTM E164	Standard Practice for Contact Ultrasonic Testing of Weldments
ASTM E1417	Standard Practice for Liquid Penetrant Testing
ASTM E1742	Standard Practice for Radiographic Examination
ASTM E238	Standard Test Method for Pin-Type Bearing Test of Metallic Materials
ASTM E9	Standard Test Methods of Compression Testing of Metallic Materials at Room Temperature
ASTM B831	Standard Test Method for Shear Testing of Thin Aluminum Alloy Products
ASTM G34	Standard Test Method for Exfoliation Corrosion Susceptibility in 2XXX and 7XXX Series Aluminum Alloys (EXCO Test)
ASTM B117	Standard Practice for Operating Salt Spray (Fog) Apparatus
ASTM G110	Standard Practice for Evaluating Intergranular Corrosion Resistance of Heat Treatable Aluminum Alloys by Immersion in Sodium Chloride + Hydrogen Peroxide Solution

B.2.3 ANSI PUBLICATIONS

Available from American National Standards Institute, 25 West 43rd Street, New York, NY 10036, Tel: 212-642-4900, www.ansi.org.

ANSI/ASQC	Sampling Procedures and Tables for Inspection by Attributes Z1.4
ANSI Z49.1	Safety in Welding, Cutting, and Allied Processes

B.2.4 AIA/NAS PUBLICATIONS

Available from Aerospace Industries Association, 1000 Wilson Boulevard, Suite 1700, Arlington, VA 22209-3928, 703.358.1000, www.aia-aerospace.org

NAS410 Certification and Qualification of Nondestructive Test Personnel

B.2.5 AWS PUBLICATIONS

Available from the American Welding Society, 550 N.W. LeJeune Rd, Miami, FL, 33126, www.aws.org

AWS D17.3 Specification for Friction Stir Welding of Aluminum Alloys for Aerospace Applications

D17.3M:2010

AWS A1.1 Metric Practice Guide for the Welding Industry

AWS A2.4 Standard Symbols for Welding, Brazing, and Nondestructive Examination

AWS B3.0 Standard Methods for Mechanical Testing of Welds

AWS B5.1 Specification for the Qualification of Welding Inspectors

AWS QC1 Standard for ASW Certification of Welding Inspectors

B.3 TECHNICAL REQUIREMENTS

B.3.1 MECHANICAL PROPERTIES

Shall be in accordance with table B-1.

Table B-1. Mechanical property minimum specifications

Friction Stir Welded or Processed Alloy	Specification
2024-T3 (based on MMPDS round-robin data package) 2198-T6 (based MMPDS round-robin data package) 2195 (?) 2219 (?) 7075-T6 (?) …	AMSxxxx/1 AMSxxxx/2 …

B.3.2 JOINT DESIGN

Unless specified in the purchasing documents or the engineering drawings, joint designs shall conform to AWS D17.3/D17.3M:2010, Clause 5.

B.3.3 JOINT CLASSIFICATION

Joints shall be classified per AWS D17.3/D17.3M:2010, Clause 4, and conform to the inspection requirements of AWS D17.3/D17.3M:2010, Clause 9, according to the classification callout.

B.3.4 WELDING AND PROCESSING PROCEDURE

Development and maintenance of the welding and processing procedure shall conform to AWS D17.3/D17.3M:2010, Clause 6. If specified, instructions in the purchasing documents or the engineering drawings shall also apply.

B.3.5 CLEANING AND CORROSION PROTECTION

Cleaning procedures shall meet the minimum requirements of AWS D17.3/D17.3M:2010, Subclause 8.3.2. Parts shall be protected from corrosion during processing and storage.

B.3.6 PRE-WELD TEMPER CONDITION

The pre-weld temper condition shall be as indicated in the Specifications listed in table B-1 of section B-3.1.

B.3.7 INSPECTION

The inspection requirements of AWS D17.3/D17.3M:2010, Clause 9, shall be met. Inspection requirements provided in the purchasing documents and/or the engineering drawings shall supplement or supersede the inspection requirements of AWS D17.3/D17.3M:2010, Clause 9.

B.3.8 QUALIFICATION

B.3.8.1 Fabricator

Facilities performing FSW and processing in accordance with this specification shall be approved as specified herein by the cognizant quality assurance organization. The fabricator shall develop and qualify welding and processing procedures according to AWS D17.3/D17.3M:2010, Clause 9, and any applicable requirements included in the purchasing documents or engineering drawings.

B.3.8.2 Personnel

All personnel performing FSW and processing and associated operations shall be trained and approved in accordance with the procedure outlined in AWS D17.3/D17.3M:2010, Clause 7.

B.3.8.3 Equipment for Friction Stir Welding and Processing

Equipment shall meet the requirements of AWS D17.3/D17.3M:2010, Subclause 8.1.

B.3.8.4 Welding and Processing Tools

Tools shall conform to AWS D17.3/D17.3M:2010, Subclause 8.2. They shall be non-consumable and made from materials that do not react with the aluminum alloys being joined or processed. The geometry of the tools shall conform to the tool-drawing requirements of the fabricator. Tools may be uncoated or coated with wear-resistance coatings.

B.3.8.5 Welding/Processing Procedures

Welding procedures shall be developed, qualified, and maintained per AWS D17.3/D17.3M:2010, Clause 6.

B.3.9 TEST METHODS

The following test methods shall be used, when applicable:

B.3.9.1 Hardness

Shall be determined in accordance with ASTM A 370, ASTM E 10, ASTM E 18, and ASTM E 384, as applicable. Hardness tests shall be performed on the thickest section, unless otherwise specified by the cognizant quality assurance organization.

B.3.9.1.1 Rockwell and Brinell Hardness Testing Machines

Shall be calibrated and verified according to ASTM E 18 and ASTM E 10 respectively.

B.3.9.2 Transverse Joint Strength (yield and ultimate) in Tension

Shall be determined in accordance with ASTM E-8, AWS B4.0, AWS D17.3, as applicable.

B.3.9.3 Stress Strain Curve Analysis

Shall be determined in accordance with AWS B4.0, as applicable.

B.3.9.4 Joint Strength (yield and ultimate) in Bearing

Shall be determined in accordance with ASTM E 238, as applicable.

B.3.9.5 Joint Strength (yield) in Compression

Shall be determined in accordance with ASTM E 9, as applicable.

B.3.9.6 Ultimate in Shear

Shall be determined in accordance with ASTM B 831, as applicable.

B.3.9.7 Corrosion Resistance

Shall be determined in accordance with ASTM G34, ASTM B117, ASTM G110, etc., as applicable.

B.3.10 ADDITIONAL PROCESSES

Parts shall not be subjected to thermal operations or straightening operations other than those specified, unless permitted by the cognizant engineering organization.

B.4 QUALITY ASSURANCE PROVISIONS

B.4.1 RESPONSIBILITY FOR INSPECTION

Unless otherwise specified by the cognizant quality assurance organization, the FSW and processing fabricator shall supply all samples for testing and shall be responsible for the performance of all required tests and inspections. The fabricator may use his or her own facilities or any commercial laboratory acceptable to the cognizant quality assurance organization. Purchaser reserves the right to sample and to perform any confirmatory testing deemed necessary to ensure that fabricator conforms to specified requirements. The cognizant quality assurance organization may review heat treating records and the results of tests and inspections to verify that heat treatment conforms to specified requirements.

B.4.2 CLASSIFICATION OF TESTS

B.4.2.1 Acceptance Tests

Acceptance tests levels will be in conformance with the specifications in table 1 of section B-3.1.

B.4.3 APPROVAL

B.4.3.1 Facilities

The approval of a facility shall be in accordance with the following criteria:

- The FSW and processing fabricator shall have a copy of his shop procedure available for the cognizant quality assurance organizations. It shall consist of a full description of all equipment and procedures that will be used to process parts to this specification and the applicable specifications listed in B-3.1.

- All equipment shall be tested in accordance with this specification and AWS D17.3/D17.3M:2010, Clauses 7 and 8.

B.4.3.2 Personnel

Training and approval of personnel shall be in accordance with B-3.8.2.

B.4.4 LOGS

A record (written or electronic storage media), traceable to machine recording information (chart(s) or electronic storage media) and to shop travelers or other documentation, shall be kept for each weld or processing procedure. The information on the combination of documents shall include: equipment identification, approved personnel's identification, date, part number or product identification, number of parts, alloy, lot identification, applicable specification(s), and Welding Procedure Specification used. When applicable, post-weld heat treatment time and temperature shall also be recorded. The log data shall be recorded in accordance with the fabricator's documented procedures.

B.4.5 RECORDS

Machine service and maintenance logs, recorder data files, all other shop records, and all test and inspection records shall be kept available to the cognizant quality assurance organization for five years after FSW and processing operations. The records shall contain all data necessary to verify conformance to specified requirements.

B.4.6 REPORT/CERTIFICATION

The heat-treating processor shall furnish, with each shipment of parts, a certified quality assurance report, traceable to the Welding Procedure Specification control number(s), stating that the parts were processed in accordance with the requirements of this specification and the related specifications listed in table B-1 of section B-3.1. The report shall include: purchase order number, part number or product identification, alloy, temper designation, quantity of parts in the shipment, identification of machine(s) used, and post-processing procedures used. When applicable, the report shall also include method of straightening (e.g. press, fixtures), actual test results (e.g., hardness, conductivity, tensile, shear, etc.), and a statement of their conformance/nonconformance to requirements. This data shall be reported in accordance with fabricator's documented procedures.

B.5 PREPARATION FOR DELIVERY

B.5.1 IDENTIFICATION

Identification of parts or product provided to the fabricator shall be maintained on the parts at delivery.

B.5.2 PACKAGING

When specified by the procuring activity, parts shall be protected with corrosion preventive compounds when shipped.

Parts shall be packaged to ensure protection from damage during shipment and storage.

Packages of parts shall be prepared for shipment in accordance with commercial practice and in compliance with applicable rules and regulations pertaining to the handling, packaging, and transportation of the parts to ensure carrier acceptance and safe delivery.

B.6 ACKNOWLEDGMENT

A vendor shall include this specification number and its revision letter in all quotations and when acknowledging purchase orders.

B.7 REJECTIONS

Parts not welded or processed in accordance with this specification, or with modifications authorized by the cognizant engineering organization, will be subject to rejection and shall be submitted for disposition in accordance with purchaser's procedures for nonconformance.

B.8 NOTES

A change bar (l) located in the left margin is for the convenience of the user in locating areas where technical revisions, not editorial changes, have been made to the previous issue of this document. An (R) symbol to the left of the document title indicates a complete revision of the document, including technical revisions. Change bars and (R) are not used in original publications, nor in documents that contain editorial changes only.

B.8.1 TERMS USED IN AMS

Terms used in AMS are clarified in ARP 1917 and as follows:

- Parts: Finished and semifinished parts, including raw mill products, friction stir welded or processed, or heat treated by the user during the fabrication process or for qualification of response to FSW or processing.

- Cognizant: The term applied to the engineering organization responsible for the design of the parts, or its allied quality assurance organization, or a designee of these organizations.

- Stress relieving: Heating or mechanical working parts, before or after the final heat treating operation, in order to relieve residual stresses caused by friction stir welding and processing or thermal cycling.

- Annealing: Heating to a suitable temperature, soaking at temperature, and slow cooling in order to get the part in its softest possible condition, usually for subsequent forming. The term “annealing” means “full annealing.”

- Aging (precipitation hardening): Heating to an intermediate temperature to cause precipitation of constituents within the material that will produce an increase in strength and hardness.

- Solution heat treating: Heating to a sufficiently high temperature, followed by cooling to hold one or more elements in solution for subsequent precipitation hardening.

- Thickness: The local dimension of the joint section of the part.

- Rockwell: Hardness testing performed in accordance with ASTM E 18.

Dimensions and properties in in./pound units and the Fahrenheit temperatures are primary; dimensions and properties in SI units and the Celsius temperatures are shown as approximate equivalents of the primary units and are presented only for information.

Purchase documents should specify not less than the following:

AMSxxxx
Size of parts
Quantity of parts
Part number or product identity
Material alloy designation of parts
Heat treating operations desired
Tensile strength, hardness, or condition that parts are to be heat treated.
……

PREPARED by DWIGHT BURFORD of the AMEC committee